Lanthanides and Quantum Dots - Time-Resolved Laser Spectroscopy of Biochemical Förster Resonance Energy Transfer (FRET) Systems

by

Niko Hildebrandt

A Dissertation
submitted to the
Mathematics-Natural Science Faculty
of the University of Potsdam
in partial fulfillment of the
requirements for the degree of
Doctor of Natural Science

Potsdam, December 2006

To Ella and Monique.

You make my life complete.

Contents

List of publications

Original publications

1. Hildebrandt N, Charbonnière LJ, Ziessel RF, Löhmannsröben H-G; "Homogeneous FRET Immunoassay Based on Lanthanides to Quantum Dots Energy Transfer" In: Osinski M, Jovin TM, Yamamoto K, editors. *Proceedings of SPIE Vol. 6448 - Colloidal Quantum Dots for Biomedical Applications II*; **2007**; 64480K (12 pages).

2. Niederkrüger M, Salb C, Marowsky G, Beck M, Hildebrandt N, Löhmannsröben H-G; "Improvement of a Fluorescence Immunoassay with a Compact Diode-Pumped Solid State Laser at 315 nm" In: *Proceedings of SPIE Vol. 6380 - Smart Medical and Biomedical Sensor Technology IV*; **2006**; 63800M (9 pages).

3. Charbonnière LJ, Hildebrandt N, Ziessel RF, Löhmannsröben H-G; "Lanthanides to Quantum Dots Resonance Energy Transfer in Time-Resolved FluoroImmunoAssays and Luminescence Microscopy" *Journal of the American Chemical Society* **2006**;128(39): 12800-12809.

4. Hildebrandt N, Charbonnière LJ, Ziessel RF, Löhmannsröben H-G; "Quantum Dots as Resonance Energy Transfer Acceptors for Monitoring Biological Interactions" In: Grzymala R, Haeberle O, editors. *Proceedings of SPIE Vol. 6191 - Biophotonics and New Therapy Frontiers*; **2006**; 61910W (9 pages).

5. Beck M, Hildebrandt N, Löhmannsröben H-G; "Quantum Dots as Acceptors in FRET Assays Containing Serum" In: Grzymala R, Haeberle O, editors. *Proceedings of SPIE Vol. 6191 - Biophotonics and New Therapy Frontiers*; **2006**; 61910X (8 pages).

6. Löhmannsröben H-G, Beck M, Hildebrandt N, Schmälzlin E, van Dongen JT; "Laser-Based Fluoroimmuno Analysis and In-Vivo Optical Oxygen Monitoring" In: Gries W, Pearsall TP, editors. *Proceedings of SPIE Vol. 6157 - Workshop on Laser Applications in Europe*; **2006**; E1-E6.

7. Hildebrandt N, Charbonnière LJ, Beck M, Ziessel RF, Löhmannsröben H-G; "Quantum Dots As Efficient Energy Acceptors in a Time-Resolved Fluoroimmunoassay" *Angewandte Chemie - International Edition* **2005**;44(46): 7612-7615.

8. Hildebrandt N, Charbonnière LJ, Beck M, Ziessel RF, Löhmannsröben H-G; "Quantenpunkte als effiziente Energieacceptoren in einem zeitaufgelösten Fluoroimmuntestsystem" *Angewandte Chemie* **2005**;117(46): 7784-7788.

Review

1. Hildebrandt N, Löhmannsröben H-G; "Quantum Dot Nanocrystals and Supramolecular Lanthanide Complexes - Energy Transfer Systems for Sensitive In Vitro Diagnostics and High Throuput Screening in Chemical Biology" *Current Chemical Biology* **2007**; accepted for publication.

Oral presentations at conferences and meetings

1. Hildebrandt N, Charbonnière LJ, Ziessel RF, Löhmannsröben H-G; "Homogeneous FRET Immunoassay Based on Lanthanides to Quantum Dots Energy Transfer" *BiOS 2007 - Biomedical Optics - Colloidal Quantum Dots for Biomedical Applications II*, San Jose, USA; **2007**.

2. Hildebrandt N, Charbonnière LJ, Beck M, Ziessel RF, Löhmannsröben H-G; "Lanthanides and Quantum Dots as Efficient Donor-Acceptor Pairs for Sensitive Homogeneous Förster Resonance Energy Transfer Fluoroimmunoassays (FRET-FIA)" *EOS Topical Meeting on Biophotonics and Biomedical Optics 2006*, Paris, France; **2006**.

3. Hildebrandt N, Charbonnière LJ, Beck M, Ziessel RF, Löhmannsröben H-G; "Lanthanide Donors and Quantum Dot Acceptors for Homogeneous FRET Immunoassays" *105. Bunsentagung 2006*, Erlangen, Germany; **2006**.

4. Hildebrandt N, Charbonnière LJ, Ziessel RF, Löhmannsröben H-G; "Quantum Dots as Resonance Energy Transfer Acceptors for Monitoring Biological Interactions" *Photonics Europe 2006 - Biophotonics and New Therapy Frontiers*, Strasbourg, France; **2006**.

5. Hildebrandt N, Flehr R, Bois E, Löhmannsröben H-G; "Optimized Homogeneous Immunoassay Based on XeCl-Laser Excited Förster Resonance Energy Transfer" *CLEO/EUROPE 2005 - Conferences on Lasers and Electro-Optics/Europe - Photonic Manipulation and Bio-Sensing*, München, Germany; **2005**.

6. Hildebrandt N, Bois E, Nuti D, Löhmannsröben H-G; "New lasers for better fluorescence immunoassays (FIA)" *OPTO 2003*, Paris - France; **2003**.

Poster presentations at conferences and meetings

1. Hildebrandt N, Bois E, Nuti D, Löhmannsröben H-G; "Sensitivity Improvement of a Laser-Based Homogeneous Fluorescence Immunoassay (FIA) Laboratory System" *EPA summer school: New Perspectives in Photochemistry*, Egmond aan See - Netherlands; **2003**.

2. Hildebrandt N, Bois E, Nuti D, Löhmannsröben H-G; "Miniaturized Laser-Based Homogeneous Fluorescence Immunoassay (FIA) Reader System" *MINIT 2003*, Potsdam, Germany; **2003**.

Abstract

Förster Resonance Energy Transfer (FRET) plays an important role for biochemical applications such as DNA sequencing, intracellular protein-protein interactions, molecular binding studies, in vitro diagnostics and many others. For qualitative and quantitative analysis, FRET systems are usually assembled through molecular recognition of biomolecules conjugated with donor and acceptor luminophores. Lanthanide (Ln) complexes, as well as semiconductor quantum dot nanocrystals (QD), possess unique photophysical properties that make them especially suitable for applied FRET. In this work the possibility of using QD as very efficient FRET acceptors in combination with Ln complexes as donors in biochemical systems is demonstrated. The necessary theoretical and practical background of FRET, Ln complexes, QD and the applied biochemical models is outlined. In addition, scientific as well as commercial applications are presented.

FRET can be used to measure structural changes or dynamics at distances ranging from approximately 1 to 10 nm. The very strong and well characterized binding process between streptavidin (Strep) and biotin (Biot) is used as a biomolecular model system. A FRET system is established by Strep conjugation with the Ln complexes and QD biotinylation. Three Ln complexes (one with Tb^{3+} and two with Eu^{3+} as central ion) are used as FRET donors. Besides the QD two further acceptors, the luminescent crosslinked protein allophycocyanin (APC) and a commercial fluorescence dye (DY633), are investigated for direct comparison. FRET is demonstrated for all donor-acceptor pairs by acceptor emission sensitization and a more than 1000-fold increase of the luminescence decay time in the case of QD reaching the hundred microsecond regime. Detailed photophysical characterization of donors and acceptors permits analysis of the bioconjugates and calculation of the FRET parameters. Extremely large Förster radii of more than 100 Å are achieved for QD as acceptors, considerably larger than for APC and DY633 (ca. 80 and 60 Å). Special attention is paid to interactions with different additives in aqueous solutions, namely borate buffer, bovine serum albumin (BSA), sodium azide and potassium fluoride (KF). A more than 10-fold limit of detection (LOD) decrease compared to the extensively characterized and frequently used donor-acceptor pair of Europium tris(bipyridine) (Eu-TBP) and APC is demonstrated for the FRET system, consisting of the Tb complex and QD. A sub-picomolar LOD for QD is achieved with this system in azide free borate buffer (pH 8.3) containing 2 % BSA and 0.5 M KF. In order to transfer the Strep-Biot model system to a real-life in vitro diagnostic application, two kinds of imunnoassays are investigated using human chorionic gonadotropin (HCG) as analyte. HCG itself, as well as two monoclonal anti-HCG mouse-IgG (immunoglobulin G) antibodies are labeled with the Tb complex and QD, respectively. Although no sufficient evidence for FRET can be found for a sandwich assay, FRET becomes obvious in a direct HCG-IgG assay showing the feasibility of using the Ln-QD donor-acceptor pair as highly sensitive analytical tool for in vitro diagnostics.

Kurzzusammenfassung

Förster Resonanzenergietransfer (FRET) spielt eine wichtige Rolle in biochemischen Anwendungen, wie z.B. DNA-Sequenzierung, intrazellulären Protein-Protein-Wechselwirkungen, molekularen Bindungsstudien, in-vitro-Diagnostik und vielen anderen. Zur quantitativen und qualitativen Analyse werden FRET Systeme normalerweise durch molekulare Erkennung von Biomolekülen, die mit Donator- und Acceptorluminophoren markiert sind, ermöglicht. Durch die besonderen photophysikalischen Eigenschaften sowohl von Lanthanidkomplexen (Ln-Komplexen), als auch Halbleiternanokristallen (sog. Quantenpunkten oder Quantumdots - QD), sind diese besonders für FRET Anwendungen geeignet. In der vorliegenden Arbeit wird effizienter FRET zwischen Ln-Komplexen und QD in biochemischen Systemen demonstriert. Die notwendigen theoretischen und praktischen Grundlagen über FRET, Ln-Komplexe, QD und die verwendeten biochemischen Modelle werden dargestellt, und wissenschaftliche als auch kommerzielle Anwendungen werden präsentiert.
FRET kann zur Messung von strukturellen Veränderungen und Dynamiken im Bereich von ca. 1 bis 10 nm verwendet werden. Der sehr starke und gut charakterisierte Bindungsprozess zwischen Streptavidin (Strep) und Biotin (Biot) wird als biomolekulares Modellsystem eingesetzt. Ein FRET System wird durch Streptavidinkonjugation mit Ln-Komplexen und QD-Biotinylierung etabliert. Drei Ln-Komplexe (einer mit Tb^{3+} und zwei mit Eu^{3+} als Zentralion) werden als Donatoren verwendet, und neben QD werden zwei weitere Acceptoren, das lumineszierende, quervernetzte Protein Allophycocyanin (APC) und ein kommerzieller Fluoreszenzfarbstoff (DY633), untersucht. FRET kann für alle Donator-Acceptor Paare nachgewiesen werden, zum einen durch sensibilisierte Acceptorlumineszenz und zum anderen durch eine über 1000-fach erhöhte Lumineszenzabklingzeit der QD mit über 100 Mikrosekunden. Mittels detailierter photophysikalischer Charakterisierung der Donatoren und Acceptoren können die Biokonjugate analysiert und die FRET Parameter berechnet werden. Für die QD FRET Systeme ergeben sich extrem große Försterradien von über 100 Å, die wesentlich größer sind als für APC und DY633 (ca. 80 bzw. 60 Å). Besondere Aufmerksamkeit gilt der Wechselwirkung mit den Zusatzreagenzien Boratpuffer, Bovines Serumalbumin (BSA), Natriumazid und Kaliumfluorid (KF) in den wässrigen Lösungen. Im Vergleich zum ausgiebig charakterisierten und vielfach verwendeten Donator-Acceptor Paar aus Europium-tris(Bipyridin) (Eu-TBP) und APC wird eine mehr als 10-fache Senkung der Nachweisgrenze für das FRET-System, bestehend aus Tb-Komplex und QD, erreicht. In azidfreiem Boratpuffer (pH 8,3) mit 2 % BSA und 0,5 M KF wird eine subpicomolare QD-Nachweisgrenze für dieses System aufgezeigt. Um den Transfer des Strep-Biot Modellsystems in eine echte in-vitro-diagnostische Anwendung zu demonstrieren, werden zwei Immuntests zum HCG-(Humanes Choriongonadotropin)-Nachweis untersucht. Sowohl HCG als auch monoklonale anti-HCG Maus-IgG-(Immunoglobulin G)-Antikörper werden mit dem Tb-Komplex bzw. mit QD markiert. Obwohl kein ausreichender Nachweis für FRET in einem immunometrischen Assay (oder Sandwichassay) erbracht werden kann, wird FRET in einem direkten HCG-IgG Assay erzielt, wodurch die Realisierbarkeit von Ln-QD Donator-Acceptor Paaren zur hochsensitiven Anwendung in der in-vitro-Diagnostik gezeigt werden kann.

Chapter 1

Introduction

Many biological and biochemical processes and functions take place on a micro- or nanometer length scale. Therefore, understanding small systems is of great importance for a thorough knowledge of fundamental life sciences as well as for many commercial applications in medicine and diagnostics. In order to analyze those systems in their natural conformation and surroundings, physiology, function and dynamics can be revealed by introducing spectroscopically accessible chemical labels. Development of the right markers, biochemical labeling and investigation of the labeled biosystems by means of highly sensitive spectroscopy affords an appropriate interaction between biology, chemistry and physics which makes this scientific field so wide and interesting.

Förster resonance energy transfer (FRET) can be used to measure structural changes or dynamics at distances ranging from approximately 1 to 10 nm, which corresponds very well to many biomolecular processes. A quantum mechanical theory for FRET was derived in 1948 by Theodor Förster [1] for allowed dipole transitions of donor and acceptor molecules of the same kind. However, the radiationless FRET process can also involve forbidden transitions, and theory as well as methods have been widely expanded (with many different donor and acceptor species), which has been described in several comprehensive books or reviews [2–18]. Due to the r^{-6} distance dependence between donor and acceptor, FRET is very sensitive to nanoscale changes and has been used for several biochemical applications such as DNA investigations, imaging, protein-protein interactions or immunoassays [10–14, 16, 18–27].

Lanthanide complexes can combine the advantegeous properties of the inner lanthanide (Ln) ion and its complexing ligand to be very good FRET donors for biochemical applications. The ligand fulfills two important requirements, namely shielding of the Ln ion from the surrounding biological medium and efficient light collection followed by energy transfer to the central ion. The Ln ion itself exhibits very special spectral properties, such as long excited state lifetimes (in the millisecond range) and narrow emission bands. The long lifetimes are especially important for FRET donors in biological applications because they allow for the distinction between short-lived background bioluminescence and the long-lived FRET signal. Ln complexes are frequently used for biochemical applications [13, 24, 28–30] and can be synthesized with functional groups for biomolecule conjugation.

Since the introduction of water soluble semiconductor quantum dot nanocrystals (QD) in the mid 1990s, they have strongly entered the biological field. The reason for this can be found in their unique optical properties. They are very photostable, have extremely high extinction coefficients and the most important aspect is their size-tunable emission wavelength. The exciton Bohr radius (which can be imagined as the hole-electron distance) of the QD semicondutor material is significantly larger than the lattice constant of the crystal. Creating nanocrystals

smaller than the Bohr radius leads to quantum confinement of motion in three dimensions (quasi zero-dimensional systems), which results in size-dependent properties as found in the early 1980s [31–33]. Thus, the narrow emission wavelength band of a QD can be shifted from the bulk semiconductor bandgap energy to higher energies (lower wavelengths) by decreasing the QD size (without changing the material). Another important fact is the very broad absorption spectrum from just below the emission onset wavelength down to the UV, caused by excitation into the energetically broad conduction band of the semiconductor. QD have been successfully applied as FRET donors, but they have been rarely used as acceptors. Although their high extinction coefficients over a wide wavelength range would make them theoretically very good acceptors, this could not be confirmed by using common organic donor molecules. The reason for this is related to the very fast radiative deactivation of the donors compared to the slow non-radiative FRET decay rate, in the presence of a QD acceptor [34]. QD surface functionalization allows for efficient biomolecule conjugation.

This work describes the possibility of using QD as very efficient FRET acceptors in combination with Ln complexes as donors in biochemical systems. The necessary theoretical and practical background of FRET, Ln complexes, QD and the applied biochemical models is outlined. In addition, scientific as well as commercial applications are presented. Three Ln complexes (one with Tb^{3+} and two with Eu^{3+} as central ion) are used as FRET donors. TbL and EuL [35–37] were synthesized at the Laboratoire de Chimie Moléculaire (CNRS Strasbourg, France) whereas Eu-TBP [37,38] is a commercial Ln complex distributed by CIS bio International (Bagnols-sur-Cèze, France). As a counterpart to these donors, three commercially available FRET acceptors are chosen. Biocompatible CdSe/ZnS core/shell QD emitting at 655 nm (QD655) are distributed by Invitrogen Corporation (Carlsbad, California, USA). The luminescent crosslinked biliprotein APC, which is used together with Eu-TBP in a commercial FRET immunoassay, can be purchased from various companies (e.g. Invitrogen Corporation). The organic fluorescence dye DY633 is distributed by Dyomics GmbH (Jena, Germany).

Both donors and acceptors are extensively characterized in several aqueous solutions by UV/Vis absorption, steady-state and time-resolved luminescence spectroscopy, and conjugation with biomolecules is described and characterized by UV/Vis and MALDI-TOF measurements. The determined photophysical properties of all donor-acceptor pairs are used to calculate the necessary FRET parameters (donor luminescence quantum yield, spectral overlap, Förster radius), which are used for further analysis of the FRET results. Time-resolved FRET experiments are performed on a modified KRYPTOR immunoreader (Cezanne, Nîmes, France) with a Nd:YAG-OPO laser system as excitation source. The strong biological binding process between biotin and streptavidin is used as a biological FRET system, in which the donors are labeled to streptavidin, whereas the acceptors are biotinylated. Several additives in aqueous solutions, namely borate buffer, potassium fluoride (KF), bovine serum albumin (BSA) and sodium azide (NaN_3) are investigated. For all FRET measurements, increasing amounts of biotinylated acceptors are added to donor labeled streptavidin containing solutions. The same experiments are performed with free Ln complexes in order to exclude dynamic energy transfer by freely diffusing donors and acceptors. For comparison of the different FRET systems, detection limits are calculated. To transfer the results from the streptavidin-biotin model to a real-life application, TbL-complex to QD655 FRET experiments with HCG (human chorionic gonadotropin) immunoassays (e.g. applied as pregnancy test) are investigated. HCG as well as monoclonal anti-HCG mouse-IgG antibodies are labeled with TbL and QD655, respectively. FRET experiments are carried out as an IgG-HCG-IgG sandwich assay and a direct HCG-IgG assay and the results are reviewed in the context of future applications.

Chapter 2

Theoretical and practical background

2.1 Förster resonance energy transfer

2.1.1 Introduction

Resonance energy transfer (RET) describes a non-radiative transfer of energy from an excited donor molecule (D^*) to an acceptor molecule (A). A first mechanism was proposed in a classical approach by Jean-Baptiste Perrin [39, 40], and his son Francis Perrin added a quantum mechanical description [41]. However, this theory yielded inexact results primarily because it was based on the assumption that the involved molecules have a discrete fluorescence frequency. Moreover, quantitative evaluation required molecular collision times which could only be roughly estimated. Theodor Förster found a classical treatment for RET in 1946 [42, 43] based on experimentally easily accessible quantities such as absorption and fluorescence spectra and excited state lifetimes. In 1948 [1] Förster published the most cited work about RET, which was a quantum mechanical formulation of his theory. This is also the reason why RET is primarily connected with Theodor Förster.
As RET is a highly sensitive spectroscopic measurement technique for processes occuring on the nanometer scale with sub-nm resolution, it has been widely used for qualitative and quantitative biochemical applications, among which are DNA sequencing, intracellular protein-protein interactions, molecular binding studies, clinical diagnostics and many others [2, 10–13, 18–27]. Several abbreviations have been created for RET in connection with e.g. Förster or fluorescence (FRET), luminescence (LRET) and bioluminescence (BRET). All of them have the common resonance mechanism of inducing a dipole oscillation in A by D^* via coulombic interactions (Figure 2.1). As FRET is the preferred abbreviation it will be used throughout this work.

2.1.2 Theoretical treatment

Most of the theory mentioned in this chapter has been taken from references [10, 17], which both cover many theoretical and practical aspects and are suggested for further reading.
For the energy difference ΔE between HOMO and LUMO of A and D, the resonance condition

$$\Delta E(\mathrm{D} \longrightarrow \mathrm{D}^*) = \Delta E(\mathrm{A} \longrightarrow \mathrm{A}^*) \tag{2.1}$$

has to be fulfilled. The transfer rate within a donor-acceptor distance of r is given by

$$k_{ET} = \left(\frac{1}{\tau_D}\right)\left(\frac{R_0}{r}\right)^6 \tag{2.2}$$

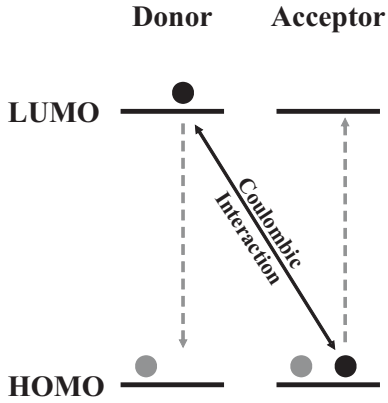

Figure 2.1: *FRET mechanism. Excitation of the acceptor molecule from HOMO (highest occupied molecular orbital) to LUMO (lowest unoccupied molecular orbital) is accomplished by inducing an acceptor dipole oscillation via coulombic interaction with the excited donor.*

where τ_D is the luminescence decay time of donor D in absence of the acceptor and R_0 is the so called Förster radius, the distance at which FRET is 50 % efficient.
Calculation of R_0 requires extensive spectroscopic knowledge of the donor-acceptor system, as the spectral overlap integral of donor emission and acceptor absorption ($J(\lambda)$), the dipole orientation factor between donor and acceptor (κ^2), the donor quantum yield (Φ_D) and the index of refraction of the surrounding medium (n_r) have to be known.

$$R_0^6 = \frac{9\,ln(10)\,\kappa^2\,\Phi_D}{128\,\pi^5\,n_r^4\,N_A} J(\lambda) = 8.79 \cdot 10^{-5} (n_r^{-4}\,\Phi_D\,\kappa^2\,J(\lambda)) \qquad \text{(in Å}^6\text{)} \tag{2.3}$$

In this equation R_0 is in Å and $J(\lambda)$ is in $\mathrm{M^{-1}cm^{-1}nm^4}$. The dipole orientation factor κ^2 describes the orientation of the transition dipole moments of D^* and A (Figure 2.2) and is calculated by

$$\kappa^2 = (cos\alpha - 3\,cos\beta\,cos\gamma)^2 \tag{2.4}$$

κ^2 can range from 0 to 4 and is equal to 2/3 for randomly oriented systems in solution (random orientation of donor and acceptor). A detailed discussion of the dipole-dipole orientation can be found in reference [3].
The spectral overlap integral is calculated with the normalized luminescence spectrum of the donor $F_D(\lambda)$ in $\mathrm{nm^{-1}}$ (with $\int F_D(\lambda)d\lambda = 1$), the extinction coefficient spectrum of the acceptor $\varepsilon_A(\lambda)$ in $\mathrm{M^{-1}cm^{-1}}$ and the wavelength λ in nm (Figure 2.3) by

$$J(\lambda) = \int F_D(\lambda)\,\varepsilon_A(\lambda)\,\lambda^4 d\lambda \tag{2.5}$$

The FRET efficiency η_{ET} is inversively proportional to the sixth power of r and is described by

$$\eta_{ET} = \frac{R_0^6}{R_0^6 + r^6} = \frac{k_{ET}}{k_{ET} + \tau_D^{-1}} \tag{2.6}$$

η_{ET} can be calculated by the donor luminescence quantum yields in absence (Φ_D) and presence (Φ_{DA}) of the acceptor or the related luminescence decay times (τ_D and τ_{DA}).

$$\eta_{ET} = 1 - \frac{\Phi_{DA}}{\Phi_D} = 1 - \frac{\tau_{DA}}{\tau_D} \tag{2.7}$$

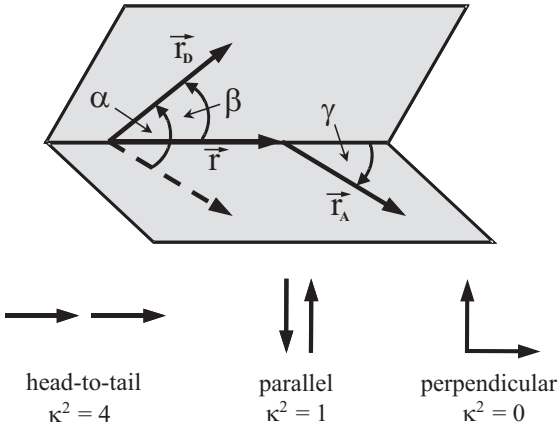

Figure 2.2: *Orientation of the donor emission transition dipole moment ($\vec{r}_D$), the acceptor absorption transition dipole moment ($\vec{r}_A$) and the influence on κ^2.*

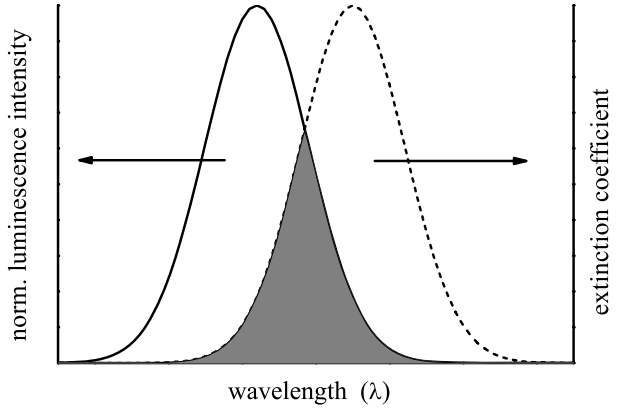

Figure 2.3: *Normalized donor emission (solid line) and acceptor extinction coefficient spectrum (dashed line) as well as spectral donor-acceptor overlap (in grey).*

If the intrinsic luminescence decay of the acceptor is much faster compared to the donor, the decay times of the donor and the FRET sensitized acceptor within a D-A complex (τ_{DA} and τ_{AD}) are equal [44]. Thus, Equation 2.7 becomes

$$\eta_{ET} = 1 - \frac{\tau_{DA}}{\tau_D} = 1 - \frac{\tau_{AD}}{\tau_D} \tag{2.8}$$

Combining Equations 2.6 and 2.7 (and recalling Equation 2.2) leads to

$$\frac{1}{\tau_{DA}} = \frac{1}{\tau_D} + \left(\frac{1}{\tau_D}\right)\left(\frac{R_0}{r}\right)^6 = \frac{1}{\tau_D} + k_{ET} \tag{2.9}$$

In biological systems, distributions of the D-A distance r have to be considered [10, 45–47]. Usually, the Gaussian distribution

$$P(r) = \frac{1}{\sigma\sqrt{2\pi}}\, exp\left[-\frac{1}{2}\left(\frac{\bar{r} - r}{\sigma}\right)^2 \right] \tag{2.10}$$

with the mean distance $\bar{r}$ and the standard deviation σ is used.
In biological systems, the donor decay in absence of the acceptor can be multiexponential [10], e.g. by multiple (n) donor species due to conformational distributions within proteins or macromolecules. In this case, the time dependent donor luminescence intensity can be described as

$$I_D(t) = \sum_{i=1}^{n} \alpha_{D_i} exp\left[- \frac{t}{\tau_{D_i}} \right] \tag{2.11}$$

where α_{D_i} are the pre-exponential factors for each ith donor luminescence decay time (τ_{D_i}) in absence of the acceptor.
Assuming that the transfer rate for each decay-time component is described by Equation 2.2 and each distance-dependent donor decay time is given by Equation 2.9, the time (t) and distance (r) dependent luminescence intensity of the donor in presence of the acceptor can be described as

$$I_{DA}(r,t) = \sum_{i=1}^{n} \alpha_{D_i} exp\left[- \frac{t}{\tau_{D_i}} - \frac{t}{\tau_{D_i}} \left(\frac{R_0}{r} \right)^6 \right] \tag{2.12}$$

and the luminescence intensity decay is given by

$$I_{DA}(t) = \int_0^\infty P(r)\, I_{DA}(r,t)\, dr \tag{2.13}$$

Because FRET is a dynamic process, determination of conformational changes as well as distance distributions within a biological FRET system can only be determined by time-resolved measurements.

2.1.3 FRET applications

The energy transfer occurs at distances ranging from ca. 1-10 nm, which corresponds very well to many biomolecular processes. Hence, FRET is an important technique for sensitive structural and dynamic measurements in this area. Finding donor-acceptor pairs with high R_0 and robustness in biological media is of great interest for efficiently measuring long distances under stable conditions.
Advantages of FRET for bioanalytical techniques include high sensitivity to nanoscale changes (luminescence measurement with r^{-6} distance dependence), the possibility of creating homogeneous immunoassays (sandwich assays with donor on one and acceptor on the other side of a biological system, e.g. two antibodies on an antigen), luminescence decay time and intensity dependence (qualitative, quantitative and real-time kinetic measurements), low environmental and safety risks (compared to techniques using radioactive labels) and the efficient quantitative use in imaging techniques.
The most often applied biological nanoscale processes using FRET for quantitative (concentration) analysis are binding between various antigens and antibodies or the well established streptavidin-biotin or avidin-biotin recognition processes known to be very efficient in biological media with a first dissociation constant of 10^{-15} M^{-1} for avidin and 10^{-13} M^{-1} for streptavidin [48]. For qualitative analysis or quantitative distance measurements, donor and acceptor can be labeled to biomolecules like proteins (e.g. analysis of protein folding) or RNA and DNA, respectively (e.g. DNA sequencing).

2.2 Luminescence quenching

Besides FRET, there are other processes which can alter the luminescence intensity and decay time of luminophores inside biological systems. Steady-state and time-resolved measurements reveal the different luminescence quenching processes, which can be static (e.g. by formation of a nonluminescent complex between luminophore and quencher) or dynamic (e.g. collisional quenching due to diffusive processes). Luminescence quenching is described by the Stern-Volmer equation [10],

$$\frac{L_0}{L} = 1 + K_{SV}[Q] \tag{2.14}$$

where L_0 and L are the luminescence intensities in absence and presence of the quencher, K_{SV} is the Stern-Volmer constant and $[Q]$ is the quencher concentration.
For dynamic quenching the Stern-Volmer constant is K_D and Equation 2.14 becomes

$$\frac{L_0}{L} = \frac{\tau_0}{\tau} = 1 + K_D[Q] = 1 + k_q\tau_0[Q] \tag{2.15}$$

with τ_0 and τ as luminescence decay times in absence and presence of the quencher and k_q being the bimolecular quenching constant.
For static quenching, the Stern-Volmer constant is given by

$$K_{SV} = K_S = \frac{[LQ]}{[L][Q]} \tag{2.16}$$

where $[LQ]$ is the complex concentration and $[L]$ is the uncomplexed luminophore concentration.
For combined dynamic and static quenching the Stern-Volmer equation can be modified to

$$\frac{L_0}{L} = (1 + K_D[Q])(1 + K_S[Q]) \tag{2.17}$$

Quenching data are usually presented in so-called Stern-Volmer plots, where L_0/L and τ_0/τ are displayed over $[Q]$. Figure 2.4 presents the different quenching processes.

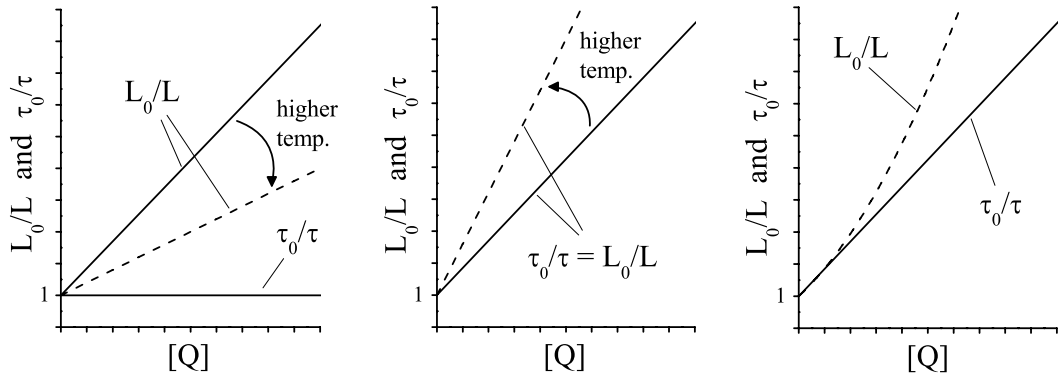

Figure 2.4: *Stern-Volmer plots of static (left), dynamic (center) and combined dynamic and static (right) quenching.*

Examples of luminescence quenching in biochemical systems are quenching of tryptophan luminescence by oxygen (dynamic) [49, 50] or quenching of coumarin C-120 luminescence by the nucleotides uridine (static and dynamic) and deoxycytidine (dynamic) [51].

2.3 Lanthanide complexes

2.3.1 Lanthanide ions

2.3.1.1 Introduction

The lanthanide (Ln) elements (also called rare earths) were discovered between 1794 (yttrium) and 1947 (promethium) [52]. From La (atomic number $Z = 57$) to Lu ($Z = 71$) they display very similar chemical as well as physical properties which is partly due to their common existence in the trivalent state.
Trivalent lanthanide ions possess unique spectral properties caused by the electronic f-f transitions within the 4f shell, which is shielded by the filled 5s and 5p shells. The shielding leads to minimal interactions with the field of surrounding ions and dipolar molecules, so there are only weak pertubations of the electronic transitions between the energy levels of the f orbitals. This results in nearly atom like narrow-line absorption and emission spectra with excited state lifetimes reaching the millisecond timescale. Luminescing Ln ions used for biochemical spectroscopy are neodymium, samarium, europium, terbium, dysprosium, erbium and ytterbium. The most important and frequently applied trivalent Ln ions for spectroscopy are those of europium (Eu^{3+}) and terbium (Tb^{3+}) with [Xe]$4f^6$ and [Xe]$4f^8$ electronic configurations, respectively. Therefore, this work will specifically address Eu^{3+} and Tb^{3+}. Detailed descriptions of the photophysical properties of lanthanide ions and their chelating complexes can be found in References [13, 28, 29, 52–58].

2.3.1.2 Spectroscopic term symbols

In order to give a detailed description of electron configurations of atoms or ions, the spectroscopic (or atomic) term symbols are used which have the form ${}^{(2S+1)}L_J$. This representation results from the determination of the total orbital angular momentum $\vec{L}$ and the total spin angular momentum $\vec{S}$. The vector sum of $\vec{L}$ and $\vec{S}$ leads to the total angular momentum $\vec{J}$. This is called L-S or Russell-Saunders coupling. It is a good approximation for lighter atoms (j-j coupling would be better for heavier atoms, where the spin and orbital angular momenta of individual electrons tend to couple and form individual electron angular momenta) and still appropriate for the luminescent transitions of Eu^{3+} and Tb^{3+} occurring within multiplets of lower energy.
The term symbol consists of the three quantum numbers L, S and J.

L is the quantum number of the total orbital angular momentum $\vec{L}$.
$\vec{L} = \sum_{i=1}^{N} \vec{l_i}$, where $\vec{l_i}$ is the orbital angular momentum of electron i.
The absolute values of $\vec{L}$ and $\vec{l_i}$ are $|\vec{L}| = \sqrt{L(L+1)} \cdot \hbar$ and $|\vec{l_i}| = \sqrt{l_i(l_i+1)} \cdot \hbar$. l_i is the orbital angular quantum number of electron i.
$M_L = \sum_{i=1}^{N} m_{l_i}$, where m_{l_i} is the magnetic quantum number of electron i.
m_{l_i} parameterizes the z component of $\vec{l_i}$ ($l_i^z = m_{l_i}\hbar$) and can take values from l_i to $-l_i$ ($m_{l_i} = l_i, l_i - 1, ..., 0, ..., 1 - l_i, -l_i$), whereas M_L can take values from L to $-L$ ($M_L = L, L-1, ..., 0, ..., 1-L, -L$).
The states of a many-electron atom (or ion) use the same code as the electronic configuration (with capital letters). For $L = 0, 1, 2, 3, 4, 5, ...$ the states are S, P, D, F, G, H, ...

S is the quantum number of the total spin angular momentum $\vec{S}$.
$\vec{S} = \sum_{i=1}^{N} \vec{s_i}$, where $\vec{s_i}$ is the spin angular momentum of electron i.
The absolute values of $\vec{S}$ and $\vec{s_i}$ are $|\vec{S}| = \sqrt{S(S+1)} \cdot \hbar$ and $|\vec{s_i}| = \sqrt{s_i(s_i+1)} \cdot \hbar = \sqrt{3}/2 \cdot \hbar$. $s_i = 1/2$ is the spin quantum number of electron i.
$M_S = \sum m_{s_i}$, where m_{s_i} is the secondary spin quantum number of electron i.
m_{s_i} parameterizes the z component of $\vec{s_i}$ ($s_i^z = m_{s_i}\hbar$) and can take values of $\pm s_i$ ($m_{s_i} = \pm 1/2$), whereas M_S can take values from S to $-S$ ($M_S = S, S-1, ..., 0, ..., 1-S, -S$).
$2S+1$ is the multiplicity of the state, e.g.:
all electrons are paired $\Rightarrow$ $S = 0$ $\Rightarrow$ $2S+1 = 1$ $\Rightarrow$ singlet state
six unpaired electrons $\Rightarrow$ $S = 3$ $\Rightarrow$ $2S+1 = 7$ $\Rightarrow$ septet state

J is the quantum number of the total angular momentum $\vec{J}$.
As $\vec{J} = \vec{L} + \vec{S}$ the maximum value of J is obtained when $\vec{L}$ and $\vec{S}$ are pointing in the same direction, so that $J = L + S$. The smallest value that J can have is when $\vec{L}$ and $\vec{S}$ are pointing in opposite directions, so that $J = |L - S|$. The values for J are obtained from $J = L+S, L+S-1, L+S-2, ..., |L-S|$

The ${}^{(2S+1)}L_J$ ground state is given by Hund's rules:

- The term with the highest spin multiplicity ($2S_{max}+1$) is the lowest in energy.
- For a given multiplicity, the term with the largest value of L lies lowest in energy.
- For atoms with less/more than half-filled shells, the level with the lowest/highest value of J is lowest in energy.

2.3.1.3 Electronic configuration

Electronic energy level calculations are rather complicated but were widely performed using tensor-operator methods originated by Racah between 1942 and 1949 [59–62] which have been described in detail by Slater [63] and Judd [64].
However, as there are only very few of these energy levels involved in the 4f transitions that are spectroscopically important, the theory will not be detailed in this work.
Some theoretical background is necessary to understand the structure of lanthanide absorption and emission spectra.
The Hamiltonian for an ion (visualized as a point nucleus of infinite mass and charge Ze surrounded by N electrons) under the influence of a ligand field (with M ligands regarded as negative charges centered around the ion) is composed of four terms:

$$H = \underbrace{\sum_{i=1}^{N} \Big(-\frac{\hbar^2}{2m_e}\nabla_i^2 - \frac{Ze^2}{4\pi\varepsilon_0 r_i} \Big)}_{H_1} + \underbrace{\sum_{i>k=1}^{N} \frac{e^2}{4\pi\varepsilon_0 r_{ik}}}_{H_2} + \underbrace{\sum_{i=1}^{N} \frac{Ze^2\hbar^2}{8\pi\varepsilon_0 c^2 m_e^2 r_i^3} \vec{s_i}\vec{l_i}}_{H_3} + \underbrace{\sum_{i=1}^{N}\sum_{l=1}^{M} \frac{Ze^2}{d_{il}}}_{H_4} \quad (2.18)$$

∇^2: Laplace operator ($\nabla^2 = \frac{\delta^2}{\delta x^2} + \frac{\delta^2}{\delta y^2} + \frac{\delta^2}{\delta z^2}$)
r_i: distance of electron i from the nucleus
r_{ik}: distance of electron i from electron k
$\vec{s_i}$: spin angular momentum of electron i

$\vec{l_i}$: orbital angular momentum of electron i
d_{il}: distance between ligand l and electron i

The H_1 term presents the undisturbed Hamiltonian (kinetic energy + coulomb potential), H_2 includes the interelectronic repulsion between the electrons and H_3 gives the contribution of the spin-orbit coupling using the L-S coupling approximation. As mentioned above, L-S coupling is valid for lighter atoms, where the quantitative splitting (energy difference between two multiplet levels) between a level with quantum number J and $J+1$ is proportional to J (Landé's interval rule). Experimentally, Landé's rule is followed fairly well for Eu^{3+} and Tb^{3+} luminescence transitions. The final H_4 term is the ligand field Hamiltonian. The energy levels of Ln ions are highly degenerate. Spectroscopic coefficients for f^n configurations have been calculated [65], and the $4f^6$ and $4f^8$ configurations for Eu^{3+} and Tb^{3+} are split into 119 $^{(2S+1)}L$ spectroscopic terms by interelectronic repulsion. Each term is further split into $2S+1$ (if $S \leq L$) or $2L+1$ (if $L > S$) sublevels, leading to 295 $^{(2S+1)}L_J$ spetroscopic levels by spin-orbit coupling. The final maximum degeneracy (or fine-splitting) into D energy levels is caused by the ligand-field where every electronic level is degenerated into maximum $2J+1$ Stark sublevels (depending on the symmetry of the Ln^{3+} ion site) [28]. D (the number of possible microstates) is given by the number of electrons (N) in the open 4f shell of $2l+1$ orbitals (with two possible spin orientations):

$$D = \binom{2(2l+1)}{N} = \binom{4l+2}{N} = \frac{(4l+2)!}{N!(4l+2-N)!} \tag{2.19}$$

For Eu^{3+} and Tb^{3+} (where $N = 6$ for Eu^{3+}, $N = 8$ for Tb^{3+} and $l = 3$ for both) $D = 3003$ with ground state levels (following Hund's rules) of $^7F_0$ and $^7F_6$, respectively. Partial energy diagrams are shown in Figure 2.5 for Eu^{3+} and Figure 2.6 for Tb^{3+}.

2.3.1.4 Optical transitions and selection rules

Optical transitions describe a resonant energy transfer from radiation to matter (absorption) or from matter to radiation (luminescence), and can be ascribed to electric transitions inside the 4f shell for lanthanide ions. $4f \leftrightarrow 4f$ transitions are very sharp in energy (narrow absorption and emission bands) because the 4f electrons are effectively shielded by the filled 5s and 5p shells.
Selection rules determine whether a transition is "forbidden" (very low probability) or "allowed" (high probability). The most important selection rules for Ln ions are the Laporte rule and the spin multiplicity rule.
The Laporte rule permits transitions only between states of opposite parity (parities are even (g) or odd (u); the parity is g, which comes from the German word "gerade", if the wavefunction is unchanged by reflexion through an inversion center and u, "ungerade", if the wavefunction changes sign by reflexion through an inversion center), which means that transitions within a single quantum shell (e.g. f-f transitions) are forbidden.
Intraconfigurational f-f transitions only become possible due to interactions with the ligand field or vibrational states, which mix electronic states of different parity into the 4f wavefunctions. Mixing states with different J (J-mixing) is another reason for allowing these transitions. They have small intensities because the interaction with other states is quite weak.
The spin multiplicity rule forbids transitions between states of different multiplicity $(2S+1)$. As the optical $f \rightarrow f$ transitions for Eu^{3+} and Tb^{3+} are of quintet $\rightarrow$ septet multiplicity, they

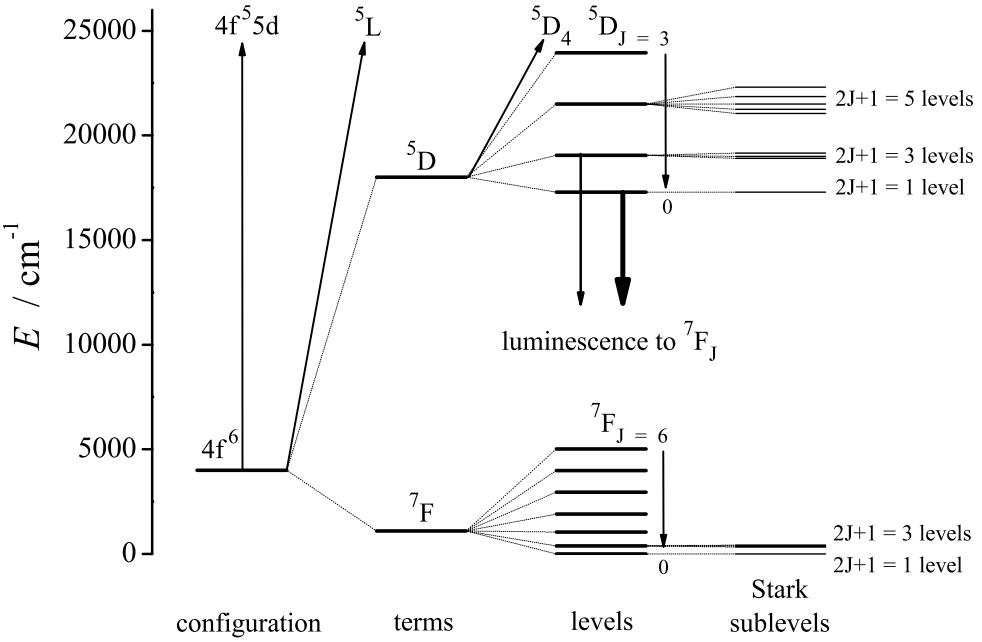

Figure 2.5: *Partial energy diagram for Eu^{3+} with the influence of interelectronic repulsion (terms), spin-orbit coupling (levels) and ligand-field (sublevels). The main luminescent transitions occur from $^5D_0$ to ^7F_J (thick downward arrow) whereas the transitions from $^5D_1$ are only weak in luminescence (thin downward arrow).*

are spin-forbidden and therefore the more general term luminescence is preferred instead of fluorescence (used in general for spin-allowed transitions in organic systems) [66]. Spin-orbit coupling (where states of different L and S but the same J admix) is the reason why the weak luminescence can nevertheless be observed.
Three mechanisms must be considered for the observed transitions in lanthanide ions [67]:

I: Magnetic dipole transitions

Magnetic dipole transitions are caused by interaction of the Ln ion with the magnetic field component of light through a magnetic dipole. They can be regarded as a charge displacement over a curved loop, which is small within the extent of an ion. Therefore, the magnetic dipole moment is small and since the intensity is proportional to the square of the transition dipole moment, the intensity of the transition is weak. Because a magnetic dipole transition can be regarded as a rotational displacement of charge (rotation is not reversed under inversion through an inversion center) it has even parity. Thus a magnetic dipole operator possesses even transformation properties under inversion and allows f-f transitions.

II: Induced electric dipole transitions

The majority of observed optical transitions in lanthanide ions are induced electric dipole transitions. They are caused by interaction with the electric field component of light through an electric dipole. f-f induced electric dipole transitions are Laporte forbidden and very weak in intensity compared to ordinary electric dipole transitions. Non-centrosymmetrical interactions cause mixing of electronic states with even parity, which makes the induced electric dipole transitions allowed. The Judd-Ofelt theory (not further discussed in this work) describes the transitions in detail and was published independently by Judd [68] and Ofelt [69].

III: Electric quadrupole transitions

Electric quadrupole transitions are much weaker than magnetic or induced electric dipole

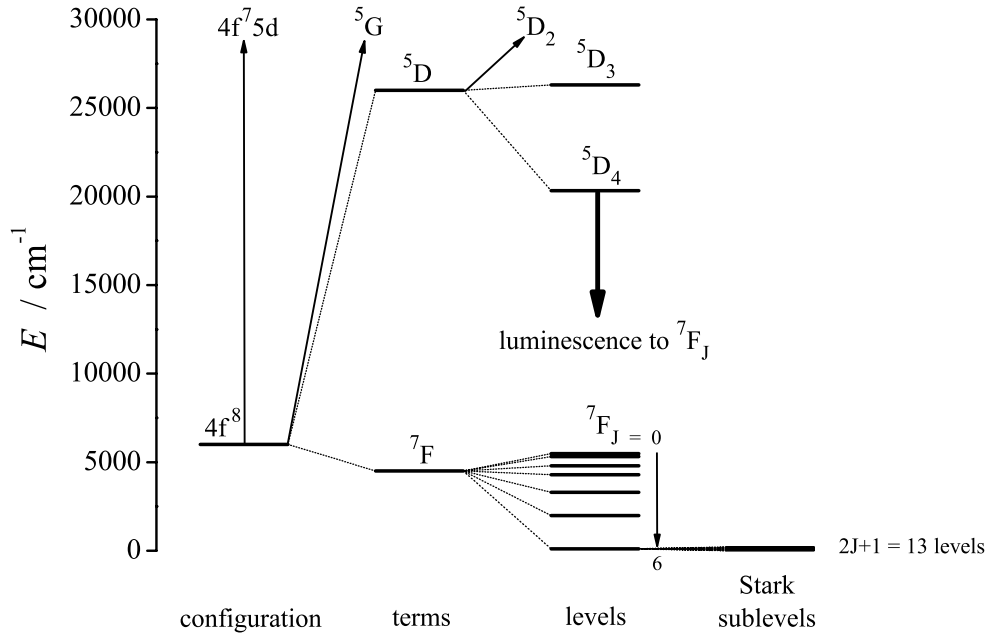

Figure 2.6: *Partial energy diagram for Tb^{3+}. Luminescent transitions occur from $^5D_4$ to ^7F_J (thick downward arrow).*

transitions. They arise from charge displacement with quadrupolar (4 point charges with overall zero charge and zero dipole moment) nature and possess even parity. Although some authors claim the existence of these transitions (e.g. Chrysochoos et al. 1973 [70]), there is no experimental evidence in Ln-spectra.
Concrete selection rules for magnetic dipole, induced electric dipole and electric quadrupole transitions can be derived from quantum mechanical calculations. They are rather complicated and only valid under certain conditions. A detailed description of the selection rules for Ln ions can be found in Reference [56].

Hypersensitive transitions
Some optical transitions are very sensitive to the environment and are usually more intense for Ln complexes than for the ion in aqueous solution. As they obey the quadrupole selection rules, they are also called pseudo-quadrupole transitons. Nevertheless, their intensities are several orders of magnitude too large for quadrupole transitions. Hypersensitive transitions were first noticed in 1930 [71] for Ln^{3+} nitrates in aqueous spectra and in 1950 [72, 73] in connection with the ligand environment. Several reviews about hypersensitive transitions have been published (e.g. Peacock et al. 1975 [74], Henrie et al. 1976 [75], Misra et al. 1985 and 1991 [76, 77]).
Hypersensitive transitions for Eu^{3+} are $^5D_1 \longrightarrow {}^7F_1$ (18700 cm^{-1}), $^5D_2 \longrightarrow {}^7F_0$ (21500 cm^{-1}) and $^5D_0 \longrightarrow {}^7F_2$ (16300 cm^{-1}) whereas non are reported for Tb^{3+} [74].
The optical transitions of Eu^{3+} and Tb^{3+} are described in Table 2.1 [28, 30].

2.3.1.5 Spectral intensities of f-f transitions

Spectral intensities of magnetic and induced electric dipole transitions can be calculated. An exact calculation is possible for magnetic dipole transitions, as suitable wavefunctions can be obtained from diagonalization of the energy matrix. Although there are few of those transitions

Table 2.1: Major characteristics of Eu^{3+} and Tb^{3+} optical transitions [28, 30].

Transition	Spectral region (nm)	Relative intensity	Dipolar character	Comments
Europium				
$^5D_0 \rightarrow {}^7F_0$	576-582	vw	ED	nondegenerate transition; appears as single, sharp line
$\rightarrow {}^7F_1$	585-600	s	MD	sharp and structured under high resolution; strong optical activity
$\rightarrow {}^7F_2$	600-635	s - vs	ED	hypersensitive transition
$\rightarrow {}^7F_3$	645-660	vw - w	ED	forbidden
$\rightarrow {}^7F_4$	680-710	m - s	ED	intensity and structure very sensitive to environment
$\rightarrow {}^7F_5$	740-770	vw	ED	forbidden, seldom ovserved
$\rightarrow {}^7F_6$	810-840	vw	ED	seldom ovserved
$^5D_1 \rightarrow {}^7F_0$	524-528	vw	MD	
$\rightarrow {}^7F_1$	530-540	vw	ED	intensity sensitive to environment
$\rightarrow {}^7F_2$	550-565	vw	ED	
Terbium				
$^5D_4 \rightarrow {}^7F_6$	480-505	m - s	ED	intensity shows moderate sensitivity to environment
$\rightarrow {}^7F_5$	540-560	s - vs	MD	strong optical activity, best probe transition
$\rightarrow {}^7F_4$	575-600	m - s	ED	intensity sensitive to environment
$\rightarrow {}^7F_3$	610-630	w - m	MD	strong optical activity, structured under high resolution
$\rightarrow {}^7F_2$	640-655	w	ED	sensitive to environment
$\rightarrow {}^7F_1$	660-670	vw	ED	
$\rightarrow {}^7F_0$	675-680	vw	ED	

ED: electric dipole; MD: magnetic dipole; vw: very weak; w: weak; m: medium; s: strong; vs: very strong

in lanthanide ions, they are very useful because their intensity is almost independent of the ligand environment. Thus they can be used as very good intensity standards.
Induced electric dipole transitions occur much more frequently in Ln ions but the disadvantage for an exact intensity calculation is that they only become allowed due to admixture of electronic states with opposite parity into the $4f^n$ configuration. Judd and Ofelt independently developed a theory for calculating induced electric dipole matrix elements. This so called Judd-Ofelt theory is used for intensity calculations with a practical parametrization in terms of Ω_λ parameters (Judd-Ofelt parameters). This work only deals with a general treatment of the f-f transition intensities. A detailed description for both magnetic and induced electric dipole transitions can be found in Reference [56].
The oscillator strength f (P is often also used) is a measure of the strength of a transition and describes the ratio of the actual intensity to the intensity radiated by one electron oscillating harmonically in three dimensions [78]. For a harmonic oscillator in three dimensions this means that $f = 1$. The oscillator strength for allowed electronic transitions is close to unity whereas $f \ll 1$ for forbidden (induced) transitions. The optical transitions of Ln ions have

oscillator strengths around $f = 10^{-6}$, and the extinction coefficient is usually close to $\varepsilon_{max} = 1\ \mathrm{M^{-1}cm^{-1}}$ except for hypersensitive transitions. The strongest $4f \leftrightarrow 4f$ transition known is the hypersensitive transition $^5G_{5/2} \longleftarrow\!\!\!- {}^4I_{1/2}$ of NdI_3 vapor with $\varepsilon_{max} = 345\ \mathrm{M^{-1}cm^{-1}}$ and $f = 5.35 \cdot 10^{-4}$ [79].
The transition of an electron in the state j, with the wavefunction ψ_j, to a state of higher energy k (wavefunction ψ_k) via the transition dipole operator $\hat{O}$ is described by the transition dipole moment $\hat{M}_{jk}$ or the dipole strength D_{jk}. Electric and magnetic dipole transitions can be regarded separately using an electric dipole moment operator $\hat{O}_{ED}$ and a magnetic dipole moment operator $\hat{O}_{MD}$ (electric quadrupole transitions are not considered).

$$D_{jk} = \hat{M}_{jk}^2 = e^2 \,|\, <\psi_j \,|\, \hat{O} \,|\, \psi_k> \,|^2 = e^2 \,|\, <\psi_j \,|\, \hat{O}_{ED} \,|\, \psi_k> \,|^2 + e^2 \,|\, <\psi_j \,|\, \hat{O}_{MD} \,|\, \psi_k> \,|^2 \quad (2.20)$$

The oscillator strength f is connected to the dipole strength and the experimental obtainable molar extinction coefficient via

$$f_{jk} = \frac{8\,\pi^2\, m_e\, \bar{\nu}}{3\, g_j\, e^2\, h}\, D_{jk} \quad (2.21)$$

$$= a\, F \int \varepsilon(\bar{\nu})\, d\bar{\nu} \quad (2.22)$$

with

$$F = \frac{9\, n_r}{(n_r^2 + 2)^2} \quad (2.23)$$

$D_{jk} = \sum_{n=1}^{g_j} \sum_{m=1}^{g_k} D_{nm}$ where g_j and g_k are the degeneracies of states j and k
$\bar{\nu}$: wavenumber of the transition (in $\mathrm{cm^{-1}}$)
a: proportionality factor ($4.32 \cdot 10^{-9}\ \mathrm{mol\,cm^{-1}}$)
F: solvent dependent correction factor
$\varepsilon(\bar{\nu})$: extinction coefficient (in $\mathrm{cm^2\,mol^{-1}}$)
n_r: index of refraction

The Einstein coefficients (in $\mathrm{s^{-1}}$) B_{jk} and A_{kj} are the rate constants for absorption and emission, respectively. They describe the probability of photon absorption or emission with the energy $h\nu$ due to electron transition from j to k or vice versa.

$$B_{jk} = \frac{1}{g_j} \frac{2\,\pi^2\, D_{jk}}{3\,\varepsilon_0\, h^2} \quad (2.24)$$

and

$$A_{kj} = \frac{1}{g_k} \frac{16\,\pi^3\,\nu^3\, n_r^3\, D_{jk}}{3\,\varepsilon_0\, c^3\, h} \quad (2.25)$$

Regarding the degeneracy of states g_j and g_k (e.g. $2J + 1$ for the ligand-field splitting in Ln ions), the relative intensities of all emission lines originating from a given excited state can be predicted with the radiative branching ratio

$$\beta = \frac{A_{kj}}{\sum_{j=1}^{2J+1} A_{kj}} \quad (2.26)$$

Experimental branching ratios can be found from the relative areas of the emission lines. The speed of depopulating an initial level can be calculated with the emission probabilities and is called radiative (or intrinsic) lifetime τ_R.

$$\tau_R = \frac{1}{\sum_j A_{kj}} \tag{2.27}$$

Quantum yield Φ is a measure of the number of photons emitted per excited ion and can be calculated with the measured luminescence decay time τ_M

$$\Phi = \frac{\tau_M}{\tau_R} \tag{2.28}$$

The effective linewidth $\Delta\lambda$ is given by

$$\Delta\lambda = \int \frac{I(\lambda)}{I_{max}}\, d\lambda \tag{2.29}$$

where $I(\lambda)$ is the intensity at the wavelength λ and I_{max} is the maximum intensity of the emission band.
Since the Judd-Ofelt intensity parameters Ω_λ have been determined for all lanthanide ions in dilute acid solution, the radiative lifetimes can be calculated. They are $\tau_R = 9.67$ ms for the $^5D_0$ excited state of Eu^{3+} and $\tau_R = 9.02$ ms for the $^5D_4$ excited state of Tb^{3+} [53].

2.3.2 Lanthanide ion complexing ligands

As already mentioned above, lanthanide ions possess very weak extinction coefficients due to the intraconfigurational f-f transitions. Thus, a direct excitation of the ion leads to very inefficient luminescent probes. The problem of insufficient absorption can be overcome by indirect excitation via organic ligands coordinated to the Ln ion. This concept was first reported by Weissman in 1942 [80] and is generally known as sensitization or antenna effect. In these compounds, the ligand absorbs light leading to an excited singlet state followed by intersystem crossing (ISC) to a ligand triplet state, where an energy transfer to the Ln ion occurs. This was first demonstrated by Crosby et al. in 1961 [81]. The basic principle of the antenna effect for Tb^{3+} as the central ion is shown in Figure 2.7.
Efficient organic ligands working as antennas for the Ln ion can exhibit extinction coefficients of approximately 30000 $M^{-1}cm^{-1}$, which is four orders of magnitude higher than the extinction of the aqueous Eu^{3+} ($\varepsilon_{max} \approx 3$ $M^{-1}cm^{-1}$ at 393 nm [82]). The light harvesting groups in Ln ion complexing ligands are usually of β-ketone, salicylate or pyridine structure [83].
Several requirements have to be fulfilled for an efficient antenna complex. First, it should possess a long-lived ligand-centered (LC) triplet state as the energy level from which the energy transfer to the metal-centered (MC) state takes place (T_1 to $^5D_4$ in Figure 2.7). In order to generate a high triplet population, ISC from the excited singlet to the triplet state should be efficient. If a ligand to metal charge transfer (LMCT) state [84] lies between the singlet and triplet energy, the singlet state can be deactivated directly via the LMCT state without populating the triplet state. Another crucial point is the energy difference between the LC triplet state and the MC energy accepting levels. If this energy difference is too high, a transfer to the lanthanide ion is inefficient or does not happen at all. If it is too small (below 1850 cm^{-1} [85]), the energy transfer is very efficient as is the backtransfer (k_B in Figure 2.7), which leads to a

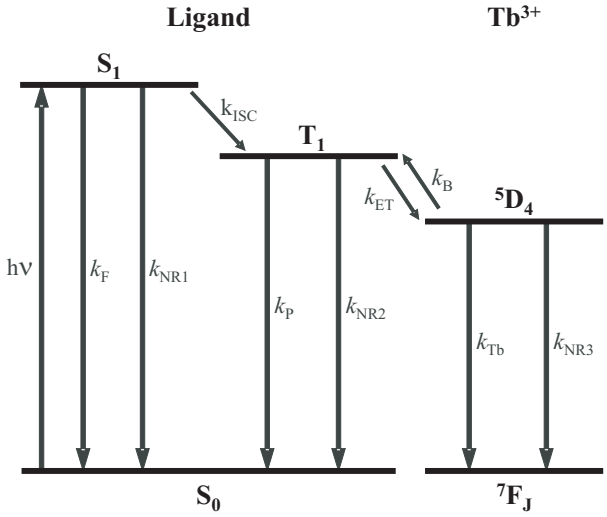

Figure 2.7: *Energy diagram and energy transfer rates k of the basic antenna effect. S_0, ligand singlet ground state; S_1, ligand excited singlet state; T_1, ligand excited triplet state; $^5D_4$, Tb^{3+} emitting quintett state; ^7F_J, Tb^{3+} septett J-manifold ground states; $h\nu$, absorption; F, fluorescence; NR, non-radiative; P, phosphorescence; ISC, intersystem crossing; ET, energy transfer; B, back transfer; Tb, Tb^{3+} luminescence.*

low total energy transfer to the Ln ion. Examples of all these transfer processes for the Gd^{3+}, Tb^{3+} and Eu^{3+} cryptates can be found in Reference [86].
Besides the antenna effect, Ln ion chelating ligands have to fulfill further requirements such as thermodynamic and kinetic stability, protection against water complexation and the possibility of labeling the complex to biomolecules.
Ln^{3+} ligand coordination is typically achieved by ionic bonding which leads to a strong preference of coordination by negatively charged groups like OH^-. In aqueous solution, water coordination results in an effective quenching of Eu^{3+} and Tb^{3+} luminescence (less than for Eu^{3+} due to the higher energy of the emitting state) via O-H vibrations and their overtones. The number of coordinated water molecules can be estimated (accuracy $\sim \pm 0.5$) with the luminescence decay times of the Ln ion in H_2O and D_2O using the Horrocks equation [87]:

$$A = C(\tau_{H_2O}^{-1} - \tau_{D_2O}^{-1}) \tag{2.30}$$

A is the number of coordinated water molecules and C is a constant which is 1.05 ms for Eu^{3+} and 4.2 ms for Tb^{3+}. The ability of the ligand to inhibit water binding in the first coordination sphere of the Ln ion is therefore of great importance in order to avoid luminescence quenching.
An important requirement for a Ln complex is efficient and easily performed coupling to biomolecules (e.g. antibodies, proteins). For this purpose, the ligands contain functional N-hydroxysuccinimide (NHS) ester, sulfo-NHS ester, maleimide, isothiocyanato, chloro-sulfonyl or amino groups. The activated complexes can then be coupled to an amino, carboxy or thiol (for maleimide activated complexes) group of the biomolecule.
To summarize, the important biological, chemical and photophysical properties of lanthanide complexes are stability in biological aqueous media, the possibility of biomolecular labeling, protection of the Ln ion against quenching by proper coordination, long luminescence decay times, strong ligand absorption with efficient energy transfer to the Ln ion, large Stokes shift and line-shaped emission spectra in a region where many dyes display excellent absorption. The properties that make Ln complexes especially interesting for use as energy donors in FRET are

strong absorption (efficient energy collection for the FRET system), long luminescence decay times (highly sensitive time-resolved measurement, discrimination between donor and acceptor emission, long-lived energy state from where the transfer to the acceptor takes place) and the emission in a wavelength region where many fluorescence dyes absorb (good spectral overlap - $J(\lambda)$ in Equations 2.3 and 2.5). Another important factor for FRET is the luminescence quantum yield of the donor (Φ_D in Equation 2.3), which is quite high for some terbium and europium complexes [35, 88]. For Ln complexes, the overall probability that the Ln ion emits a photon after photon absorption by the ligand is

$$\Phi_{tot} = \Phi_{Ln} \cdot \Phi_{trans} \tag{2.31}$$

with the Ln ion quantum yield Φ_{Ln} and the transfer efficiency from ligand to ion Φ_{trans} [88]. As the donor for FRET is the lanthanide ion itself, only Φ_{Ln} has to be taken into account for Φ_D. Φ_{trans} is relevant for the total brightness of the sample, which has no effect on FRET efficiency, but on the signal intensity. Hence, it can influence the sensitivity of a FRET immunoassay (signal to background).
Very high values for $J(\lambda)$ and extremely large Förster radii (~ 100 Å) are reported for FRET systems using lanthanide complexes as energy donors [24].

2.3.3 Biochemical applications of lanthanide complexes

Due to their special photophysical and biological properties, lanthanide complexes are widely used in biochemical applications. Their long luminescence decay times allow for efficient discrimination of short-lived background signals such as autofluorescence of biological materials or optical components (filters etc.). There are several luminescent lanthanide complexes which have been used in various bioanalytical methods, among which are homogeneous and heterogeneous immunoassays in medical and clinical diagnostics, drugscreening, photodynamic therapy, protein-protein interactions, DNA hybridization, study of ion channels in living cells, structure analysis of biomolecules (spectroscopic ruler), characterization of individual binding sites and bioimaging. Many books and reviews have been published over the last 30 years [24, 28, 29, 83, 89–97].
This work is focused on time-resolved fluoroimmunoassays (TRFIA), a widely commercially used application for in vitro diagnostics (IVD). A well known example for a heterogeneous TRFIA is DELFIA (dissociation enhanced lanthanide fluoroimmunoassay), which was scientifically developed in the 1970s by Soini and Hemmilä [95] and patented in 1982 by Wallac (now part of Perkin Elmer) [98]. DELFIA consists of two steps. First, the Ln ion is chelated by a labeling reagent (e.g. derivates of diethylene triamine pentaacetic acid - DTPA) for kinetic stability and biological labeling. The second step enables sensitization by luminescence enhancing ligands (e.g. β-diketonates). Another example is CYBERFLUOR, in which 4,7-bis(chlorosulfonylphenyl)-1,10-phenanthroline-2,9-dicarboxylic acid (BCPDA) is used as the chelator and antenna at the same time [99, 100]. These and other methods were extensively reviewed in References [101] and [83]. For commercial methods, homogeneous measuring techniques are much more interesting than heterogeneous ones, as no time-consuming washing and separation steps are required. Several stable luminescent lanthanide complexes have been synthesized in order to fulfill all the necessary requirements of coordinating and protecting the Ln ion, efficient sensitization, stability, biolabeling and biocompatibility [24, 28–30, 82, 83, 94, 97, 101–103].
In lanthanide complexes used for biochemical applications, derivates composed of one to four

conjugated pydirines are the most commonly used antenna groups. Most of these complexes can be efficiently used as FRET donors in biochemical measurements. Figure 2.8 shows four representative pyridine based lanthanide complexes. Two of them are used in successfully commercialized systems. Europium tris(bipyridine) (Eu-TBP) [38] (Figure 2.8a) is used in the KRYPTOR immunoreader system (Cezanne, Nîmes, France). This method was commercialized by CIS bio and is used under the trade names TRACE (time-resolved amplified cryptate emission) and HTRF (homogeneous time-resolved fluorescence) [104]. Ln^{3+} chelates of dichlorotriazinyl (DTA) activated phenylethynylpyridine tetra acetate [105] (Figure 2.8b) are used in the LANCE (lanthanide chelate excitation) technology of Perkin Elmer [106]. The terpyridine-bis(methylenamine) tetraacetic acid (TMT) chelate of europium [107] is commercially available as isothiocyanate (Figure 2.8c) from Amersham Biosciences. The sulfo-NHS activated LnL complex [35] (Figure 2.8d), where ligand L is based on a glutamate skeleton N-functionalized with two anionic bipyridyl chromophoric units, is a non-commercial Ln complex which has been successfully used as the FRET donor with quantum dots as the acceptor in a biological immunoassay [36, 37, 108]. Detailed results of these FRET systems can be found in Chapter 3.

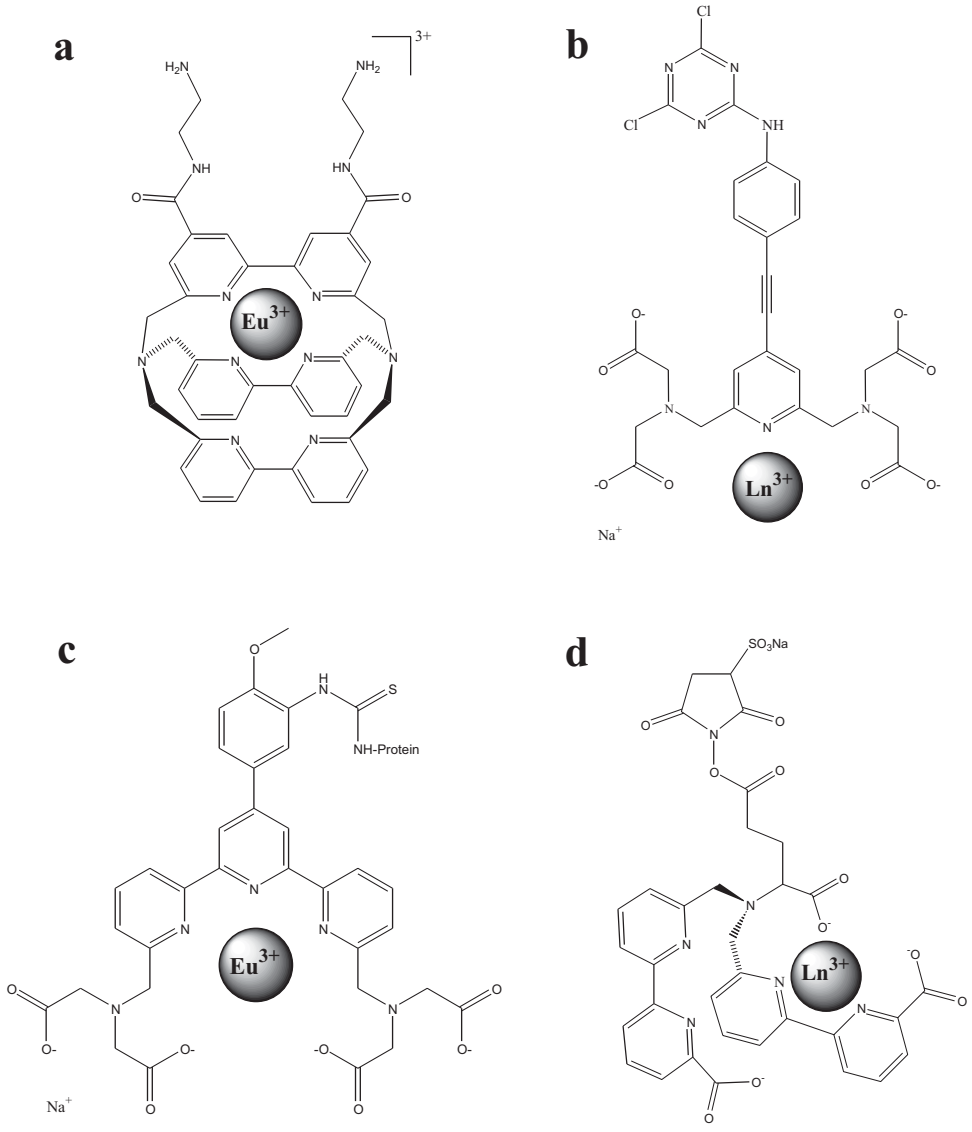

Figure 2.8: *Representative Ln^{3+} complexes for use in FRET immunoassays (description see text).*

2.4 Quantum dot semiconductor nanocrystals

2.4.1 Introduction

The scientific field of semiconductor quantum dots (also called nanocrystals) is much younger than the one of lanthanides. Although properties of quasi-zero-dimensional structures were studied much earlier for small metal particles [109, 110], the size-dependent properties of quantum dots (QD) due to quantum confinement effects were first investigated in the early 1980s by Ekimov et al. [31], Éfros and Éfros [32] and Rossetti et al. [33]. Some of the important original papers about fundamental aspects of QD have been recently gathered in a SPIE Milestone Series (Volume MS 180) [111], and comprehensive books [112–114] as well as many reviews [115–120] can be found about this topic.
For a better understanding of the special photophysical properties of QD, basic theoretical principles of semiconductor crystals and quantum confinement will be addressed (detailed descriptions can be found in textbooks about quantum mechanics [78, 121]). As this work is focused on the spectroscopic properties of QD in biological systems, synthesis is only briefly mentioned, whereas special attention is payed to biochemical applications. Biocompatible QD typically consist of an emitting semiconductor core, a passivating semiconductor shell and a biocompatible coating for labeling biomolecules to the surface. The different functions of the quantum dots will therefore be explained in the order from inside to outside.

2.4.2 The quasiparticle approach in semiconductor crystals

In many-body systems (e.g. a large number of interacting positive nuclei and negative electrons), the consideration of many interacting particles is replaced by a few non-interacting quasiparticles, which are described as elementary excitations of the system. In a semiconductor crystal, this elementary excitation in the conduction band is an electron with negative charge, whereas the quasiparticle in the valence band is a hole with positive charge. The ground state of such a crystal would be the vacuum state with neither the electron in the conduction band nor the hole in the valence band. The first excited state can be seen as the creation of an electron-hole pair by the promotion of an electron to the conduction band as a result of e.g. photon absorption. In the reverse way, a photon can be created by annihilation of the electron-hole pair.
When the electron and hole interact via a Coulomb potential, they generate another quasiparticle, the exciton, which can be well compared to the hydrogen atom. In the hydrogen atom Hamiltonian, the electron mass (m_e) is replaced by the effective mass of the electron (m_e^*), the proton mass (m_p) with the effective mass of the hole (m_h^*) and the dielectric constant of the crystal (ε) is added. This leads to the exciton Hamiltonian

$$H = -\frac{\hbar^2}{2m_e^*}\nabla_e^2 - \frac{\hbar^2}{2m_h^*}\nabla_h^2 - \frac{e^2}{4\,\pi\,\varepsilon_0\,\varepsilon\,r_{eh}} \tag{2.32}$$

where r_{eh} is the distance between electron and hole. The exciton Bohr radius is

$$a_B^{ex} = \frac{4\,\pi\,\varepsilon_0\,\varepsilon\,\hbar^2}{\mu\,e^2} = \varepsilon\frac{m_e}{\mu}\,\cdot\,0.53\ \text{Å} \tag{2.33}$$

with the hydrogen Bohr radius of 0.53 Å and where μ is the electron-hole reduced mass

$$\mu^{-1} = (m_e^*)^{-1} + (m_h^*)^{-1} \tag{2.34}$$

The exciton Rydberg energy is

$$E_R^{ex} = \frac{e^2}{8\,\pi\,\varepsilon_0\,\varepsilon\,a_B^{ex}} = \frac{\mu\,e^4}{32\,\pi^2\,\varepsilon_0^2\,\varepsilon^2\,\hbar^2} = \frac{\mu}{m_e\,\varepsilon^2}\;\cdot\;13.6\text{ eV} \tag{2.35}$$

with the hydrogen Rydberg energy equal to 13.6 eV. As the reduced electron-hole mass is smaller than the electron mass, and the dielectric constant of the crystal ε is much larger than that of the vacuum, the Bohr radius is significantly larger (10 - 100 Å) and the Rydberg energy significantly smaller (1 - 100 meV) than the hydrogen atom values. For CdSe with $m_e^* = 0.13\,m_e$, $m_h^* = 0.45\,m_e$ and $\varepsilon \approx 9$, a Bohr radius of 49 Å and a Rydberg energy of 16 meV are obtained [113].
The band structures of semiconductors are normally displayed as dispersion curves where parabolic energy states are shown over the wavevector and the effective mass gives the curvature. The difference between the energy maximum of the valence band (E_v) and the minimum of the conduction band (E_c) is called band gap energy $E_g = E_c - E_v$ and corresponds to the minimum energy necessary for creating a pair of free charge carriers (hole and electron). The complete dispersion curve for a crystal can be complicated with several minima and maxima as the effective mass cannot be considered as constant. However, in the most important cases, events in the close vicinity of E_c and E_v are considered and are therefore described by the approximation of a constant effective mass. The exciton dispersion function can be expressed as

$$E_n(\boldsymbol{K}) = E_g - \frac{E_R^{ex}}{n^2} + \frac{\hbar^2\boldsymbol{K}^2}{2M} \tag{2.36}$$

where n is the principle quantum number, $M = m_e^* + m_h^*$ and $\boldsymbol{K}$ is the exciton wavevector. Exciton creation by photon absorption leads to a discrete set of energies

$$E_n = E_g - \frac{E_R^{ex}}{n^2} \tag{2.37}$$

Figure 2.9 shows a partial bandstructure diagram of a direct-gap semiconductor in close vicinity of E_c and E_v, where the dispersion curves of electron (conduction band), hole (valence band) and exciton are displayed.

For a given temperature T, the concentrations of excitons n_{ex} and of free electrons and holes $n_e = n_h$ are related via the Saha equation:

$$n_{ex} = n_e^2\left(\frac{2\,\pi\,\hbar^2}{\mu\,k\,T}\right)^{3/2} exp\left[\frac{E_R^{ex}}{k\,T}\right] \tag{2.38}$$

Only when $k\,T \leq E_R^{ex}$, a significant number of excitons exists, whereas they are ionized when $k\,T \gg E_R^{ex}$ and free holes and electrons play the major role. The absorption spectrum of a direct-gap semiconductor monocrystal consists of a distinct exciton peak at $h\nu = E_g - E_R^{ex}$, some smaller peaks at E_n (for $n > 1$) and a broad continuum for absorption energies higher than the bandgap energy.

2.4.3 Quantum confinement

For many semiconductors, the exciton Bohr radius a_B^{ex} is significantly larger than the lattice constant of the crystal. Thus, it is possible to create nanocrystals smaller than a_B^{ex} but larger

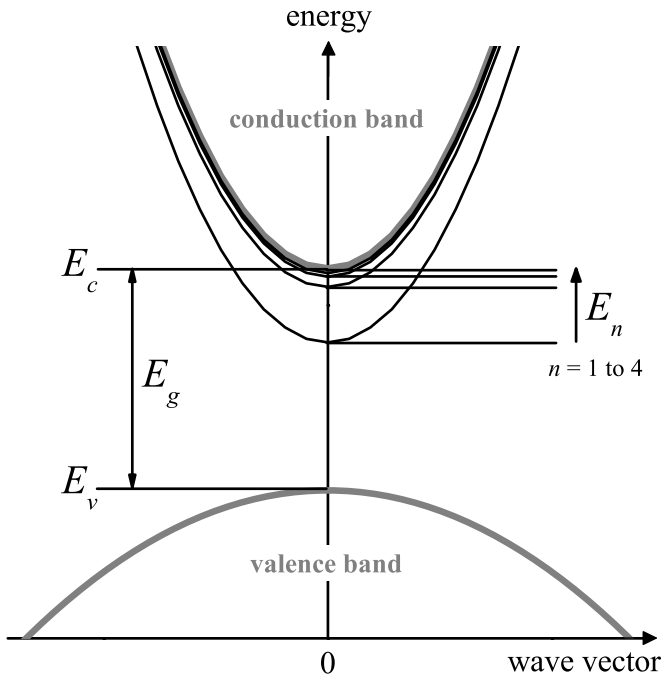

Figure 2.9: *Dispersion curves of the electron (with conduction band above) and hole (with valence band below) depicted in grey as well as exciton dispersion curves with $n = 1$ to 4 in black.*

than the lattice constant, which leads to quantum confinement (finite motion) along the confinement axis and infinite motion in the other directions. If the restriction of motion is one-, two-, or three-dimensional, the crystal structure is called quantum well (quasi two-dimensional system), quantum wire (quasi one-dimensional system) or quantum dot (quasi zero-dimensional system). Going from a bulk semiconductor crystal to a QD, the density of electron states changes from a steady square root function to a set of δ-functions (discrete energies). In 1980 it was experimentally discovered by Ekimov et al. [31] that a size quantization in a semiconductor sphere leads to a wavelength shift with the sphere radius, and Éfros and Éfros proposed a theoretical explanation for this phenomenon in 1982 [32]. In order to explain the physical properties of quantum confinement in QD, the effective masses of the quasiparticles (electrons, holes, excitons) are considered to be the same as in an ideal infinite crystal (effective mass approximation), and the finite size of the QD (regarded as a sphere) is implied as an infinetely high potential wall surrounding the crystal. There are three cases, which have to be examined. The first one is when the sphere radius a is smaller than the Bohr radius of the electron a_B^e and the hole a_B^h ($a \ll a_B^e$ and $a \ll a_B^h$). The second case is $a_B^h \ll a \ll a_B^e$, leading to the same mathematical result in a first approximation, and means that the size quantization is determined by only the electron mass. These two cases are called strong confinement, whereas weak confinement occurs for $a_B^e \ll a$ and $a_B^h \ll a$.
Regarding the dispersion law of an exciton in a crystal (Equation 2.36), the kinetic energy of a free exciton has to be replaced by a solution derived for a particle in a spherical box. The exciton in the weak confinement is characterized by the principle quantum number n, describing internal exciton states that arise from the Coulomb electron-hole interaction, and by the two additional numbers l and m (orbital angular quantum number l and magnetic angular quantum number m), describing the states connected with the center-of-mass motion in the presence of

an external potential barrier. Taking the roots of the spherical Bessel functions χ_{ml} (tabulated in [122], m is the number of the root and l is the order of the function) the exciton energy spectrum is then

$$E_{nml} = E_g - \frac{E_R^{ex}}{n^2} + \frac{\hbar^2 \chi_{ml}^2}{2\,M\,a^2} \tag{2.39}$$

This results in the lowest exciton energy state of

$$E_{110} = E_g - E_R^{ex} + \frac{\hbar^2 \pi^2}{2\,M\,a^2} \tag{2.40}$$

Using Equations 2.33 and 2.35, this can be written as

$$E_{110} = E_g - E_R^{ex} + \frac{\mu}{M}\left(\frac{\pi\, a_B^{ex}}{a}\right)^2 E_R^{ex} \tag{2.41}$$

resulting in a positive energy shift of

$$\Delta E_{110} = \frac{\mu}{M}\left(\frac{\pi\, a_B^{ex}}{a}\right)^2 E_R^{ex} \tag{2.42}$$

whereas the bandgap energy is shifted by

$$\Delta E_g = \left(\frac{\pi\, a_B^{ex}}{a}\right)^2 E_R^{ex} \tag{2.43}$$

Both shifts are small regarding the initial conditions of $a_B^e \ll a$ and $a_B^h \ll a$.
For both cases of strong confinement, Éfros and Éfros found that in a first approximation the optical shift is determined by only the electron size quantization and therefore both cases can be treated equally ($a \ll a_B^{ex}$). As the crystal size in this case is much smaller than the Bohr radius, the electron and hole are assumed to be in the unbound state. Considering that the electron and hole confinement are of the order of $\frac{\hbar^2}{m_e^* a^2}$ and $\frac{\hbar^2}{m_h^* a^2}$ respectively, and the Coulomb interaction between the electron and hole is $\sim \frac{e^2}{\varepsilon\, a}$, the latter can be ignored for $a \ll a_B^{ex}$. Selection rules allow optical transitions that couple electron and hole states with the same principle and orbital quantum number which results in an absorption spectrum with discrete bands:

$$E_{nl} = E_g + \frac{\hbar^2 \chi_{nl}^2}{2\,\mu\,a^2} \tag{2.44}$$

Brus [123] included the Coulomb interaction, which is not negligible for a approaching a_B^{ex}. He proposed an energy of the lowest electronic transition of

$$E_{10} = E_g + \frac{\hbar^2 \pi^2}{2\,\mu\,a^2} - 1.8\,\frac{e^2}{4\,\pi\,\varepsilon_0\,\varepsilon\,a} \tag{2.45}$$

or

$$E_{10} = E_g + \pi^2\left(\frac{a_B^{ex}}{a}\right)^2 E_R^{ex} - 1.786\,\frac{a_B^{ex}}{a} E_R^{ex} - 0.248\,E_R^{ex} \tag{2.46}$$

including some further corrections [124–126]. Figure 2.10 displays the size dependence of the lowest electronic transition energy. The graph shows the strong impact of quantum confinement for high ratios of $\frac{a_B^{ex}}{a}$ ($a \ll a_B^{ex}$).

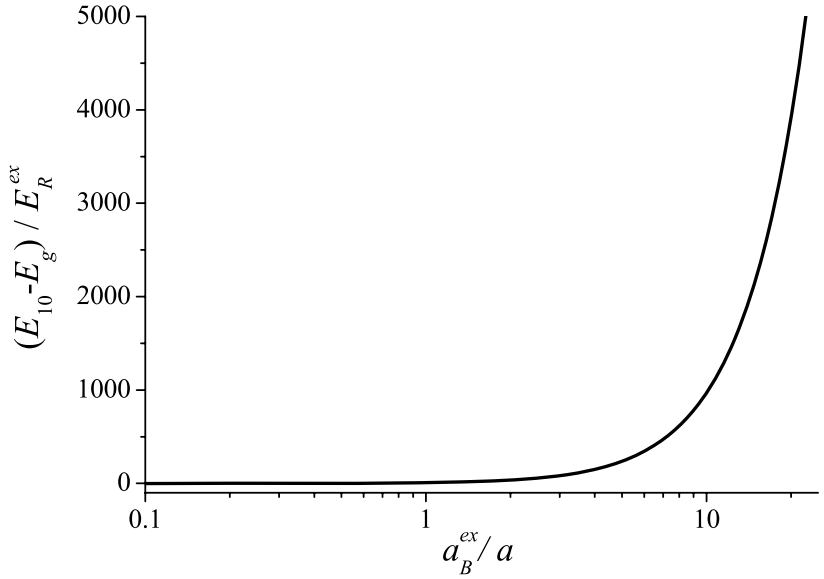

Figure 2.10: *Size dependence of the lowest electronic transition state of an ideal spherical QD. Equation 2.46 is changed in order to receive a dimensionless energy over a dimensionless ratio of Bohr radius to QD radius.*

It has to be mentioned that these calculations are applicable for ideal spherical QD with infinite potential barrier at the nanocrystal surface. Finite barriers, surface polarization effects due to a different dielectric constant of the surrounding medium, heavy and light hole effects, hole effective mass differences for different crystal directions and spin-orbit interactions are not considered here, but the theoretical treatment can be found in Reference [113]. Nevertheless, the effect of quantum confinement is the same and the effective mass approximation gives a good description of crystal size dependency of QD electronic properties due to three dimensional confinement of quasi-particles.
Absolute values of the absorption onset energy over crystal radius (calculated with Equation 2.46 for $a < 2a_B^{ex}$ and with Equation 2.41 for $a \geq 2a_B^{ex}$) for different materials are presented in Figure 2.11. Here the lowest radius was chosen to be 2 nm (QD contains less than 1000 atoms) because the approximations mentioned above still give good results for $a > 2$ nm. Lower values can be treated with an energy dependent effective mass approach.

Methods for fabricating QD can be found in the literature. Besides the text books [112–114], there are several articles about QD preparation [111, 117, 120, 127, 128]. Basically, two methods exist. The more chemical approach uses synthetic preparation where atomic or ionic precursor materials react in solution in order to yield colloidal QD. The other approach relies on solid state physics or engineering. Here QD are made from semiconductor substrates by lithography or electrochemical methods. Both approaches can also be combined.

2.4.4 Core/shell semiconductor QD

Nanocrystals provide a high surface-to-volume ratio resulting in a significant effect of the surface properties on the optical properties of the QD. Therefore, QD surfaces are capped by organic layers such as TOP (tri-*n*-octylphosphine) or TOPO (tri-*n*-octylphosphine oxide), which passivate the surface and permit slow steady crystallite growth [117]. While the absorp-

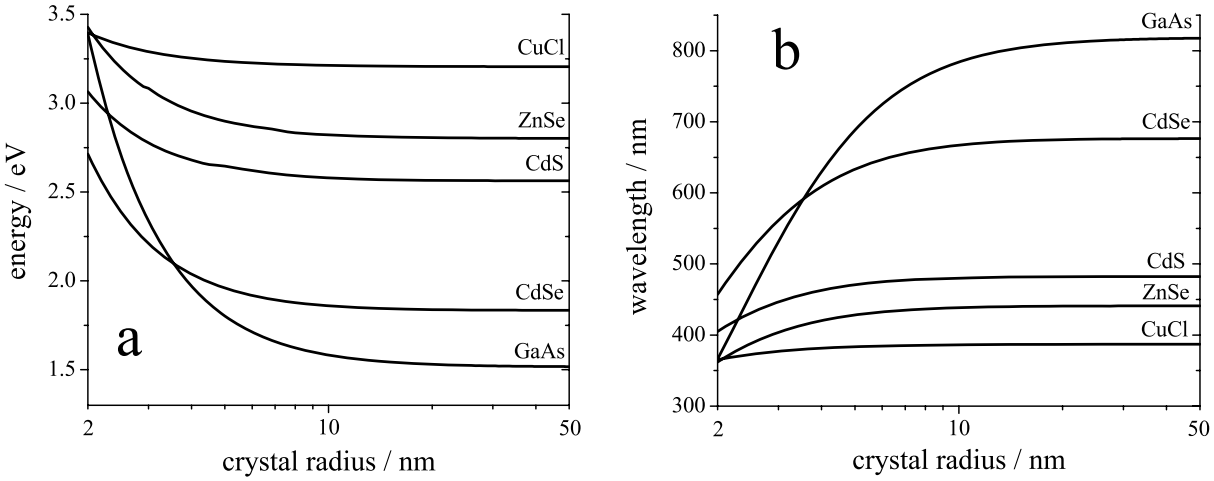

Figure 2.11: *Energy (a) and wavelength (b) absorption onset over crystal radius for some representative semiconductor materials. Strong quantum confinement becomes obvious at small crystal radii. Bohr radii taken from Reference [113] are* 0.7 *nm for CuCl,* 3.8 *nm for ZnSe,* 2.8 *nm for CdS,* 4.9 *nm for CdSe and* 12.5 *nm for GaAs.*

tion characteristics are only mildly influenced, the emission efficiency, spectrum and kinetics are very strongly affected by the capped surfaces. This passivation of gap surface states, arising from surface nonstoichiometry, unsaturated bonds, etc., is the key to highly luminescent QD [128]. Although organically capped QD have already quantum yields around 10 % at room temperature reaching 90 % at 10 K [117, 129], further improvement of luminescence properties and stability is possible.

Capping a size-tunable lower bandgap core nanocrystal with a higher bandgap shell is an attractive possibility to enhance luminescence and stability of the QD. This concept has been successfully realized, e.g. with ZnS capped CdSe core nanocrystals [127, 128, 130, 131]. The reason for using a shell around the core QD is the high surface to volume ratio of the nanocrystal. At a semiconductor surface, bonds and atomic sites reorder to achieve a minimum energy structure (surface reconstruction). This process leads to a different and quite complex lattice structure at the surface, which is influenced by the crystal growth conditions and the surface surrounding medium. Particularly important are defects due to incorporation of atoms different from the semiconductor materials, lattice vacancies or surface adsorbates. They can lead to so called trap states for interacting electrons and holes within the bandgap, resulting in a lower exciton energy. The emission from trap states is therefore red shifted and broad due to several trap states of different energy. Oxidation at the surface (e.g. CdSe QD oxidation results in selenium oxide formation) is another major drawback for QD luminescence and leads to low quantum yields [130].

Dabbousi et al. [130] have published an extensive spectroscopic study about CdSe/ZnS core/shell quantum dots, where many properties of CdSe surface passivation by ZnS layers of varying thickness are discussed and the composite QD synthesis is described. They found that a ZnS thickness of 1.3 monolayers (ca. 4 Å) gives the best results with a quantum yield of 50 %, which decreases below and above this layer thickness. Figure 2.12 shows absorption and luminescence spectra taken from this article. The influence of size-tunability and surface passivation is well demonstrated within these spectra. Also the broad and red-shifted trap state emission becomes obvious for the smallest uncoated CdSe nanocrystal, which is eliminated for the coated QD.

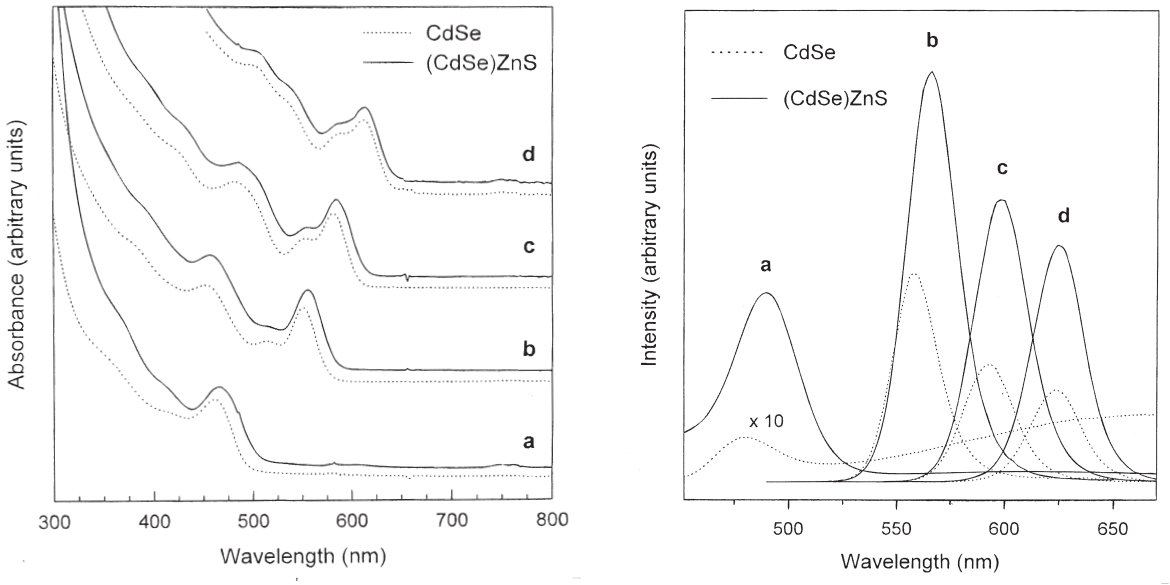

Figure 2.12: *Absorption (left) and emission (right) spectra of uncoated (dashed lines) and* 1 *to* 2 *monolayer ZnS overcoated (solid lines) CdSe QD with core sizes of (a)* 23*, (b)* 42*, (c)* 48 *and (d)* 55 *Å. Quantum yields are* 40*,* 50*,* 35 *and* 30 *%, respectively. Reprinted with permission from Reference [130]. Copyright (1997) American Chemical Society.*

Efficient core/shell QD are usually capped by organic layers, as well. They are thermodynamically stable, resistent against photobleaching, have size-tunable luminescence and absorption spectra with narrow emission bands and high quantum yield, have extremely high extinction coefficients (increasing with absorption energy) over a wide wavelength range and are therefore very well suited for highly sensitive spectroscopic methods like FRET.

2.4.5 Biocompatible QD

Besides the surface passivating shell for luminescence and stability enhancement, several methods for creating water soluble, biocompatible QD have been developed [132–136]. QD surface functionalization with polymers [137], proteins [138], peptides [139, 140] or hydrophilic molecules [127, 141–145] was performed for their use in aqueous media. Due to this progress in cytotoxicity suppression and biological surface functionalization, there are several biological applications such as cellular assays [146], in vivo imaging [147–149], DNA detection [150, 151], multiplexed bioanalysis [152–154] and other biological assays found in several reports and reviews [155–161]. In a recent review by Ron Hardman, dealing with toxicity of many different QD used in various applications [162], the author arrives at the conclusion that not all QD are alike, and toxicity depends on multiple physicochemical as well as environmental factors. Although QD are most often used in research, they are commercially available as CdSe/ZnS and CdTe/ZnS core/shell QD from Molecular Probes/Invitrogen (www.qdots.com) and Evident Technologies (www.evidenttech.com).
There are several examples of QD-based FRET in biological and other applications [34, 36, 37, 108, 132, 155, 163–177]. Most of these reports deal with the use of QD as FRET donors and there are few examples where QD are used as FRET acceptors, e.g. with other QD as donors [165], in

solid state devices [172,173], quantum wells [178], or polymer based matrices [179]. Although it was assumed that FRET to QD in solution should be possible from tryptophane to CdTe QD conjugated to bovine serum albumin (BSA) [138], a thorough study by Mattoussi et al. [34] showed that organic dyes such as Cy3 or AlexaFluor 488 were unable to generate FRET to CdSe QD. Unefficient energy transfer was related to the very fast radiative deactivation of these donors compared to the FRET process. To confirm their hypothesis, long-lived triplet emitter complexes of ruthenium were used as donors, but this approach remained inconclusive. However, in some recent publications we demonstrated that terbium and europium luminescent complexes with millisecond decay times can be excellent energy donors for FRET to QD in biological systems in solution [36, 37, 108, 174]. Another article reports about bioluminescence resonance energy transfer (BRET) to QD from a variant of *Renilla reniformis* luciferase [180]. The field of QD and their implementation in biological measurements is especially interesting as they have not thus far been used in commercial applications.

2.5 Biochemical FRET systems

In order to obtain a biochemical FRET system, one has to bring a FRET donor-acceptor couple in close proximity (around 1 to 10 nm), e.g. through a biochemical binding process. As mentioned in 2.1.3 many biomolecular processes occur within this distance. Well known systems are biotin-avidin, biotin-streptavidin and binding of antibodies to specific targets (e.g. in immunoassays).

2.5.1 Immunoassays

Immunoassays are analytical tests that use antibodies for binding a specific target. These analytes can be natural or artificial chemicals, biomolecules, cells and viruses. Antibodies have exceptional specificity for their target with a very high binding strength. These properties have made immunoassays a major diagnostic tool in medicine and life sciences. In this section only basic immunoassay principles are addressed. For a detailed description of immunoassays including many examples and applications "The Immunoassay Handbook" [96] is an excellent resource.

2.5.1.1 Heterogeneous immunoassays

There are several types of immunoassays including the immunometric design (Figure 2.13a) as one of the simplest test mechanisms. An antibody is immobilized onto a surface (e.g. a polystyrene test plate) and binds the analyte (usually called antigen) after addition of the sample. A different antibody (the so-called tracer), labeled e.g. with a luminophore, enzyme or radioactive isotope, is added and binds to another epitope of the antigen. As antibodies and antigen form a sandwich complex, immunometric assays are also called sandwich immunoassays. After a separation step where all unbound tracers are washed away, bound tracers can be measured. If an antibody is to be detected, the antigen is immobilized and the tracer will be a second antibody which is specific for the first one (Figure 2.13b). For both assays the signal is proportional to the antigen concentration (Figure 2.14).

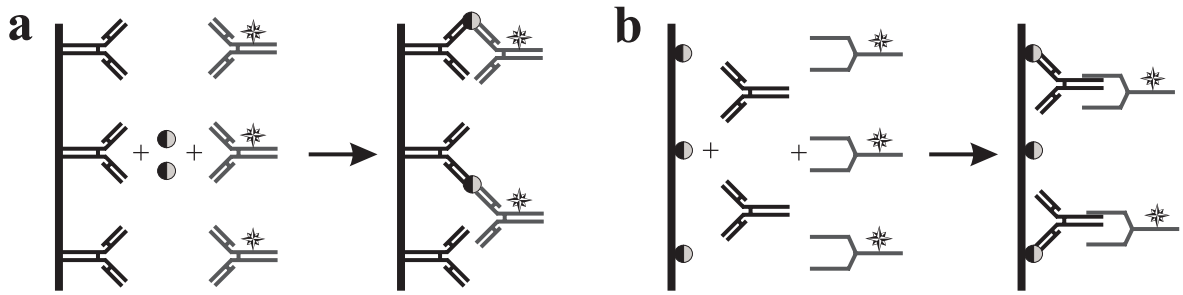

Figure 2.13: *a) Immunometric immunoassay for antigen detection: capture antibodies (black) are surface immobilized and antigens (balls) as well as tracers (grey) are added (left side). After incubation and separation (right side), the signal of the sandwich complexes, which is proportional to antigen concentration, can be measured. b) Immunometric immunoassay for antibody detection: capture antigens (balls) are surface immobilized and antibodies (black) as well as tracers (grey) are added (left side). After incubation and separation (right side), the signal of the sandwich complexes, which is proportional to antibody concentration, can be measured.*

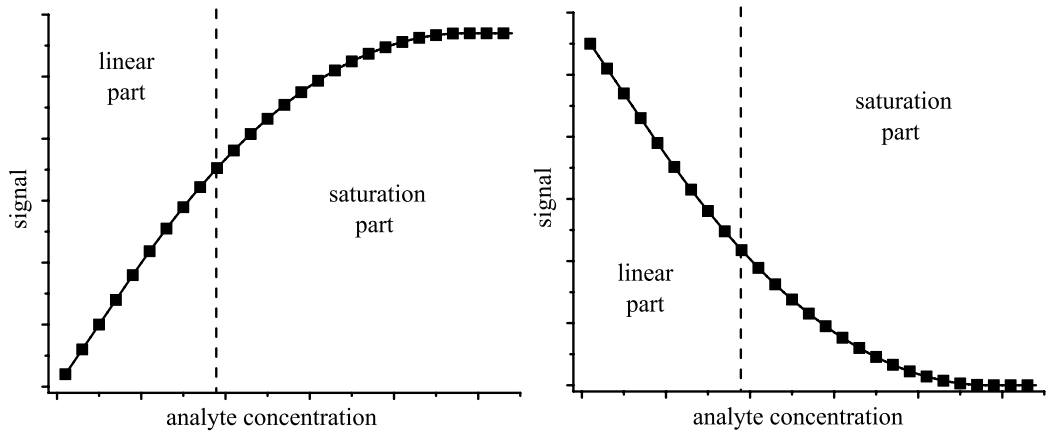

Figure 2.14: *The signal of an immunometric immunoassay (left) is proportional to the analyte (antigen or antibody) concentration. The saturation part of the graph is caused by saturation of the capture antibody/antigen or the tracer antibody by the analyte. The signal of a competitive immunoassay (right) is indirectly proportional to the analyte concentration. The saturation part of the graph is caused by saturation of the capture antibody by free analyte.*

An important immunometric immunoassay is the so-called ELISA (enzyme-linked immunosorbent assay), where the tracers are labeled with enzymes that can catalyze the reactions of a specific substrate, which is added to the assay after the separation step. Usually, these reactions generate a specific colour or luminescence signal which is again proportional to the analyte concentration. As each enzyme can activate many substrate molecules, ELISAs are very sensitive immunoassays.
Immunometric immunoassays work with large antigens because they need to possess at least two epitopes for binding the antibodies. Detection of smaller molecules (e.g. in drug screening) is performed by competitive immunoassays. Figure 2.15 shows the assay principle, where the capture antibodies are surface immobilized, and analyte and tracer are added. The tracer is the same analyte, labeled with a suitable signal generator (e.g. luminophore, enzyme, radioisotope). Both labeled and unlabeld antigens compete for the binding sites of the antibodies, leading to a signal indirectly proportional to analyte concentration (Figure 2.14).

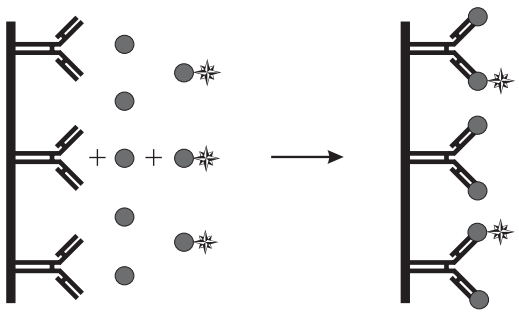

Figure 2.15: *Competitive immunoassay for small analyte detection: capture antibodies (black) are surface immobilized and antigens (balls) as well as tracer antigens (labeled balls) are added (left side). After incubation and separation (right side), the signal of the antibody-antigen complexes, which is indirectly proportional to antigen concentration, can be measured.*

All of the immunoassays mentioned so far require a separation step before measuring in order

to generate a signal which is directly or indirectly proportional to the analyte concentration. These assays are called heterogeneous assays.

2.5.1.2 Homogeneous FRET immunoassays

Immunoassays without necessary separation steps are called homogeneous assays. As the analyte specific signal is only generated when the tracer binds to the analyte, this assay format requires only the mixing of sample and immunochemical reagents, followed by detection. Another advantage is the short incubation time because the binding reaction is not limited by slow diffusion to a surface. Theoretically, homogeneous immunoassays are even more sensitive than heterogeneous ones, which are more error-prone and tend to reverse weak binding reactions. However, interference with the non-separated assay constituents often repeals the sensitivity advantage and techniques to overcome non-specific signals (e.g. autofluorescence of biological constituents, background luminescence or light scattering) have to be developed.
One of these concepts is the time-resolved FRET immunoassay using lanthanide complexes as FRET donors. This sensitive technique has been successfully applied in commercial systems (see section 2.3.3). The principle of such a homogeneous sandwich immunoassay is presented in Figure 2.16.

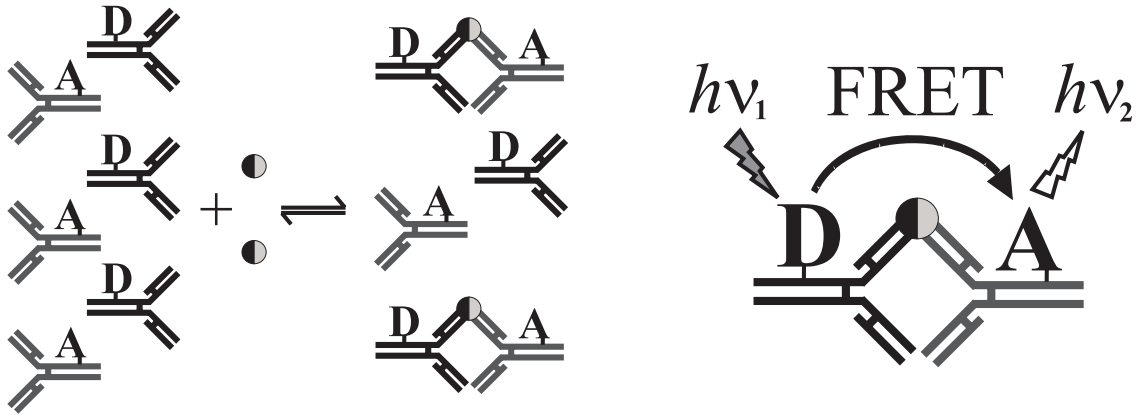

Figure 2.16: *Homogeneous sandwich FRET immunoassay. Left: two different capture antibodies are labeled with a FRET donor and acceptor, respectively, and after analyte addition, sandwich complexes are formed. Right: once the donor is excited ($h\nu_1$), FRET can occur to the acceptor when the sandwich complex is formed. The acceptor can then luminesce ($h\nu_2$) and this luminescence signal is proportional to analyte concentration.*

For elimination of spurious background signal, which occurs on the nanosecond timescale, a long luminescence lifetime component is necessary within the FRET assay. For two reasons, this is preferably the donor. If the donor luminescence lifetime is short compared to the FRET process the donor luminescence has decayed before FRET to the acceptor can happen. The second reason is that a long-lived excited state of the acceptors would be a big disadvantage in connection with a short-lived donor excited state. As the donor can be excited several times during the acceptor excited-state lifetime, the acceptor is already saturated for FRET and the donor would decay ineffectively.
As mentioned above, lanthanide complexes with long luminescence decay times can be effectively used as FRET donors in immunoassays. The FRET couple of Eu-TBP (Figure

2.8a) as donor and a crosslinked allophycocyanin (APC) as acceptor has a Förster radius of up to 90 Å [181] and is used for commercial homogeneous immunoassays in the KRYPTOR immunoreader (see also section 2.3.3). Delayed emission detection (from 50 to 450 μs) of the APC signal eliminates background and provides a proportional signal to analyte concentration. In order to ensure a correction for biological medium interferences or laser energy fluctuations, a ratiometric measurement is performed where the measurement signal is the ratio of APC emission and Eu-TBP emission. A typical signal ratio over analyte concentration graph (calibration curve) for a TPSA (total prostate specific antigen) is presented in Figure 2.17.

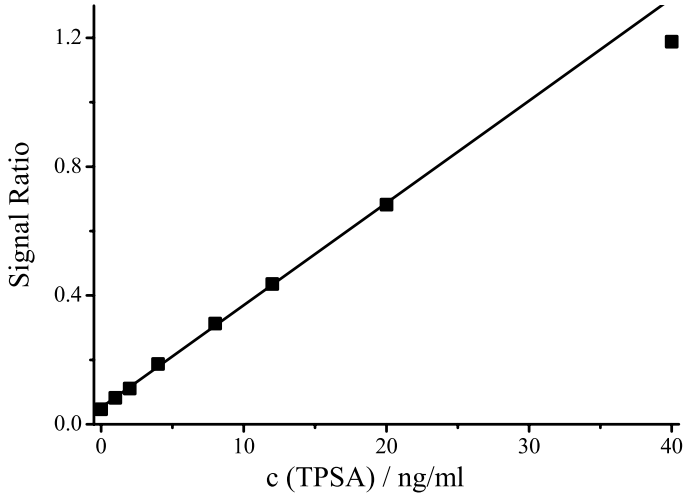

Figure 2.17: *Calibration curve for a homogeneous TPSA FRET immunoassay. The ratio of the FRET signal (from APC) and the reference signal (from Eu-TBP) is measured in a time-gate (*50 *to* 450 *μs) and plotted against TPSA concentration c(TPSA). The ratio at 40 ng/ml TPSA is in the saturation part of the curve as it lies below the linear fit (line).*

The limit of detection (LOD - the lowest concentration of an analyte that the analytical process can reliably detect [182]) is determined by the standard deviation of the blank σ_0 (blank concentration of the analyte $c_a = 0$) and the sensitivity S, which is the slope of the calibration curve.

$$S = \frac{\Delta\text{signal}}{\Delta\text{concentration}} \tag{2.47}$$

The LOD corresponding to a confidence level of 99 % is defined as

$$LOD = 3\,\frac{\sigma_0}{S} \tag{2.48}$$

Besides LOD other definitions are also used, e.g. the limit of quantitation LOQ [182](the concentration range at which the analyte concentration can be accurately quantified) which is 3 x LOD. As different sources use different interpretations of LOD, one should always check the exact definition that is used. Throughout this work the definition in Equation 2.48 is applied.

2.5.2 Biotin-(strept)avidin

The biotin-(strept)avidin system is one of the most frequently used biological binding systems in research and there are several reviews [183–186] and a volume of *Methods in Enzymology* [187] dedicated to this topic. The reason for this is the fast and strong binding between

biotin and (strept)avidin characterized by a formation constant of 10^{15} M^{-1} for avidin and 10^{13} M^{-1} for streptavidin [48,188], which is some orders of magnitude higher than for interaction of ligands with their specific antibodies [185]. Probably the most cited work on the high affinity binding of biotin to avidin is from Green, published in 1975 [189].
Avidin is a 67-kDa glycoprotein consisting of four subunits of 128 amino acids each. The protein is found in egg white whereas streptavidin is from the bacterial source *Streptomyces avidinii*. Both proteins provide four binding sites for biotin. The neutral isoelectric point and the lack of carbohydrates result in less non-specific binding for streptavidin, which makes this protein more useful for biological assays than avidin. The most frequently applied streptavidin has a molecular mass of ca. 55 kDa and is called "core" or "truncated" streptavidin as it can be converted to this lower-mass form from the native protein (with $66 - 75$ kDa).
Biotin (also known as vitamin H) is found in minute amounts in every living cell and has a molecular weight of 244.31 Da. It is well suited for bioconjugation and one of the major advantages is that biotinylation does usually not alter the properties of the biotinylated molecule.

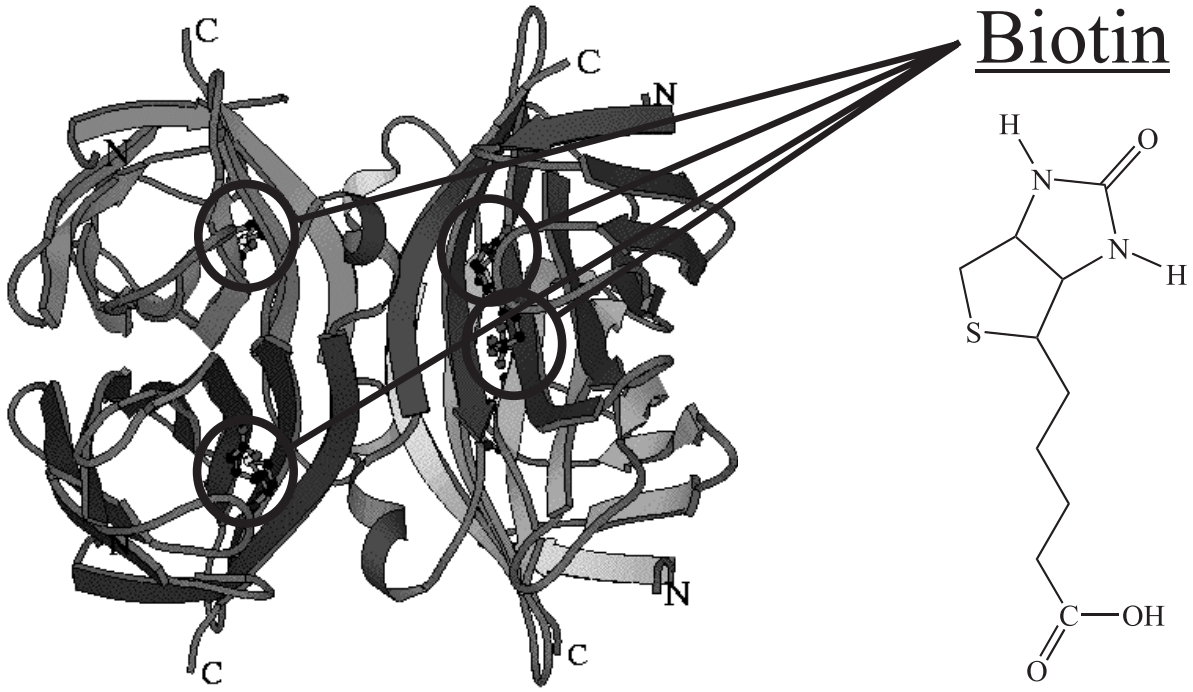

Figure 2.18: *Left (taken from [190]): each of the four streptavidin monomers binds one biotin molecule. Right: chemical structure of biotin.*

Both labeling of (strept)avidin and biotinylation of molecules is quite simple and a lot of (strept)avidin conjugates as well as biotinylated molecules [185] are already commercially available for biological applications. Nevertheless, most of the available immunoassay methods rely on direct labeling of the antibodies and antigens, and the biotin-(strept)avidin system is usually used in research applications. In this work the biotin-streptavidin system was used as a well characterized model system for biological binding in order to generate FRET systems. For this reason the theory is only briefly addressed and the reviews mentioned above should be used for detailed desriptions.

2.5.2.1 Biotin-streptavidin binding

Each monomer of the tetrameric streptavidin binds one biotin molecule (Figure 2.18). The three different binding mechanisms that have been described to be involved in the strong biotin binding of streptavidin [188, 191–194] are displayed in Figure 2.19. The side chains of mainly four tryptophans (Trp79, Trp92, Trp108 and Trp120) bind biotin via hydrophobic and van der Waals interactions. A hydrogen bonding network is the second binding mechanism, in which asparagine, serine and tyrosine (Asn23, Asn49, Ser27, Ser88 and Tyr43) bind to the oxygen atoms, serine and aspartate (Ser45 and Asp128) bind to the nitrogen atoms and threonine (Thr90) binds to the sulfur atom of biotin. The third binding mechanism is a surface loop (consisting of the residues 45 to 52) which closes for biotin binding. All three mechanisms (see Figure 2.19) are described in References [191, 193] in detail.

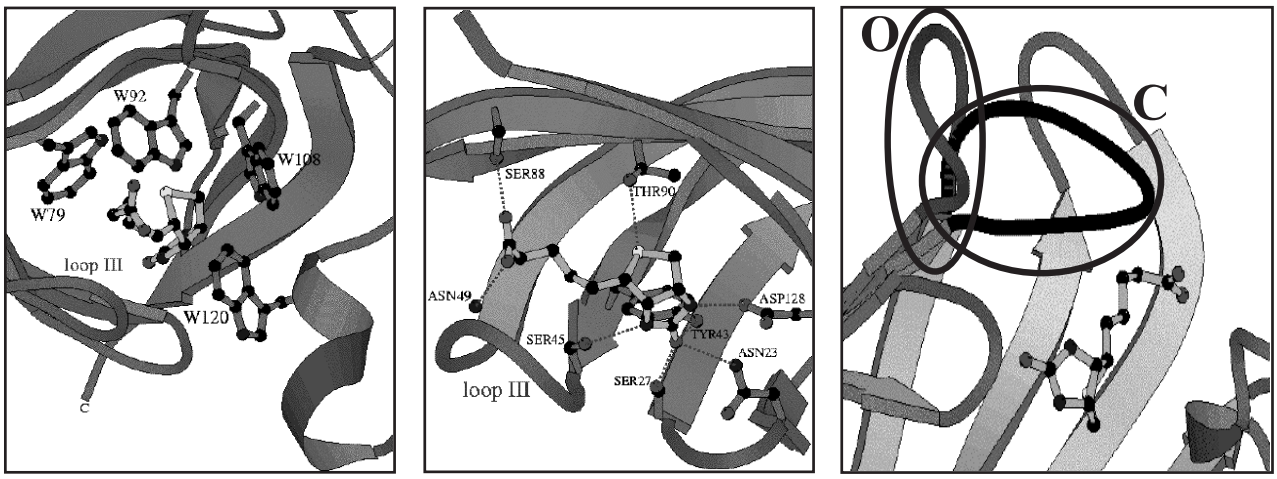

Figure 2.19: *The three binding mechanisms of streptavidin with biotin (taken from [190]). Left: hydrophobic and van der Waals interactions of tryptophan (W79, W92, W108 and W120) residues with biotin. Center: hydrogen bonding network. Right: open (O) and closed (C) surface loop incorporating biotin.*

2.5.3 Conjugation methods

For both immunoassays and biotin-streptavidin, conjugation of the biomolecules with donor or acceptor luminophores is necessary to establish a FRET system. Many of these conjugation methods have been described in the literature [96, 195–198]. Two examples of very common coupling reactions to amines and sulfhydryls are presented.

The most common reactive groups for conjugating molecules to proteins are the N-hydroxysuccinimide (NHS) or N-hydroxysulfosuccinimide (sulfo-NHS) esters which react with amine nucleophiles. The binding reaction is an acylation where the active carbonyl group of the NHS ester undergoes addition to the amine with the release of the NHS or sulfo-NHS leaving group (Figure 2.20). Principally, these amines are the α-amines at the N-terminals and the ε-amines of lysine side chains. Compared to NHS esters, the sulfo-NHS esters are relatively water-soluble, long-lived and hydrolyze slower in water.

A thiol-reactive reaction is another common method for bioconjugation. Maleic acid imides (maleimides) are functional groups where the C-C double bond undergoes alkylation with

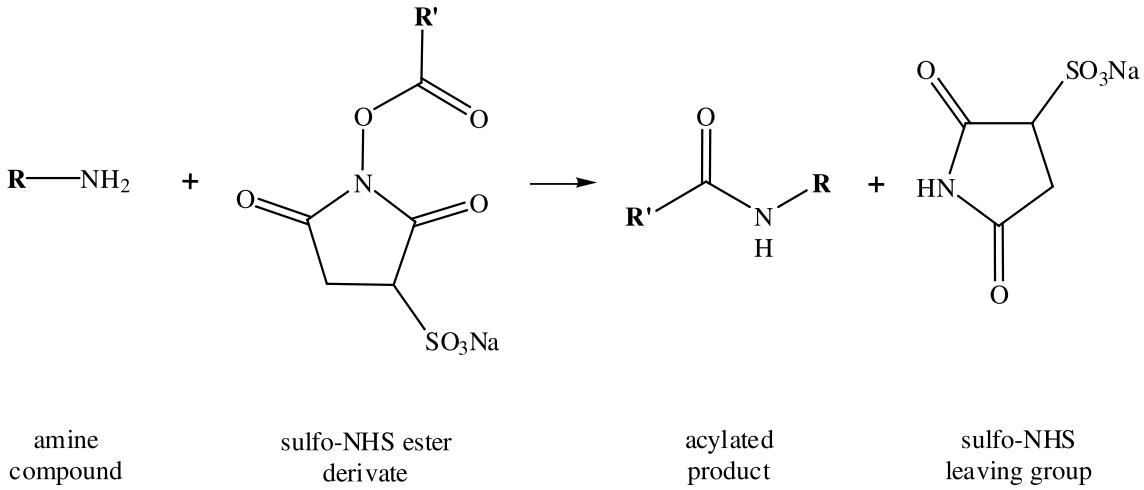

Figure 2.20: *The sulfo-NHS ester reacts with the amine nucleophile releasing the sulfo-NHS leaving group to form an acylated product.*

sulfhydryl groups to form a stable thioether bond (Figure 2.21).

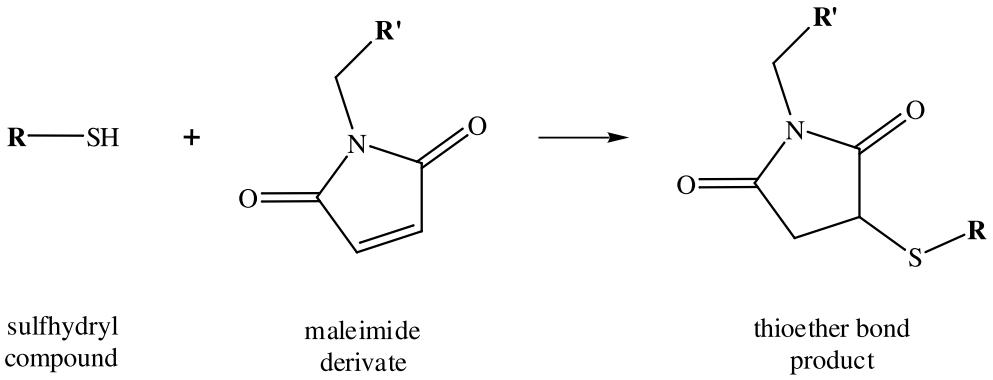

Figure 2.21: *One of the maleimide carbons undergoes nucleophilic attack by the thiolate to generate a stable thioether bonded product.*

This method is especially used for labeling IgG antibodies without blocking the antigen binding site. The antibodies are reduced (usually with MEA - 2-mercaptoethylamine) to cleave the disulfide bonds between the two heavy chains in the hinge region of the antibody, whereas the disulfide bonds between heavy and light chains are not affected. This reduction creates two half-antibody fragments with one light and heavy chain, one antigen binding site and two free sulfhydryl groups to couple the maleimide activated molecule.

Chapter 3

Experimental section

3.1 Measuring solutions

The main solutions used in the experiments were:

SA: pure water
SB: pure water + 0.5 M KF
SC: 50 mM borate buffer pH 8.3
SD: 50 mM borate buffer pH 8.3 + 2 % BSA
SE: 50 mM borate buffer pH 8.3 + 2 % BSA + 0.5 M KF
SF: 50 mM borate buffer pH 8.3 + 2 % BSA + 0.05 % NaN_3
SG: 50 mM borate buffer pH 8.3 + 2 % BSA + 0.5 M KF + 0.05 % NaN_3

3.2 FRET donors and acceptors

Donors
The FRET lanthanide donor substances used in this work are the terbium complex of TbL [35–37] as well as the europium complexes of EuL [35–37] and Eu-TBP [37, 38] (see also Figure 2.8).
TbL and EuL labeling to streptavidin and TbL labeling of monoclonal mouse-IgG antibodies (B24BF10 [199]) and to human chorionic gonadotropin (HCG) was performed by mixing 0.5 mg of the sulfo-NHS activated esters of TbL or EuL (dissolved in 2 μl DMSO) with 1 mg of streptavidin, IgG or HCG in 200 μl PBS buffer. After one day of incubation on a shaker at room temperature, unlabeled TbL was removed by dialysing twice for one day against 1 l of PBS buffer. Labeling and purification as well as supply of IgG and HCG were realized by Frank Sellrie (Universität Potsdam, Institut für Biochemie und Biologie, Professur für Biotechnologie, Karl-Liebknecht-Str. 24-25, Haus 25, 14476 Potsdam-Golm, Germany). Streptavidin was supplied by Promega GmbH (High-Tech-Park, Schildkrötstr.15, 68199 Mannheim, Germany).
TbL, EuL and their sulfo-NHS activated complexes were supplied by Loïc Charbonnière (Laboratoire de Chimie Moléculaire, UMR 7509 CNRS, ECPM 25 rue Becquerel, 67087 Strasbourg cedex 02, France).
Eu-TBP and Eu-TBP labeled streptavidin (Pierce Biotechnologie,Inc., P.O.Box 117, Rockford, IL 61105, USA) inside phosphate buffer containing bovine serum albumin (BSA) were supplied by Cezanne SA (280, Allée Graham Bell, Parc Scientifique, Georges Besse, 30035 Nîmes cedex 1, France).

Acceptors
The FRET acceptor substances used in this work are QDot655 semiconductor nanocrystals [200], crosslinked allophycocyanin (APC) [201, 202] and DY633 [203].
QDot655 biotin conjugate kit (5 to 6 biotins/QDot) was supplied by Quantum Dot Corporation (26118 Research Road, Hayward, CA 94545, USA), now part of Invitrogen Corporation (1600 Faraday Avenue, Carlsbad, CA 92008, USA). Invitrogen kindly supplied a free sample of the QDot655 antibody conjugation kit. IgG antibodies (B20CA2 [199]) were labeled with maleimide activated QDots using the procedure described in the QDot655 antibody conjugation kit user manual (www.qdots.com).
Biotinylated DY633 (1 biotin/DY633) was supplied by Dyomics GmbH (Winzerlaer Str.2A, 07745 Jena, Germany).
APC and biotinylated APC (10 to 15 biotins/APC) were supplied by Cezanne SA (280, Allée Graham Bell, Parc Scientifique, Georges Besse, 30035 Nîmes cedex 1, France).

3.3 Analytical methods

3.3.1 Stationary absorption and luminescence spectroscopy

UV/Vis absorption measurements were performed on a Cary500 absorption spectrometer (Varian Inc., 3120 Hansen Way, Palo Alto, CA 94304-1030, USA) with 5 mm or 10 mm quartz cells. For correction of absorption and scattering of biological buffers the optical reference path as well as single path buffer measurements were used for background correction.
Steady-state luminescence measurements were performed (with 5 mm or 10 mm quartz cells) on a Fluoromax3 fluorescence spectrometer (HORIBA Jobin Yvon GmbH, Chiemgaustr. 148, 81549 München, Germany) in a 90° setup using the system-internal quantum correction and a UV filter for excitation light suppression.

3.3.2 Time-resolved luminescence spectroscopy and fluoro immunoassays

Time-resolved luminescence measurements and fluoro immunoassays (FIA) were performed on three spectrometer systems:

1. Modified KRYPTOR system (Cezanne) for time-resolved integrated single photon counting at two photomultiplier (PMT) channels (545 and 665 nm for Tb and 620 and 665 nm for Eu, filter based wavelength separation) with 2 μs integration steps over 8 ms using fiber-coupled laser excitation. The samples were measured inside a multi-well plate with 300 wells of 150 μl sample volume. The optical path of excitation light to the sample and luminescence light to the PMTs is shown in Figure 3.1.

2. Andor iStar time-resolved ICCD camera (Andor Technology PLC, 7 Millennium Way, Springvale Business Park, Belfast BT12 7AL, Northern Ireland) coupled to a MS257 spectrometer (Oriel Instruments, 150 Long Beach Boulevard, Stratford, CT 06497-0872, USA). Samples were measured (with 5 mm or 10 mm quartz cells) in a 90° setup with direct or fiber-coupled laser excitation.

ICCD specifications: 1024x256 pixels, min. gatewidth < 10 ns, min. stepwidth < 500 ps.
MS257 specifications: 270 nm < λ < 920 nm, 2 gratings: 300 and 1200 lines/mm.

3. FLS920 fluorescence spectrometer (Edinburgh Instruments Ltd., 2 Bain Square, Kirkton Campus, Livingston EH54 7DQ, UK). Samples were measured (with 5 mm or 10 mm quartz cells) in a 90° setup with direct laser excitation from a LDH-P-635 picosecond diode laser head (635 nm output wavelength) with PDL800-B picosecond pulsed diode laser driver (PicoQuant GmbH, Rudower Chaussee 29 (IGZ), 12489 Berlin, Germany).

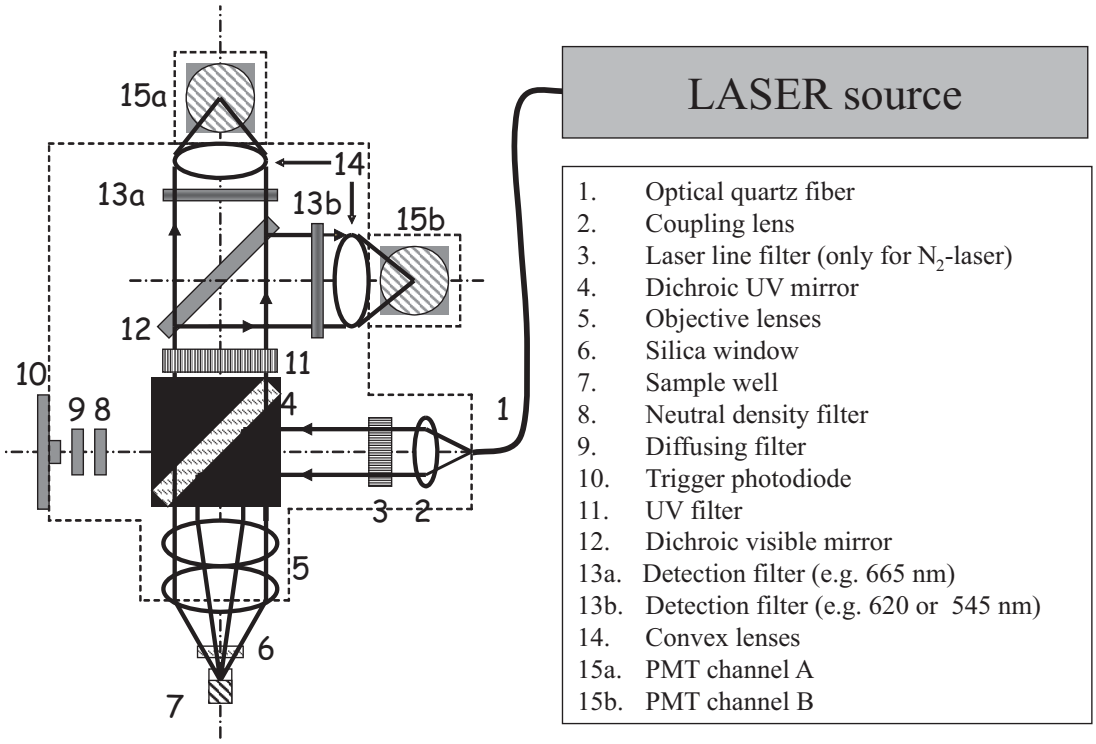

Figure 3.1: *Schematic setup of the KRYPTOR detection system.*

The laser sources used for sample excitation with the spectrometer setups **1** and **2** were:

1. Vibrant-LD-355-II OPO (Opotek Inc., 2233 Faraday Avenue, Suite E, Carlsbad, CA 92008, USA) pumped with a Brilliant Nd:YAG laser (Quantel SA, 17, Avenue de l'atlantique, 91941 Les Ulis cedex, France) with 20 Hz repetition rate and spectral tunability from 250 to 2400 nm. Due to insufficient performance this system had to be returned to the manufacturer after some months and is no longer available in our labs.
2. LAB-170-20PLUS Nd:YAG laser (Spectra-Physics, 1330 Terra Bella Ave., Mountain View, CA 94039, USA) pumping a versaScan OPO (GWU-Lasertechnik Vertriebsgesellschaft m.b.H., Talstr. 3, 50374 Erftstadt, Germany) with 20 Hz repetition rate and spectral tunability from 240 - 2550 nm.
3. OPTex XeCl excimer laser (Lambda Physik AG, Hans-Böckler-Straße 12, D-37079 Göttingen, Germany) with 20 Hz repetition rate and 308 nm output wavelength.
4. VSL-337i nitrogen laser (Spectra-Physics, 1330 Terra Bella Ave., Mountain View, CA 94039, USA) with 20 Hz repetition rate and 337.1 nm output wavelength.

3.3.3 MALDI-TOF

Analysis of labeled streptavidin was realized with Matrix Assisted Laser Desorption/Ionization Time of Flight (MALDI-TOF) mass spectrometry [204]. The measurements were performed by Dr. Sophie Haebel (Universität Potsdam, Interdisziplinäres Zentrum für Massenspektrometrie von Biopolymeren, Karl-Liebknecht-Strasse 24-25, Haus 20, 14476 Potsdam-Golm) on a REFLEX II MALDI-TOF mass spectrometer (Bruker BioSciences Corporation, 40 Manning Road, Billerica, MA 01821, USA).

3.4 Data processing

For data processing, mathematical calculations and fitting procedures as well as graphical data presentation, the computer software Origin7G (OriginLab Corporation, One Roundhouse Plaza, Suite 303, Northampton, MA 01060, USA) and MicrosoftExcel2000 (Microsoft Corporation, One Microsoft Way, Redmond, WA 98052, USA) were used.

Chapter 4

Results and discussion

4.1 Characterization of the FRET donors

The donors used for FRET experiments were the long-luminescing lanthanide complexes of Eu-TBP and LnL (see Figure 2.8 a and d in Section 2.3.3). These complexes were labeled to streptavidin, IgG antibodies and HCG (the two latter for TbL only) in order to obtain biocompatible FRET donors. Structural and spectroscopic data important for FRET are described in this section.

4.1.1 Bioconjugation

Bioconjugation was performed as described in the experimental section (Chapter 3). Assuming the absence of strong electronic perturbations due to the labeling process, it was possible to quantify the labeling ratio (the number of complexes per biomolecule) by deconvolution of the UV/Vis spectra of the labeled biomolecule into a linear combination of the spectra of the pure label and pure biomolecule. For concentration calculations, the molar absorption coefficients ε of the biomolecules at the absorption maximum around 280 nm, of LnL at the maximum around 308 nm and of EuTBP at the maximum around 305 nm were used. The absorbance of a protein at 280 nm depends on the content (number of residues) of tryptophan (n_{Trp}), tyrosine (n_{Tyr}) and the disulfide bonds between to cysteine residues (also called cystine) (n_{dsb}) and can be predicted using the equation [205]

$$\varepsilon(280\text{nm}) = n_{Trp} \cdot 5500 \; + \; n_{Tyr} \cdot 1490 \; + \; n_{dsb} \cdot 125 \quad \text{M}^{-1}\text{cm}^{-1} \tag{4.1}$$

With $n_{Trp} = 6$, $n_{Tyr} = 6$ and $n_{dsb} = 0$ for the used streptavidin monomer, the absorption coefficient is $\varepsilon(280\text{nm}) = 42000$ $\text{M}^{-1}\text{cm}^{-1}$ for a monomer and $\varepsilon(280\text{nm}) = 168000$ $\text{M}^{-1}\text{cm}^{-1}$ for the complete tetramer.
Determination of the HCG and IgG absorption coefficients is not as easy as for streptavidin, as the used HCG contains many sugars and the amino acid sequence of the used IgG is not completetly known. Coefficients of $\varepsilon(280\text{nm}) = 40000$ $\text{M}^{-1}\text{cm}^{-1}$ for HCG (absorbance = 1 for 1 mg/ml, molecular weight = 40 kDa) and $\varepsilon(280\text{nm}) = 210000$ $\text{M}^{-1}\text{cm}^{-1}$ for IgG (absorbance = 1.4 for 1 mg/ml, molecular weight = 150 kDa) were used, as suggested by the supplier.
For the Ln complexes, absorption coefficients of $\varepsilon(308\text{nm}) = 20800$ $\text{M}^{-1}\text{cm}^{-1}$ for TbL [35], $\varepsilon(308\text{nm}) = 19700$ $\text{M}^{-1}\text{cm}^{-1}$ for EuL [35] and $\varepsilon(305\text{nm}) = 30000$ $\text{M}^{-1}\text{cm}^{-1}$ for Eu-TBP [86] were used.

The spectra of labeled streptavidin are presented in Figure 4.1. For both Eu-TBP and TbL, labeling ratios close to 4 were obtained (4.1 and 3.7, respectively), meaning an average value of one label per monomeric unit composing the tetrameric streptavidin protein. For EuL, a poor labeling ratio of 1.2 could be obtained. A much better labeling ratio of approximately 10 TbL/streptavidin could be achieved by a secondary labeling step of already TbL-labeled streptavidin with 2 mg of sulfo-NHS activated TbL dissolved in 300 μl DMSO. As hydrolysis of the active sulfo-NHS ester to nonreactive sulfo-NHS and a nonreactive TbL complex is the main competing reaction to the amine conjugation described in Section 2.5.3, aqueous stock solutions of the sulfo-NHS activated complexes should be used immediately. Stronger hydrolysis of the activated EuL complex due to longer dissolving times in the aqueous stock solution could be a reason for the low labeling ratio of 1.2. On the other hand, the use of a DMSO stock solution for the secondary labeling step with TbL prevents early hydrolysis and could be the reason for the high labeling ratio. Nevertheless, one has to take care that high amounts of DMSO do not damage the protein, which has to be labeled.

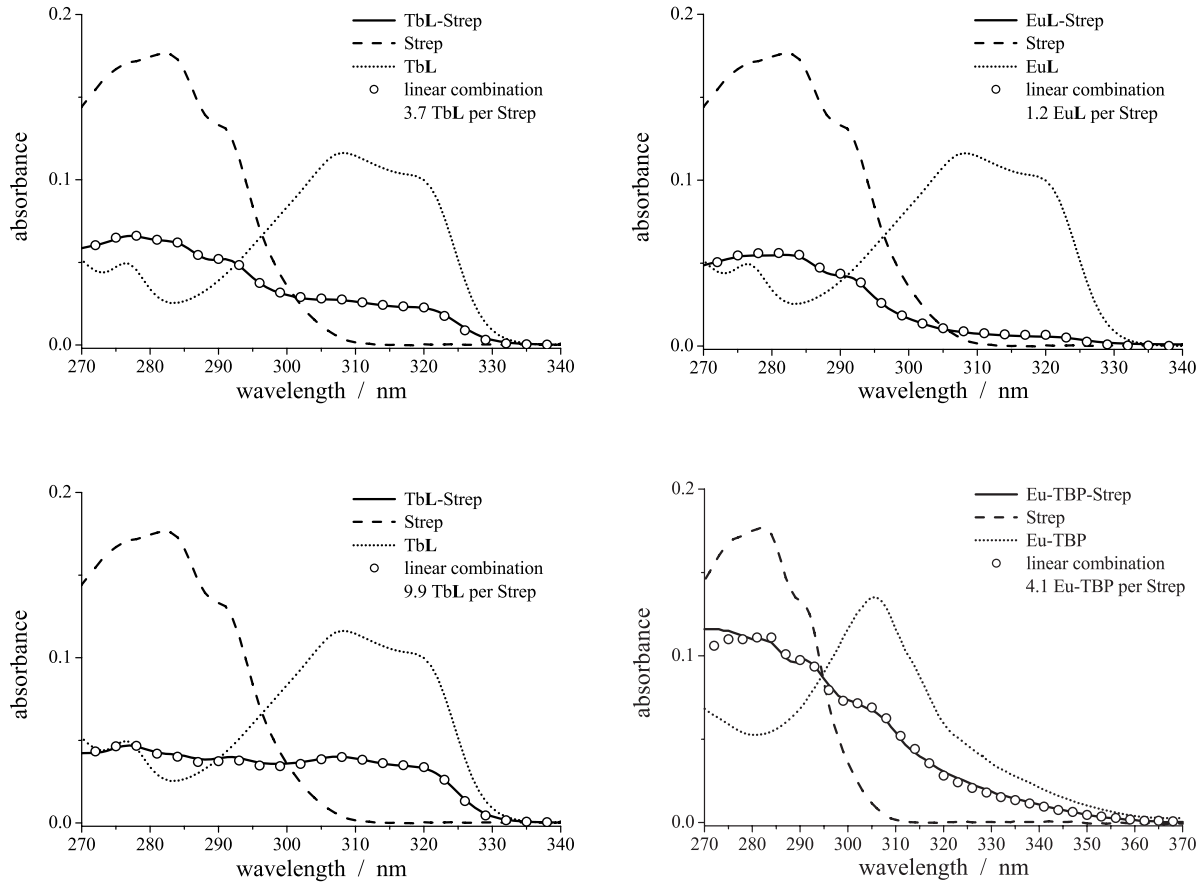

Figure 4.1: *Labeling of streptavidin with Ln complexes. UV/Vis spectra of streptavidin (Strep, $c = 1 \cdot 10^{-6}$ M), TbL ($c = 5.6 \cdot 10^{-6}$ M), EuL ($c = 5.9 \cdot 10^{-6}$ M), Eu-TBP ($c = 4.5 \cdot 10^{-6}$ M), Ln complex labeled streptavidin and linear combinations of streptavidin and Ln complex. Labeling ratios of 4.1 Eu-TBP/Strep, 1.2 EuL/Strep, 3.7 TbL/Strep and 9.9 TbL/Strep (two step labeling) were achieved.*

In order to confirm these labeling ratios, the Ln complex streptavidin conjugates were

characterized by MALDI-TOF mass spectrometry. The spectra of the 4.1 Eu-TBP/Strep, the 1.2 EuL/Strep and the 3.7 TbL/Strep complexes are shown in Figure 4.2. Depending on the cleavage of the native protein, the molecular mass of the "core" streptavidin monomer ranges from 12930 Da [206] to 13300 Da (specified by Promega Corp. for streptavidin). The pure streptavidin spectrum shows five peaks at 12970, 13040, 13115, 13185 and 13265 Da (all ±10 Da) indicating a streptavidin sample composed of differently cleaved monomers. Nevertheless, these five peaks can also be found in the spectra of all labeled streptavidin compounds, refering to unlabeled streptavidin monomers. This accumulation of peaks can be found shifted to higher molecular weight in steps of approximately 600 to 700 Da, which corresponds to the molecular weight of the Ln complexes without the central Ln ion (which is detached from the complex during the ionization process). For LnL, besides the unlabeled monomer, proteins labeled with one complex are the predominant species, coexisting with minor amounts of double and triple labeled ones. For Eu-TBP-Strep single and double-labeled monomers are dominant with minor amounts of triple and quadruple labeled ones. These spectra point to multiple possible environments for the Ln complex label.

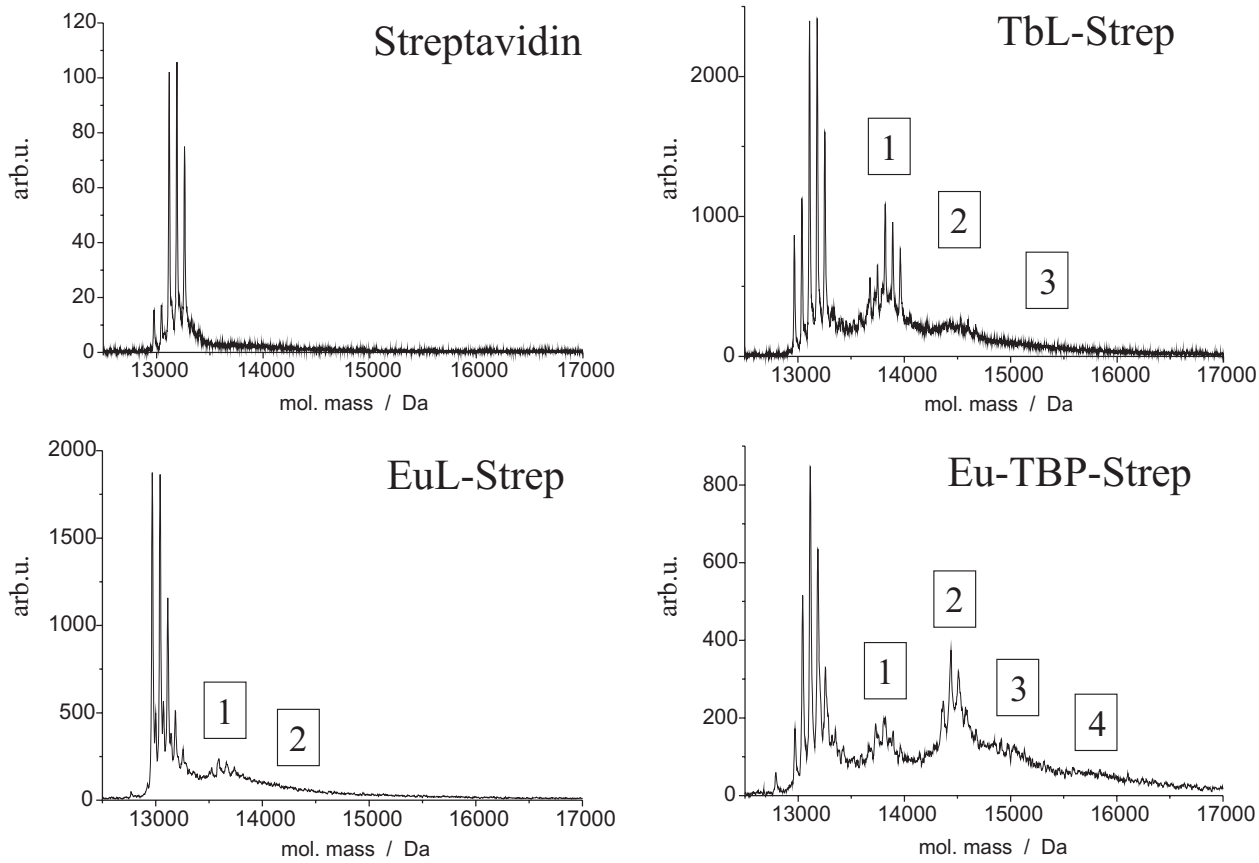

Figure 4.2: *MALDI-TOF spectra of streptavidin monomer and its three Ln complex labeled bioconjugates. The number of Ln complexes per streptavidin monomer are displayed on top of the peaks. All spectra show single charged biomolecules (m/z = m = mol. mass).*

Labeling of IgG and HCG with TbL was characterized by UV/Vis spectroscopy (Figure 4.3). Although several lysine residues should be available at the proteins for sulfo-NHS labeling,

both labeling ratios of 2.1 for IgG and 0.4 for HCG are quite low. Reasons for that could be hydrolysis of the sulfo-NHS complex or to few accessible lysine residues on the protein surface.

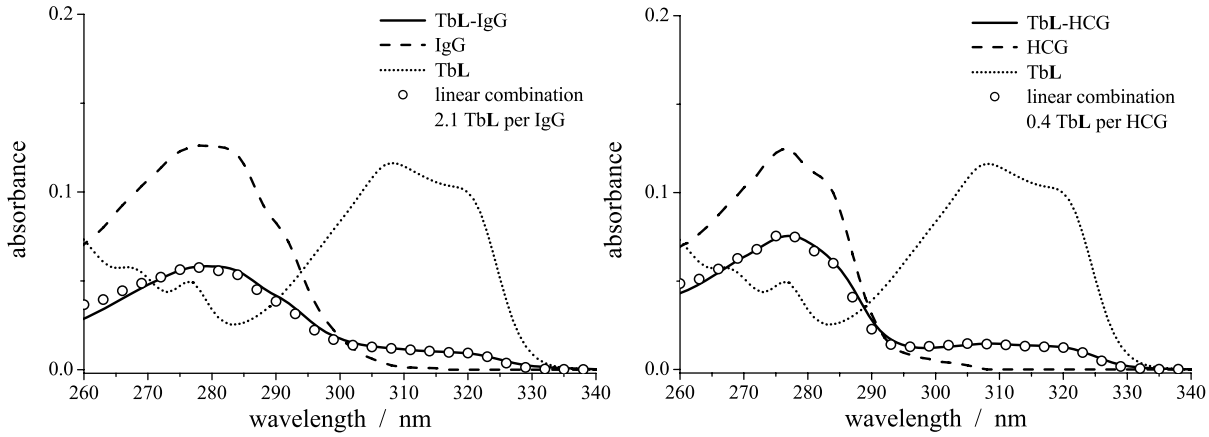

Figure 4.3: *Labeling of IgG and HCG with TbL. UV/Vis spectra of IgG ($c = 6 \cdot 10^{-7}$ M), HCG ($c = 3.1 \cdot 10^{-6}$ M), TbL ($c = 5.6 \cdot 10^{-6}$ M), Ln complex labeled IgG and HCG and linear combinations of TbL and IgG and HCG, respectively. Labeling ratios of 2.1 TbL/IgG and 0.4 TbL/HCG were achieved.*

4.1.2 Photophysical characterization

As mentioned in Section 2.3.2, the photophysical properties of Ln complexes are characterized both by the Ln ion itself as well as the surrounding ligand. The energy level diagram of Figure 2.7 is basically the same for the used Ln complexes.
The lowest singlet state of the LnL ligand is around 30000 cm^{-1}, as characterized by the absorption spectrum with a maximum at 308 nm and 318 nm and a cut-off wavelength at around 340 nm. States of higher energy can also be observed in this spectrum (peaks at 276 nm, 268 nm and 253 nm). The ligand triplet state lies at ca. 22100 cm^{-1} which is 1800 cm^{-1} above the Tb^{3+} $^5D_4$ state at approximately 20300 cm^{-1} [58]. Although this value is lower than 1850 cm^{-1} (see Section 2.3.2), strong backtransfer could not be observed at room temperature [35]. The Eu^{3+} levels, which can receive energy from the ligand triplet state, lie at ca. 17300 cm^{-1} ($^5D_0$), 19050 cm^{-1} ($^5D_1$) and 21500 cm^{-1} ($^5D_2$) [58]. Energy backtransfer to the ligand triplet state is not problematic in this case because the two higher levels deactivate directly to the $^5D_0$.
For Eu-TBP the lowest singlet state is around 30000 cm^{-1} as well, characterized by the absorption maximum at 305 nm and a weak shoulder in the absorption spectrum around 325 nm. The cut-off wavelength is at approximately 370 nm. Eu-TBP possesses a LCMT state allowing for direct deactivation of the singlet state. The LCMT state energy is unknown but expected to lie between the singlet and triplet state of the ligand which is at 21600 cm^{-1} [86].

4.1.2.1 Absorption spectra

Absorption spectra of the lanthanide complexes are characterized by the ligand (the antenna - see Section 2.3.2), which collects the light and transfers the photon energy to the central Ln ion. As the antenna absorbs in the UV region, there is a strong overlap with the biomolecule absorption as shown in Figures 4.1 and 4.3. Some biomolecules luminesce strongly, which can interfere with the luminescence signal of interest. Moreover, a strong biomolecule absorption withdraws photons from the ligand excitation process. For these reasons excitation should be performed with a wavelength that is not (or only slightly) absorbed by the biomolecule. Excitation wavelengths above 305 nm usually fulfill this requirement.
For comparison, the absorption spectra of the three Ln complexes with maxima of 20800 $M^{-1}cm^{-1}$ at 308 nm for TbL [35], 19700 $M^{-1}cm^{-1}$ at 308 nm for EuL [35] and 28000 $M^{-1}cm^{-1}$ at 305 nm for Eu-TBP [86] are shown in Figure 4.4. Looking at these spectra, a wavelength around 250 nm would be possible for exciting the complexes. Taking into account common laser sources, the 4th harmonic of a Nd:YAG laser at 266 nm would result in a better excitation than using the 3rd harmonic at 355 nm. In a biological assay the use of 266 nm is not possible due to the reasons mentioned above. Unfortunately, near the excitation maxima of the complexes above 305 nm only large and expensive laser systems are commercially available (e.g. XeCl excimer laser at 308 nm or Nd:YAG laser pumped OPO or dye laser systems). This may sometimes not be a problem for the use in scientific laboratories. For commercial applications small and inexpensive lasers are necessary. In the case of the KRYPTOR immunoreader (see Section 3) a nitrogen laser (337.1 nm) is used in the standard setup for economic reasons. This wavelength is quite far away from the absorption maximum, and Eu-TBP excitation is weak but still possible. Small and inexpensive diode pumped solid state laser concepts using a frequency-tripled 930 nm Nd:YAlO or 946 nm Nd:YAG laser were proposed [207] and successfully realized in the case of the Nd:YAG [208]. Unfortunately these concepts have not yet been commercialized.

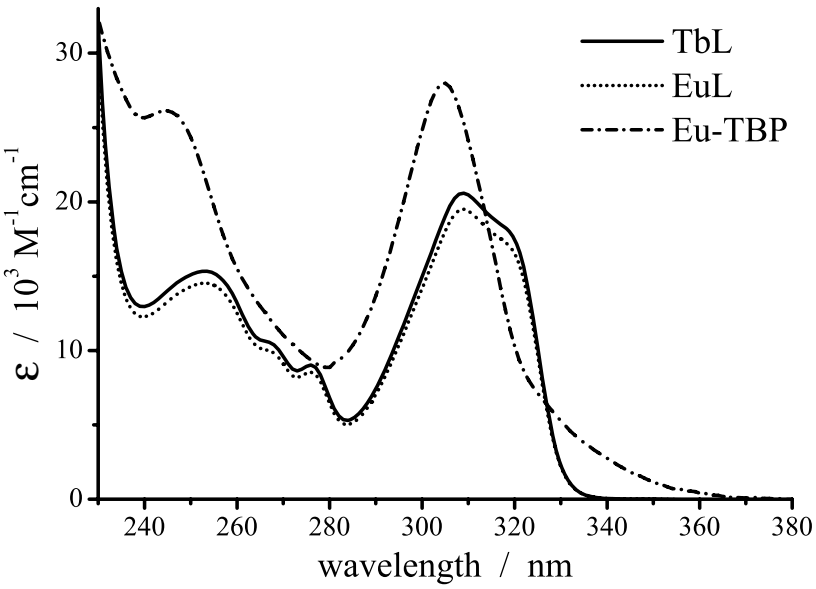

Figure 4.4: *Absorption spectra (extinction coefficient ε) of the Ln complexes TbL, EuL and Eu-TBP in 50 mM phosphate buffer pH 7.5.*

4.1.2.2 Emission spectra

Emission spectra of the Ln complexes are composed of the typical narrow-band luminescence lines of the central Ln ion due to the $^5D_4 \rightarrow {}^7F_J$ transitions for Tb^{3+} and the $^5D_0 \rightarrow {}^7F_J$ and $^5D_1 \rightarrow {}^7F_J$ transitons of Eu^{3+}. In the latter case, the $^5D_1 \rightarrow {}^7F_J$ transitions are extremely weak and cannot be easily observed at room temperature.
In order to estimate the influence of different assay constituents on the donor properties, emission spectra were investigated in the presence of water, borate buffer and BSA. The presence of potassium fluoride (KF) was also tested, as fluoride anions are known to have a dramatic influence on the luminescence properties of lanthanide complexes in general [209,210] and on charged macropolycyclic cryptates such as Eu-TBP in particular [181]. This hard lanthanophylic anion is able to compete with water and other anionic species and to alleviate their negative impact on the luminescence of lanthanides. The influence of sodium azide (NaN_3), which is used as antibacterial agent in biological solutions, was also investigated. Solutions **SA** to **SG** (see Section 3) were used for the experiments.
Streptavidin labeled and unlabeled Ln complexes were measured in **SA**, **SB**, **SC**,**SF** and **SG**. The complete spectra are shown in the appendix (Section 6.3) and only representative spectra are displayed here. All spectra are intensity-normalized to the maximum emission peak because Ln complex emission intensities are not important for FRET. In Equation 2.5, the integrated donor emission is normalized to unity over the complete wavelength range. The donor quantum yield (Φ_D in Equation 2.3) is the quantum yield of the central Ln ion itself (Φ_{Ln}) and not the one of the whole Ln complex. Φ_{Ln} will be calculated in Section 4.1.2.3.

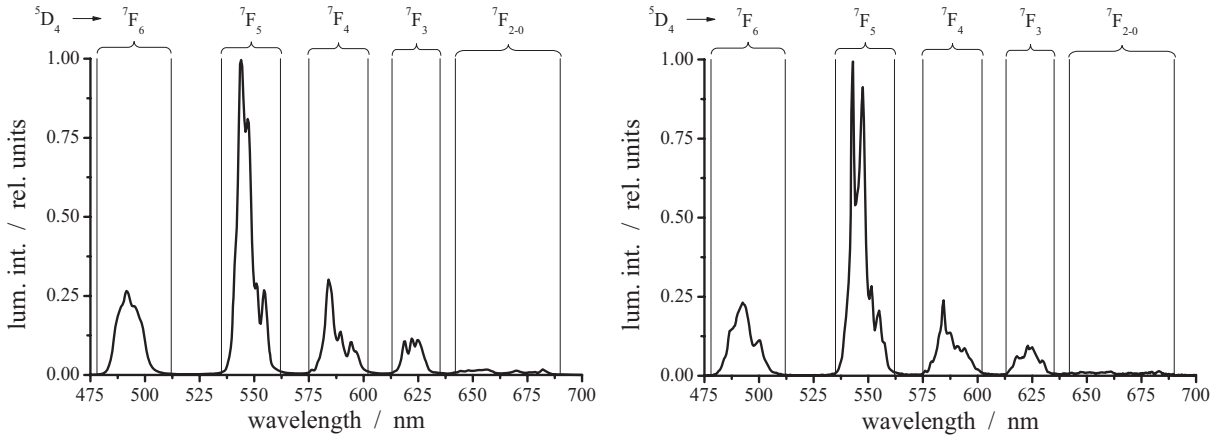

Figure 4.5: *Intensity-normalized emission spectra of TbL-Strep in* ***SA*** *(left) and TbL in* ***SG*** *(right). The estimated optical transitions are displayed on top of the graphs. Complete spectra are displayed in the appendix (Section 6.3).*

TbL and TbL-Strep are relatively insensitive to the different conditions. Even addition of KF results only in small changes of the emission spectrum. Figure 4.5 shows the emission spectra of TbL-Strep in **SA** and TbL in **SG**. Depending on addition of KF, the other spectra are almost identical to the ones in Figure 4.5. Especially for KF spectra the fine-splitting of the energy levels becomes visible. The typical intensity distribution for the different transitions (see Table 2.1) can be found as well.
Although **EuL and EuL-Strep** are not very sensitive to the different conditions a stronger influence of KF addition on the emission spectra becomes visible (Figure 4.6). This influence is strongest for the hypersensitive $^5D_0 \rightarrow {}^7F_2$ transition. Like with TbL and TbL-Strep, the

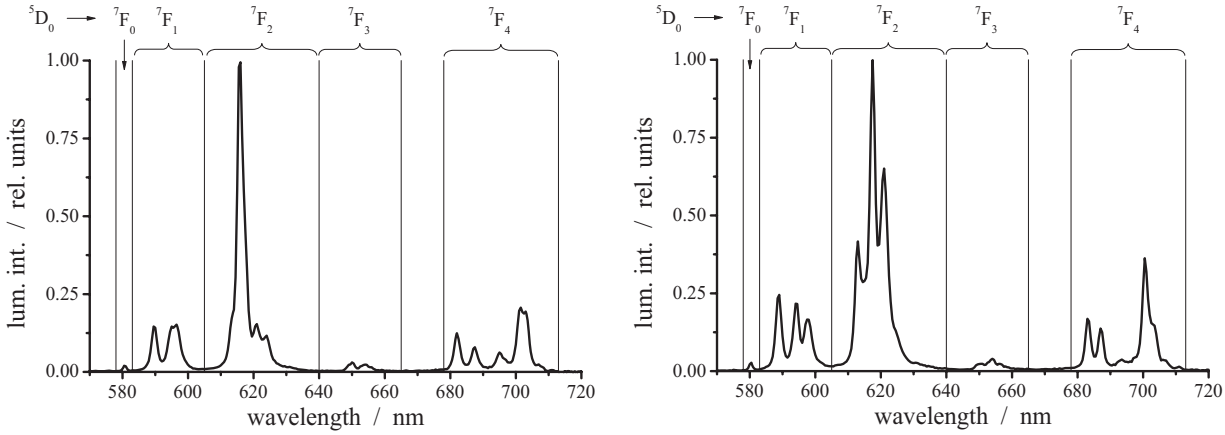

Figure 4.6: *Intensity-normalized emission spectra of EuL-Strep in* ***SA*** *(left) and EuL in* ***SG*** *(right). The estimated optical transitions are displayed on top of the graphs. Complete spectra are displayed in the appendix (Section 6.3).*

emission spectra show energy level fine-splitting and a typical intensity distribution for the different transitions.

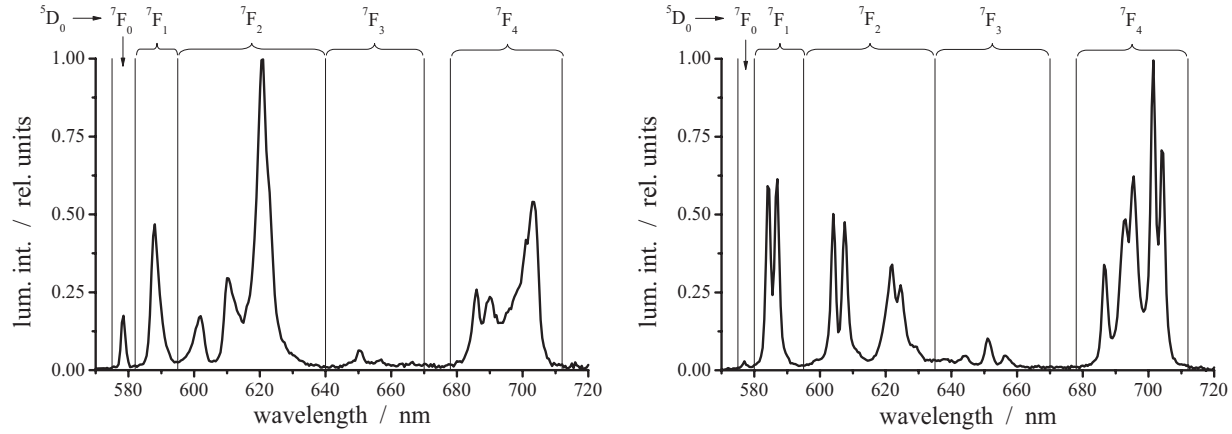

Figure 4.7: *Intensity-normalized emission spectra of Eu-TBP-Strep in* ***SA*** *(left) and Eu-TBP in* ***SG*** *(right). The estimated optical transitions are displayed on top of the graphs. Complete spectra are displayed in the appendix (Section 6.3).*

Unlike TbL, TbL-Strep, EuL and EuL-Strep, **Eu-TBP and Eu-TBP-Strep** are very sensitive to the different solution conditions. This becomes very obvious regarding KF addition, which results in a spectral shift of the emission lines as well as a different intensity distribution. Especially the hypersensitive $^5D_0 \rightarrow {}^7F_2$ transition is affected by the addition of KF. Figure 4.7 displays two representative spectra for the various conditions. Similar to the two other Ln complexes, the energy level fine-splitting is apparent in the emission spectra.

4.1.2.3 Luminescence kinetics

Besides line-like emission bands, the long luminescence decay times are characteristic photophysical properties of Ln complexes. Luminescence decay times are very important for an extensive analysis of FRET, quenching processes and Ln complex properties (cf. Chapter 2). Moreover, the long decay times are necessary for homogeneous FRET immunoassays.

Luminescence kinetics of streptavidin labeled and unlabeled Ln complexes in solutions **SA** to **SG** were measured.

Table 4.1: Luminescence decay times (τ) and Ln centered quantum yields (Φ_{Ln}) of the unlabeled Ln complexes in different solutions.

	TbL		EuL		Eu-TBP	
Solution	τ (μs)	Φ_{Ln}	τ (μs)	Φ_{Ln}	τ (μs)	Φ_{Ln}
SA	1560	0.52	620	0.24	[1] 395 [2] 95 & 400 [3] 90 & 430	0.23 0.22 0.18
SB	2370	0.78	1390	0.54	1190	0.70
SC	1540	0.51	620	0.24	520 (70%) 250 (30%)	0.26
SD	1330	0.44	700	0.27	790 (45%) 320 (55%)	0.31
SE	1990	0.66	1350	0.52	1180	0.69
SF	640	0.21	750	0.29	1020 (70%) 200 (30%)	0.45
SG	1250	0.41	1350	0.52	1150	0.68
$\mathbf{D_2O}$[a]	2530	0.84	2480	0.96	1700	1.0
$\mathbf{H_2O}$[a,b]	1480	0.49	620	0.24	340	0.20

Experimental uncertainty for τ ca. ±5 % (±10 % for bi-exponential decays); calculated max. error for Φ_{Ln} ca. ±20%. In case of two-exponential decays, the relative amounts of the two decay components to the total luminescence are given in brackets. For Eu-TBP in water, the decay behaviour changes with incubation time after dilution: [1] 5 min.; [2] 30 min.; [3] 2.5 h.

a Taken from Reference [35] for TbL and EuL and from Reference [86] for Eu-TBP; **b** Values (in pure water at 300 K) taken as τ^0 and Φ^0_{Ln} for Equation 4.2

The measured luminescence decay times can be used to calculate the Ln centered quantum yields (Φ_{Ln}), which are relevant for FRET (cf. Section 2.3.2), by Equation 2.28. The radiative lifetime of the Ln ion inside the complex is the ratio of measured luminescence decay time and Ln quantum yield. It was calculated for each complex with the decay time in pure water (at 300 K) τ^0 and the corresponding Φ^0_{Ln} (see Table 4.1). The resulting values (with a max. error of ±15%) are $\tau_R = 3.0$ ms for TbL, $\tau_R = 2.6$ ms for EuL and $\tau_R = 1.7$ ms for Eu-TBP. Assuming that τ_R of each complex is independent of the medium, Φ_{Ln} is given by

$$\Phi_{Ln} = \Phi^0_{Ln} \frac{\tau}{\tau^0} \tag{4.2}$$

The different solution conditions also have an influence on Φ_{trans} (Equation 2.31), which has no impact on the FRET efficiency, but can alter the FRET immunoassay sensitivity due to variable amounts of energy available for FRET (cf. Section 2.3.2).

Table 4.2: Luminescence decay times (τ) and Ln centered quantum yields (Φ_{Ln}) of the streptavidin labeled Ln complexes in different solutions.

	TbL-Strep		**EuL-Strep**		**Eu-TBP-Strep**	
Solution	τ (μs)	Φ_{Ln}	τ (μs)	Φ_{Ln}	τ (μs)	Φ_{Ln}
SA	1450	0.48	680	0.26	840 (55%) 320 (45%)	0.36
SB	2100	0.70	1400	0.54	1080	0.64
SC	1220	0.40	650	0.25	650 (65%) 230 (35%)	0.29
SD	1220	0.40	650	0.25	690 (65%) 230 (35%)	0.31
SE	1900	0.63	1400	0.54	1100	0.65
SF	680	0.23	680	0.26	1030 (65%) 220 (35%)	0.44
SG	1430	0.47	1430	0.55	1110	0.65

Description see Table 4.1

Tables 4.1 and 4.2 summarize the luminescence decay times τ and the Ln quantum yields Φ_{Ln} of streptavidin labeled and unlabeled TbL, EuL and Eu-TBP in the different solutions. The corresponding decay spectra can be found in the appendix (Section 6.4).
Regarding these results, one can clearly see that EuL and EuL-Strep are influenced very little by borate, BSA or NaN_3. In contrast, KF greatly increased the luminescence lifetime and quantum yields, as expected by the replacement of water molecules in the first coordination sphere with fluoride anions. The average number of coordinated water molecules (calculated by Equation 2.30) in water is 1.3 and 1.1 for EuL and EuL-Strep, respectively. Addition of KF leads to an average of 0.3 water molecules for both complexes.
For TbL and TbL-Strep, a surprising decrease of τ was observed upon addition of NaN_3, while borate buffer and BSA have only minor influence. The azide quenching effect was further confirmed by titration experiments at different concentrations of added anions (Figure 4.8). Such titrations also showed that a bi-exponential luminescence decay can be found for TbL-Strep at azide concentrations of 0.05 % and higher, as observed in previous experiments [36].
The quenching effect of N^{3-} anions on lanthanide luminescence has already been documented [211], but it was reported to be far more efficient for Eu than for Tb. Thus, these variations can possibly be attributed to first coordination sphere perturbations [212]. TbL

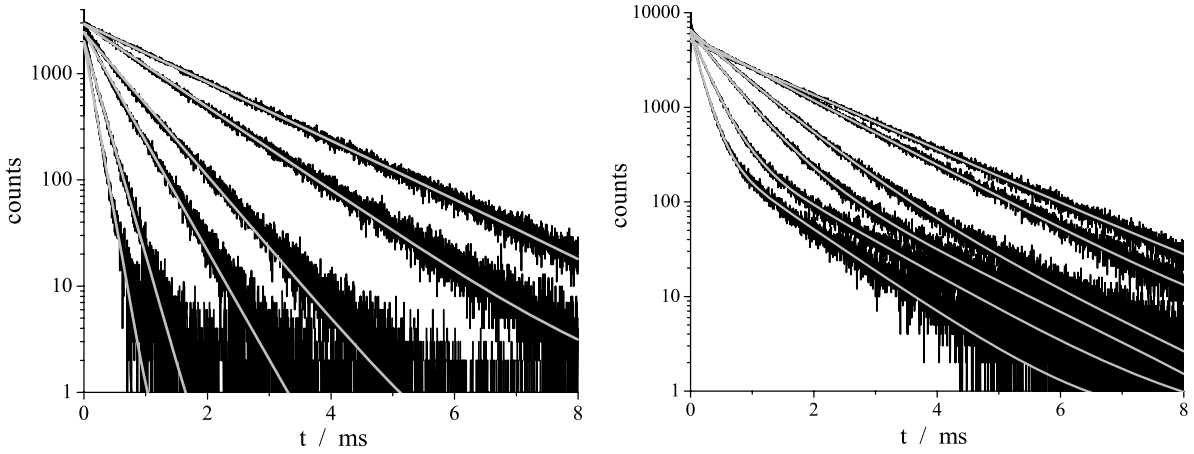

Figure 4.8: *Influence of azide concentration on TbL (left) and TbL-Strep (right). Concentrations: [TbL] = $2 \cdot 10^{-6}$ M; [TbL-Strep] = $4 \cdot 10^{-8}$ M). [NaN_3] is 0, 0.01, 0.05, 0.1, 0.25 and 0.5 % from top to bottom, respectively.*

provides a relatively small energy difference between the ligand centered triplet state and the Tb $^5D_4$ emitting level (cf. Section 4.1.2), and subtle changes in the coordination sphere of Tb may improve the energy back transfer processes from Tb^{3+} to the ligand. Interestingly, fluoride anions strongly enhanced the luminescence lifetime of Tb, nearly reaching values obtained in pure D_2O, and in the presence of all constituents inside the solution, the combined effects of NaN_3 and KF are compensated to afford luminescence decay times similar to TbL-Strep in water. The average number of coordinated water molecules in water is 1.0 and 1.2 for TbL and TbL-Strep, respectively. KF addition leads to an average number of 0.1 for TbL and 0.3 for TbL-Strep.

Unlike the other complexes, Eu-TBP and Eu-TBP-Strep luminescence shows an obvious two-exponential decay behaviour in water as well as in borate buffer with or without NaN_3, likely due to the presence of two distinct emitting species. Moreover, for Eu-TBP an incubation time dependent luminescence decay was observed (Table 4.1 and Figure 6.23). This is probably caused by a time-dependent water coordination of Eu in the Eu-TBP complex which might hydrolize at low concentrations (in this case ca. $3 \cdot 10^{-8}$ M). While the luminescence decay is mono-exponetial with a decay time around 400 μs directly after dilution from a ca. $2 \cdot 10^{-6}$ M stock solution, a second decay time of ca. 100 μs appears after ca. 30 min., becoming obvious after approximately 2.5 h. In order to avoid the well known negative influence of water on Eu-TBP, it is usually supplied in a phosphate buffer, which enhances the luminescence decay time [213] and stability. The major influence on Eu-TBP and Eu-TBP-Strep is, as expected, due to fluoride anions, which removed water from the first coordination sphere and resulted in a mono-exponential luminescence decay. The average number of coordinated water molecules in water is 2.0 and 1.1 for Eu-TBP and Eu-TBP-Strep, respectively. Addition of KF leads to an average number of 0.3 for Eu-TBP and 0.4 for Eu-TBP-Strep. These results show that Eu-TBP should be used with KF or at least in phosphate buffer for reliable spectroscopic experiments.

4.2 Characterization of the FRET acceptors

The acceptors used for the FRET experiments were commercially available (Invitrogen Corporation) CdSe/ZnS core/shell quantum dot nanocrystals emitting at 655 nm (QD655), crosslinked allophycocyanin (APC) and the fluorescence dye DY633.
QD655 are spherical nanoparticles made of semiconductor materials with a CdSe core diameter of ca. 6 nm surrounded by a surface passivation ZnS shell, resulting in an overall diameter of approximately 8 nm. Due to the organic passivating shell these nanocrystals are not soluble in water, which has been overcome by several concepts (see Section 2.4.5). QD655 are coated with a polymer shell, which also provides the possibility of labeling biomolecules to the surface [214]. The complete QD has a diameter of ca. 10 - 12 nm.
The ca. 100 kDa biliprotein allophycocyanin is an important component of phycobilisomes (macromolecular photosynthetic antenna complexes of cyanobacteria and red algae). Crosslinked allophycocyanin consists of an $(\alpha\text{-}\beta)_3$ trimer with $(\alpha\text{-}\beta)$ as the only major intersubunit, leading to better stability compared to untreated allophycocyanin [201]. The three $(\alpha\text{-}\beta)$ monomers are arranged around a 3-fold axis to form a discshaped trimer of approximately 3 nm in thickness and ca. 10 - 13 nm in diameter (depending on the algae source) with a cavity in the center [215, 216].
In contrast to QD655 and APC, DY633 is a relatively small fluorescence dye comparable to other conventionally used red absorbing dyes such as Cy5 or Alexa Fluor dyes [217, 218].

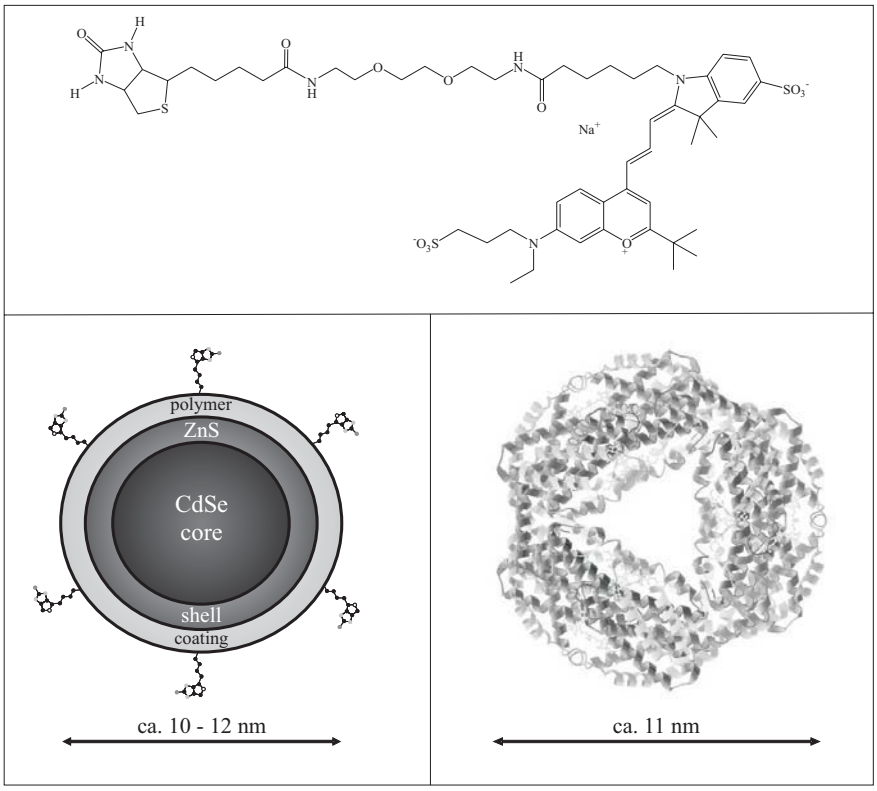

Figure 4.9: *Top: chemical structure of biotinylated DY633 red-absorbing fluorescence dye (Biot-DY633). Bottom left: schematic representation of the biotinylated CdSe/ZnS core/shell (Biot-QD655) with ca. 6 biotin molecules (not to scale) attached to the surface. Bottom right: representative structure of the APC $(\alpha\text{-}\beta)$ trimer from Porphyra yezoensis taken from www.pdb.org [216] without biotin molecules.*

4.2.1 Bioconjugation

QD655, APC and DY633 are commercially available in their biotinylated forms Biot-QD655, Biot-APC and Biot-DY633. Nevertheless, methods for biotinylation are described in the literature mentioned in Section 2.5.3. Each QD655 contains 5 - 7 biotin molecules labeled to the polymer coating on the surface of the dots. APC contains between 10 and 15 biotins. DY633 and biotin are supplied as a 1:1 complex, because they have approximately the same size. IgG antibodies were labeled with maleimide activated QD655 using the procedure described in the QDot655 antibody conjugation kit user manual (www.qdots.com). The three biocompatible FRET acceptors are shown in Figure 4.9.

4.2.2 Photophysical characterization

In order to perform efficient FRET, the acceptors need high extinction coefficients with absorption spectra overlapping well with the donor luminescence (cf. 2.1). Other important properties for distinguishing between donor and acceptor luminescence are short decay times and well separated emission spectra compared to the donors.

4.2.2.1 Absorption spectra

The absorption spectra of Biot-QD655, Biot-APC and Biot-DY633 are shown in Figure 4.10. Biot-QD655 displays the typical absorption spectrum described in Section 2.4, with three major exciton peaks around 650, 610 and 520 nm, two minor ones at ca. 580 and 460 nm and a broad continuum towards the UV from energies higher than the bandgap energy. Compared to other luminescence dyes, the extinction coefficients are extremely high over the complete absorption spectrum.

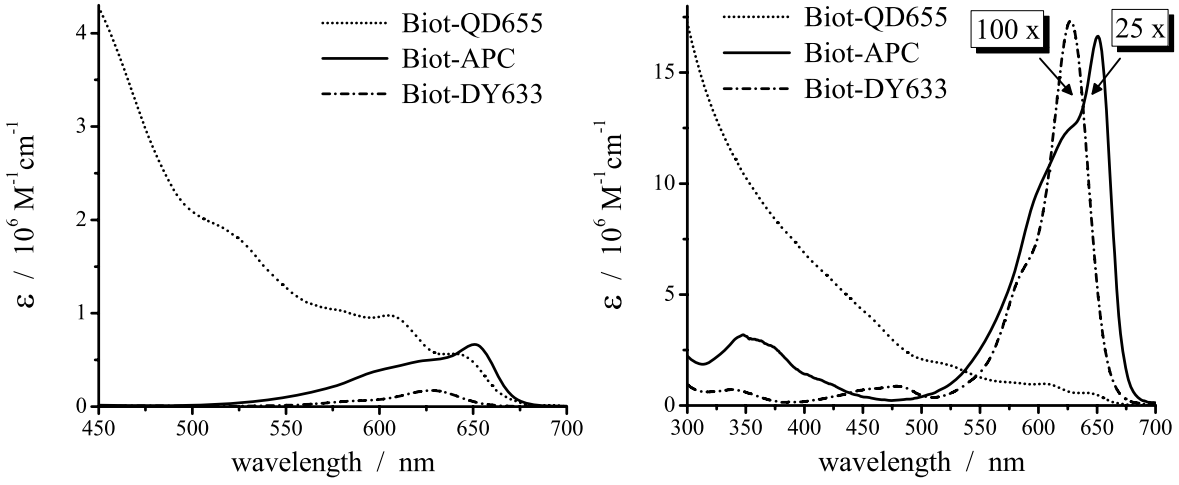

Figure 4.10: *Absorption spectra (extinction coefficients ε as suggested by the suppliers) of Biot-QD655 (in* ***SF****), Biot-APC and Biot-DY633 (in 20 mM phosphate buffer, pH 7.5). For better comparison, the spectra of Biot-APC and Biot-DY633 (right) are magnified by a factor of 25 and 100, respectively.*

Biot-APC has a broad absorption peak with the maximum at 650 nm, providing a very high extinction coefficient of ca. $7 \cdot 10^5$ $M^{-1}cm^{-1}$ [219]. There are two further shoulders in the falling

slope of the peak towards the blue at ca. 625 and 600 nm. Another minor absorption region lies around 350 nm, as is typical for phycobiliproteins [215].
The Biot-DY633 absorption spectrum is similar to the one of Biot-APC with a maximum of approximately 175000 $M^{-1}cm^{-1}$ at 628 nm (as suggested by the supplier) and a shoulder at 580 nm. There are two further absorption regions around 475 and 340 nm.

4.2.2.2 Emission spectra

Emission spectra of the three acceptors are presented in Figure 4.11. They all have a strong emission peak with 30 - 40 nm FWHM (full width at half maximum) in the wavelength region above 600 nm. The maximum Biot-QD655 emission lies around 654 nm, the one for Biot-APC at 660 nm and the one for Biot-DY633 at ca. 651 nm. The emission spectra of the two latter acceptors show a further shoulder next to the maximum around 705 nm for DY633 and 725 nm for APC.

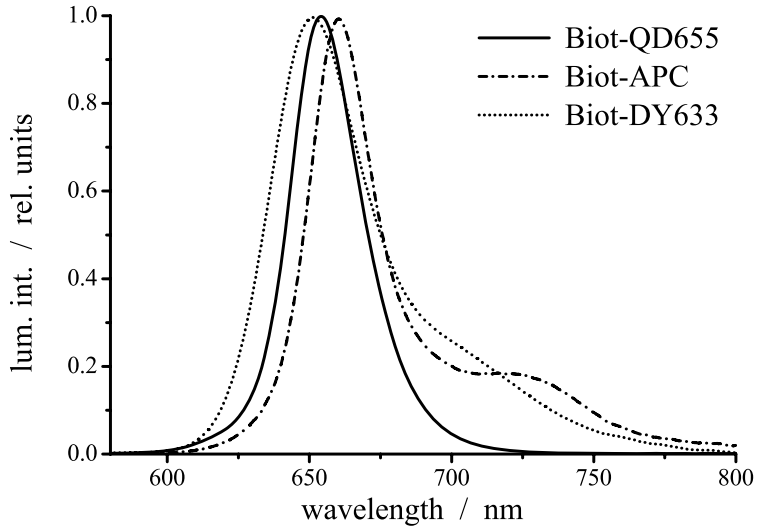

Figure 4.11: *Intensity-normalized emission spectra of Biot-QD655 (in **SF**), Biot-APC and Biot-DY633 (in 20 mM phosphate buffer, pH 7.5).*

4.2.2.3 Luminescence kinetics

In contrast to the donors, Biot-QD655, Biot-APC and Biot-DY633 display short luminescence decay times in the ns range. These short decay times are important in order to have an equal luminescence decay time of donor and FRET sensitized acceptor within a D-A complex (cf. Equation 2.8 in Section 2.1.2). While the fluorescence decay times of DY633 and Biot-DY633 are different, the larger QD655 and APC molecules are not disturbed by the small biotin resulting in the same decay times for both biotinylated and free species of QD655 and APC, respectively.
The Biot-QD655 luminescence decay (Figure 4.12) shows a multi-exponential behavior and the decay function could be conveniently fitted by two main components of 23 and 47 ns (41 and 53 % of the overall luminescence), and a minor one of 160 ns (6 % of the overall luminescence). This behavior is commonly observed for the luminescence decay of quantum dot nanocrystals and arises from the QD size distribution and their anisotropy [152, 220, 221].

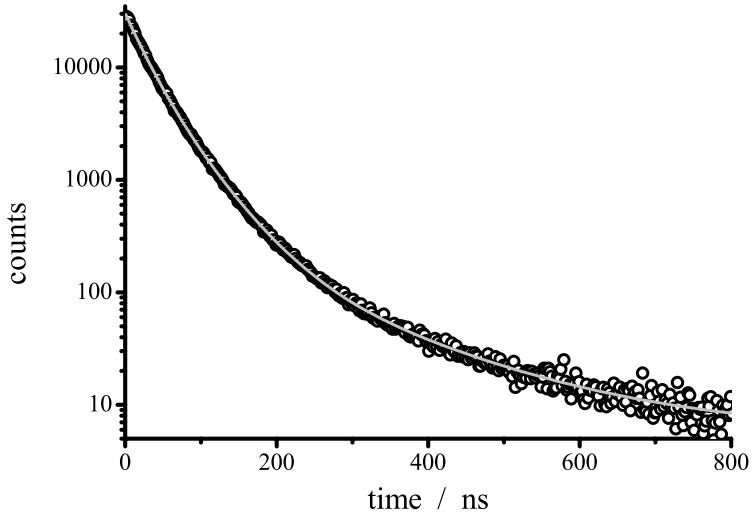

Figure 4.12: *Luminescence decay (integrated intensity (in counts) from 625 - 685 nm) of Biot-QD655 (in **SF**) with decay times of 23 ns (41 % of the overall luminescence intensity), 47 ns (53 %) and 160 ns (6 %). Excitation wavelength 308 nm.*

The luminescence decays of Bio-APC and Biot-DY633 are mono-exponetial with decay times of 1.5 ns and 0.6 ns, respectively (Figure 4.13). The decay time of unbiotinylated DY633 (not displayed) is with ca. 0.2 ns much shorter than for Biot-DY633, showing the influence of biotin on the small molecule DY633. Similar values can be found in the literature for other DY dyes [217] and APC [215].

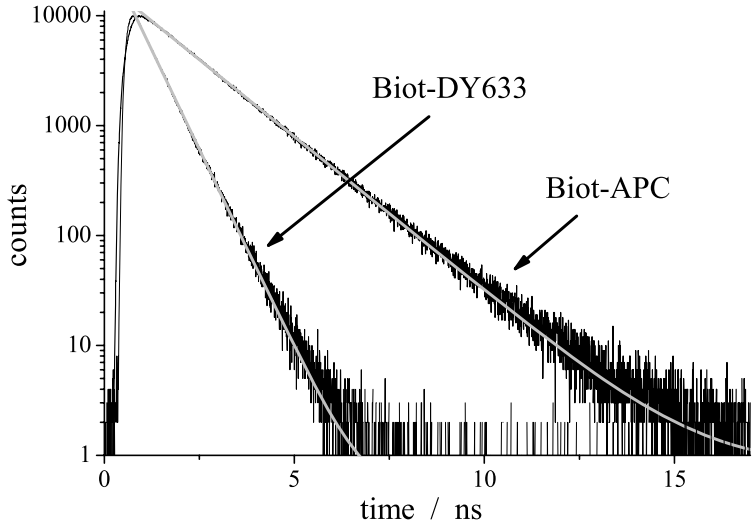

Figure 4.13: *Luminescence decay times τ (measured at 665 ± 1 nm in 20 mM phosphate buffer, pH 7.5) of Biot-APC ($\tau = 1.5$ ns) and Biot-DY633 ($\tau = 0.6$ ns).*

4.3 FRET experiments

The biochemical FRET systems used in this work were the binding of biotin by streptavidin and a homogeneous sandwich immunoassay of HCG with two different IgG antibodies. The FRET experiments were performed on a modified KRYPTOR system, equipped with a well plate reader, using laser excitation at 315 nm (see Section 3). This wavelength was chosen in order to have a comparable extinction coefficient of the different donors and to avoid biomolecule absorption (cf. 4.1.2). Concerning the acceptors, all of them (especially QD655) are excited at this wavelength, and strong short-lived emission by direct acceptor excitation can be expected. For this reason, time gated (250 - 1000 μs for experiments with QD655 and 50 - 1000 μs for the others) donor emission intensities I_D at 545 ± 5 nm for Tb and 620 ± 5 nm for Eu as well as acceptor emission intensities I_A at 665 ± 5 nm were recorded. A ratiometric analysis, in which the acceptor signal is divided by the donor reference signal, was performed for concentration correction of the titration experiments and for suppression of laser intensity fluctuations.

4.3.1 Streptavidin-biotin FRET system

The streptavidin-biotin system is a good model for studying FRET in biological systems because it is well known and provides extremely strong binding properties (cf. Section 2.5.2). Using the calculated quantum yields Φ_{Ln} (Table 4.2), the normalized donor luminescence spectra $F_D(\lambda)$ (cf. Sections 4.1.2.2 and 6.3), the acceptor absorption spectra $\varepsilon_A(\lambda)$ (Figure 4.10), a refractive index of $n = 1.4$ for biomolecules in aqueous solution [10] and a dipole orientation factor of $\kappa^2 = \frac{2}{3}$ (considering a statistical distribution of the donor-acceptor dipoles within the luminescence decay time of the donor [24]), the Förster radii R_0 for the different donor-acceptor pairs can be calculated using Equations 2.3 and 2.5. Table 4.3 shows the Förster radii for all donor-acceptor pairs in the different solutions. It should be mentioned that the R_0 values in

Table 4.3: Förster radii R_0 (in Å) of all donor-acceptor pairs in different solutions.

	TbL-Strep			**EuL-Strep**			**Eu-TBP-Strep**		
Solution	QD	APC	DY	QD	APC	DY	QD	APC	DY
SA	98	71	55	84	76	61	85	78	63
SB	104	76	59	95	86	70	91	82	64
SC	95	69	54	83	76	61	83	75	61
SD	95	69	54	83	76	61	84	76	61
SE	102	75	58	95	86	70	91	83	65
SF	86	63	49	84	76	61	89	81	65
SG	97	71	55	95	86	70	91	83	65

QD is Biot-QD655, APC is Biot-APC and DY is Biot-DY633. Max. error for R_0 ca. ± 10 %.

SA and **SB** are theoretical values for Biot-QD655 as acceptors because they are not stable in water at low concentrations.
As a result of the high $\varepsilon(\lambda)$ for QD655 and the good spectral overlap with the lanthanide complexes, the R_0 values are considerably larger than the ones of APC or DY633, reaching ca. 100 Å in some cases. These values are even higher than the Förster radii of the Eu-TBP-APC

system under ideal conditions (approximately 90 Å in phosphate buffer) [181] and unbound donor-acceptor pairs (71 - 98 Å) [24]. Nevertheless, all donor-acceptor pairs possess large Förster radii compared to conventional donor-acceptor pairs (with distances ranging from 21 - 61 Å) [44] or pairs containing QD as donors (39 - 65 Å) [175, 177, 222].
The main focus of this work lies on FRET from Ln complexes to QD. For this reason the measuring solutions for the FRET experiments were chosen to yield the best performance for these donors and acceptors. Biot-QD655 are delivered with (and stored in) 50 mM borate buffer, pH 8.3, containing 2 % BSA and 0.05 % NaN_3 as a preservative (**SF**). The positive influence of KF on Ln luminescence was shown in Section 4.1.2. As Biot-QD655 are not stable in water at low concentrations, 50 mM borate buffer (**SC**) was chosen as solution without further additives to obtain "pure" conditions. The three used buffering media were **SC**, **SF** and **SG**(see Section 3).
For the purpose of comparison, two further acceptors were used besides Biot-QD655, namely Biot-APC and Biot-DY633. Among the various donor-acceptor couples with Ln complexes as donors, one of the most studied is probably that using Eu-TBP as donor and APC as acceptor [181, 223, 224]. Furthermore, this system can be found in commercialized applications (see e.g. Sections 2.5.1.2 and 2.3.3). Biot-DY633 was used as a common fluorescence dye among the acceptor species. Because this dye is commercially available but has not yet been extensively studied in the literature, it is an interesting candidate to be used in the FRET experiments. It should be mentioned that **SC**, **SF** and **SG** are not perfectly suited for these acceptors. Nevertheless, the solutions were used due to a better direct comparison with the Biot-QD655 systems.
The FRET experiments were realized by the stepwise addition of increasing acceptor amounts into a solution containing the donor in **SC**, **SF** and **SG**. Figure 4.14 shows a schematic representation of Ln-Strep titration by Biot-QD655.

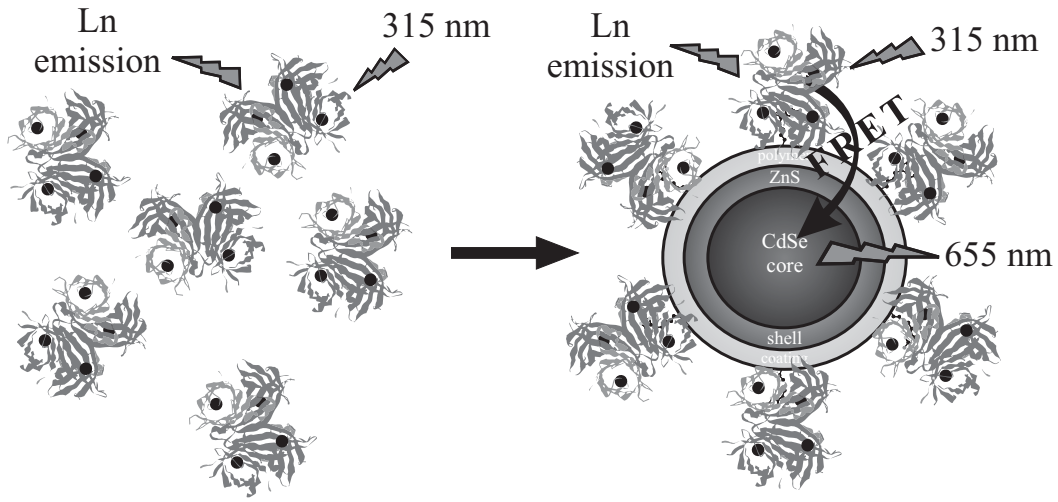

Figure 4.14: *Schematic representation of the FRET experiment between Ln-Strep and Biot-QD655. Ln-Strep before (left) and after addition of Biot-QD655, which results in a formation of a Ln-Strep-Biot-QD655 complex.*

For the analysis of the titration experiments, the normalized ratio $R_I = \frac{I_A}{I_D}$ was plotted against acceptor concentration. In order to follow the donor concentration decrease caused by dilution with the acceptor, a second x-coordinate with relative donor concentrations is also displayed.

By this means, it was possible to follow the entire kinetic evolution of the biochemical system at low concentrations of reactants (typically 10^{-10} M), and to monitor the influence of the constituents of the buffering media on the assay efficiency. Figure 4.15 represents the kinetic profiles observed for TbL-Strep-Biot-QD655 in **SG**. It appeared that at such low levels of streptavidin the assay took ca. five hours to be fully equilibrated.

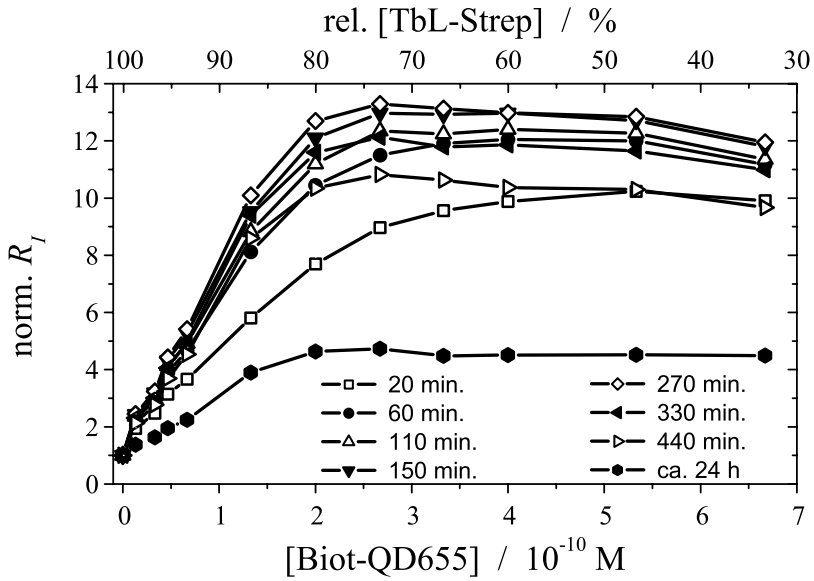

Figure 4.15: *Kinetic evolution of the normalized intensity ratio R_I as a function of [Biot-QD655] and relative [TbL-Strep](**SG**, initial concentration [TbL-Strep] = $1 \cdot 10^{-9}$ M).*

Similar results (see Figures 6.26 and 6.25) were found for Eu-TBP-Strep-Biot-QD655 (ca. 5 h) and EuL-Strep-Biot-QD655 (ca. 2 h; the shorter time could be due to the lower labeling ratio of EuL to streptavidin, which causes less interference of the label with the protein). This very slow kinetic equilibration was attributed to two reasons. The first one is the presence of large amounts of BSA, known to create non-specific binding with streptavidin [225]. Before the streptavidin-biotin recognition process can occur, the BSA must first be "peeled off" from streptavidin, a process which takes a few hours. The second reason has to be connected with Biot-QD655 because the slow equilibration was not examined with APC or DY633 as acceptor. Here the equilibration times were much shorter with ca. one hour for APC and approximately 15 - 30 minutes for DY633. These values lead to the conclusion that the size and rigidity of the acceptor play an important role. While the small Biot-DY633 can bind relatively quickly to streptavidin, the bigger biotinilated protein APC needs more time. The high amount of biotins (10-15) per APC and the flexibility of the disc shaped protein allow faster biotin binding to streptavidin than for Biot-QD655. The large and rigid Biot-QD655 therefore needs much longer for an equilibrated binding between biotin and streptavidin. However, these are possible conclusions and further investigations would be expedient for a more evident argumentation.

4.3.1.1 Biot-QD655 as acceptor

To compare the different conditions on the assay efficiency, solutions **SC**, **SF** and **SG** were investigated. Increasing amounts of Biot-QD655 were added to a stocksolution of Ln-Strep ([TbL-Strep] = $1 \cdot 10^{-9}$ M, [EuL-Strep] = [Eu-TBP-Strep] = $3 \cdot 10^{-9}$ M). To generate sufficient

and comparable emission signals, the concentrations of EuL-Strep, Eu-TBP-Strep and of Biot-QD655 (for titration to the Eu donors) had to be chosen three times higher than for TbL-Strep. The results obtained for the evolution of the normalized values of R_I as a function of added Biot-QD655 after the optimal equilibration time are displayed in Figures 4.16 and 4.17. Similar evolutions are observed inside **SF** and **SG**, with R_I increasing rapidly until the [Biot-QD655]/[Ln-Strep]-ratio reached a value of approximately $\frac{1}{6}$, in good agreement with the number of biotin molecules per QD (5 to 7). For larger [Biot-QD655], R_I remained stable at a plateau value. Noteworthy, the presence of KF in the assay (**SG**) significantly increased the measured intensity ratio, as expected on the basis of the observed influence of KF on the luminescence efficiency (cf. Section 4.1.2).

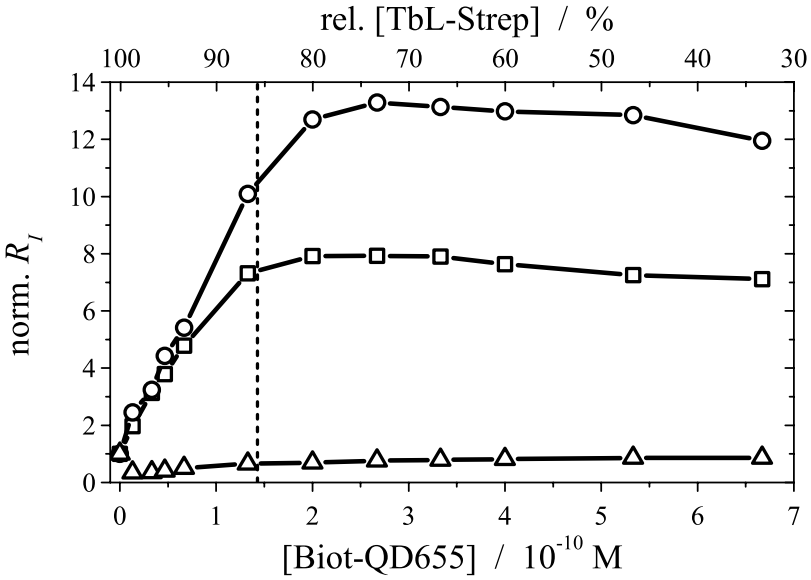

Figure 4.16: *Evolution of R_I as a function of [Biot-QD655] added to TbL-Strep in **SC** after ca. 7 hours incubation time (triangles), **SF** after ca. 5 hours (squares) and **SG** after ca. 4 hours (circles). Initial concentration [TbL-Strep] = $1 \cdot 10^{-9}$ M. The dotted line indicates a ratio of 6 TbL-Strep per Biot-QD655.*

For all three FRET systems, the strong increase of R_I with Biot-QD655 concentration was due to long-lived emission of Biot-QD655 (I_A), whereas the Ln emission (I_D) decreased with Ln-Strep concentration (see Figures 6.27 to 6.29). The decrease of I_D is directly proportional to [TbL-Strep], whereas it decreases more slowly for EuL-Strep. The reason for this behaviour is the three times larger Biot-QD655 concentration in the case of EuL-Strep as donor. Due to direct excitation of Biot-QD655, an extremely strong short-lived emission occurs, which can still be measured at longer delay times because of the high spectrometer sensitivity. In the case of Eu-TBP as donor, an almost 2-fold increase of I_D can be measured before it starts to decrease with Eu-TBP-Strep concentration. This effect is attributed to the streptavidin-biotin binding. The responsible mechanism is currently under investigation in our group [226].
A surprising result was observed for **SC**. In absence of BSA and NaN_3, the intensity ratio of the LnL containing donor-acceptor systems was observed to drop dramatically for the very first aliquots of added Biot-QD655 before it increased again. Careful examination of the data showed this drop to be due to a very large increase of the intensity of the LnL emission (I_D, cf. Figures 6.27 and 6.28). Regarding the negative impact of NaN_3 on the luminescence efficiency of TbL (cf. Figure 4.8), this behavior was tentatively attributed to the BSA present in Biot-QD655

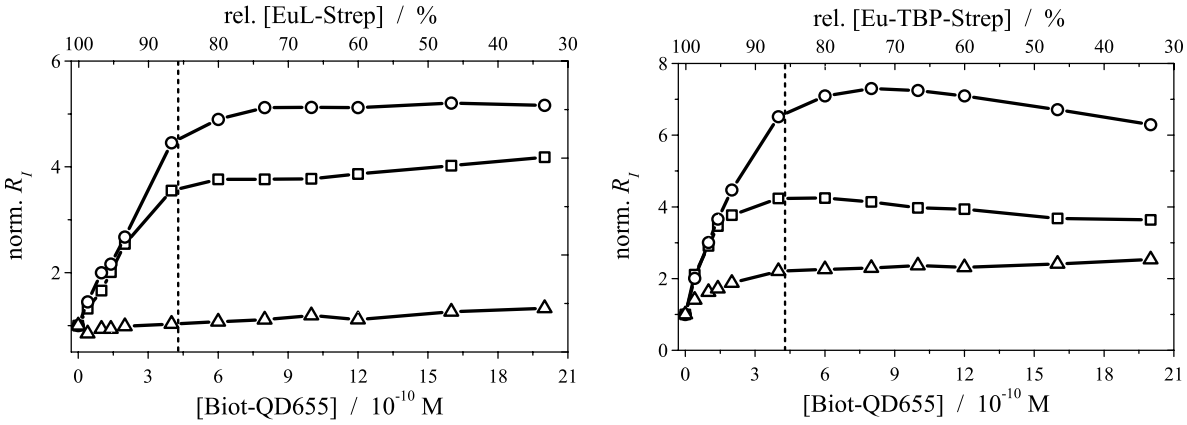

Figure 4.17: *Evolution of R_I as a function of [Biot-QD655] added to EuL-Strep (Eu-TBP-Strep) in **SC** after ca. 1 h (2 h) incubation time (triangles), **SF** after ca. 3.5 h (5.5 h)(squares) and **SG** after ca. 2 h (5.5 h) (circles). Initial concentrations [EuL-Strep] = [Eu-TBP-Strep] = $3 \cdot 10^{-9}$ M. The dotted line indicates a ratio of 6 EuL-Strep or Eu-TBP-Strep per Biot-QD655.*

buffer. To confirm this hypothesis, a titration was performed in which increasing amounts of BSA were added to a TbL-Strep or EuL-Strep containing solution. The results, displayed in Figure 4.18, showed that in both cases the lanthanide luminescence largely increased after an incubation time of 5 hours.

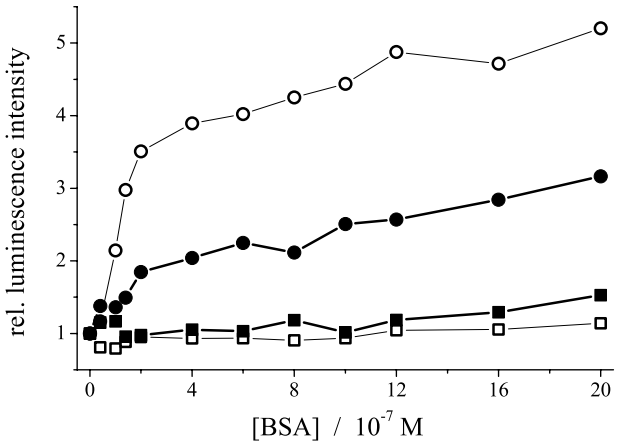

Figure 4.18: *Relative luminescence of EuL-Strep (full symbols) and TbL-Strep (hollow symbols) after 20 min. (squares) and 5 h (dots) incubation time as a function of [BSA]. [TbL-Strep] = $1 \cdot 10^{-9}$ to $3.4 \cdot 10^{-10}$ M and [EuL-Strep] = $3 \cdot 10^{-9}$ to $1 \cdot 10^{-9}$ M.*

This phenomenon was attributed to the use of polystyrene (PS) well plates in the measuring setup, where adsorption of proteins occurs due to hydrophobic binding. At such low concentrations (10^{-9} to 10^{-10} M), streptavidin is adsorbed to the PS walls of the well plate and addition of BSA allowed for desorption of the protein. In contrast, the phenomenon could not be observed for Eu-TBP-Strep (Figure 4.17), which was supplied in a BSA containing solution. This unambiguously corroborated the influence of BSA on the adsorption phenomena and justified the use of BSA in the assay.
In order to exclude that direct QD excitation or dynamic FRET is responsible for the R_I increase, control experiments with free lanthanide complexes (no streptavidin) were performed

(see Figures 6.30 to 6.32). Here only a weak increase of R_I with [Biot-QD655], resulting from a stronger decrease of I_D compared to I_A, could be observed. Thus, the strong increase of R_I with [Biot-QD655] is a clear evidence for FRET from the Ln donors to the QD acceptors.

Table 4.4: Luminescence decay times (τ), donor-acceptor distances (r), FRET rates (k_{ET}) and FRET efficiencies (η_{ET}) for the three Ln-Strep donors with Biot-QD655 as acceptor in solutions SF and SG.

	TbL-Strep		**EuL-Strep**		**Eu-TBP-Strep**	
Solution →	**SF**	**SG**	**SF**	**SG**	**SF**	**SG**
τ_D (μs)	620	1360	680	1400	1050 230	1100
τ_{DA} (μs)	410	440	490	680	400 90	700
r (Å)	95	87	100	95	83	101
k_{ET} (s^{-1})	830	1500	560	760	1550 7100	520
η_{ET} (%)	34	67	27	52	62	36

Experimental uncertainty for τ ca. ±5 % (ca. ±10 % for Eu-TBP-Strep in **SF**); calculated max. error for r, k_{ET} and η_{ET} ca. ±10 % (ca. ±15 % for Eu-TBP-Strep in **SF**). Incubation times: TbL-Strep in **SF** ca. 5 h and in **SG** ca. 4 h; EuL-Strep in **SF** ca. 3.5 h and in **SG** ca. 2 h; Eu-TBP-Strep in **SF** and in **SG** ca. 5.5 h.

In order to confirm this evidence, a luminescence decay time analysis was performed (considering multiple donor species, where more than one donor decay time was measured (cf. Equation 2.11)) for the measurements in **SF** and **SG**. The intrinsic Biot-QD655 decay is very prompt compared to the luminescence decay of the lanthanide ions. This means that the long-lived Biot-QD655 luminescence in the presence of Ln-Strep is due to the fraction x of the donor energy transferred to the acceptor, $x \cdot I_{DA}(r,t)$ (cf. Equation 2.12), characterized by a decay time $\tau_{DA} = \tau_{AD}$ (cf. Equation 2.9). The overall emission intensity in the acceptor channel $I_A(r,t)$ is the sum of the Biot-QD655 emission resulting from FRET, plus background emission $I_{BG}(t)$, emanating from non-transferring lanthanide donors (especially for europium), parasitic emission from the measurement apparatus (light scattering, fluorescence from the well plate reader), and from strong short-lived Biot-QD655 fluorescence which appears partly as pseudo long-lived component due to a short-time-scale saturation of the photomultipliers (working at 1.2 kV).

$$I_A(r,t) = I_{BG}(t) + xI_{DA}(r,t) \tag{4.3}$$

From the measurement of $I_{BG}(t)$ obtained in absence of the acceptor, $I_A(r,t)$ allowed for fitting of the donor-acceptor distance r and then for calculation of the energy transfer rates k_{ET_i}, for the decay times τ_{DA_i} of each donor in the presence of the acceptor, as well as for the FRET efficiency η_{ET} using Equations 2.2, 2.6 and 2.9. The results are summarized in Table 4.4.
Compared to pure Biot-QD655, the luminescence decay times in presence of the donors (τ_{DA})

are more than 1000-fold increased (cf. Figure 4.12). This is another strong evidence for QD655 FRET sensitization by the Ln complexes. The resulting average donor-acceptor distances are in the range of 83 - 101 Å, which is in good agreement with the binding model depicted in Figure 4.14, with the structural parameters of Biot-QD655 (ellipsoidally shaped with 100 - 120 Å length along the main axis - cf. Figure 4.9), and with streptavidin in the solid state (54 x 58 x 48 $Å^3$) [192]. A noticeable exception arose with Eu-TBP-Strep in absence of KF (**SF**), where a shorter 83 Å distance is observed. In that case, the charged Eu complexes may provide particular electrostatic interactions with Biot-QD655 that shortened the distance.
For LnL-Strep the best FRET efficiencies could be achieved in **SG** because of both higher Förster radii and energy transfer rates. For Eu-TBP-Strep the optimal FRET efficiency is accomplished in **SF**, mainly because of the shorter average donor-acceptor distance compared to **SG**.

4.3.1.2 Biot-APC and Biot-DY633 as acceptors

To compare the results obtained for Biot-QD655, the measurements were repeated with Biot-APC and Biot-DY633 as acceptors. The concentrations of donors and acceptors were the same as for the Biot-QD655 experiments with the exception of a 5-fold higher Biot-DY633 concentration, which was chosen due to the lower labeling ratio of DY633 to biotin (1:1). The results obtained for the evolution of R_I as a function of added acceptor are displayed in Figures 4.19 to 4.21. The graphs for the intensity functions (I_A and I_D) and for the control experiments can be found in Figures 6.33 to 6.38 and Figures 6.39 to 6.41, respectively.

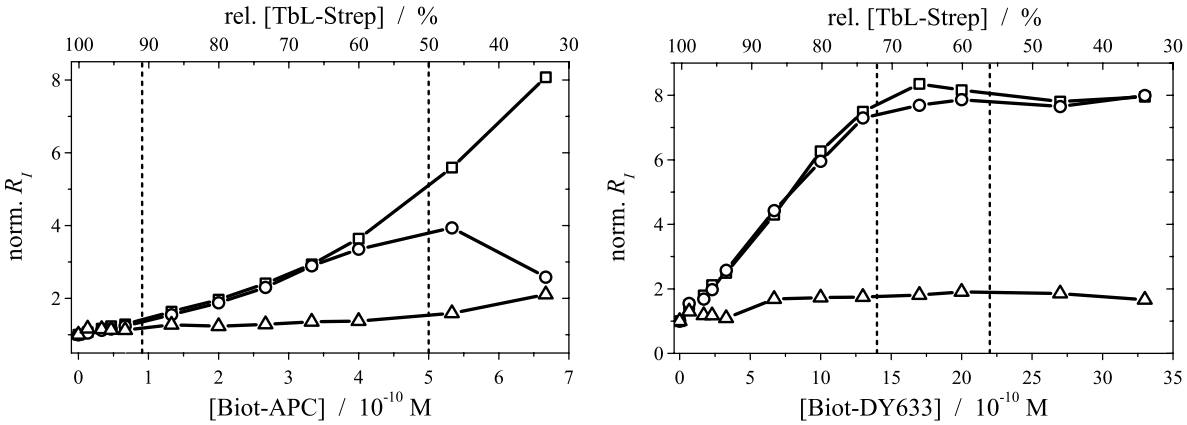

Figure 4.19: *Evolution of R_I as a function of [Biot-APC] ([Biot-DY633]) added to TbL-Strep in **SC** after ca. 1 h (1 h) incubation time (triangles), **SF** after ca. 2 h (1 h) (squares) and **SG** after ca. 2 h (1 h) (circles). Initial concentration [TbL-Strep] = $1 \cdot 10^{-9}$ M. The dotted lines indicate a ratio of 1 (at 50 % [TbL-Strep]) and 10 TbL-Strep per Biot-APC as well as 0.25 (at ca. 56 %) and 0.5 TbL-Strep per Biot-DY633.*

Concerning the measuring medium conditions, nearly the same results as for the Biot-QD655 systems could be observed. For all donor-acceptor systems **SC** gives the worst results without sufficient evidence for a FRET process occuring under these conditions. The positive influence of KF on the assays can only be monitored for Eu-TBP-Strep, whereas for both TbL-Strep and EuL-Strep, **SF** and **SG** lead to approximately the same results. Nevertheless, FRET is obvious for all donor-acceptor pairs in **SF** and **SG**, which is confirmed by the increasing R_I

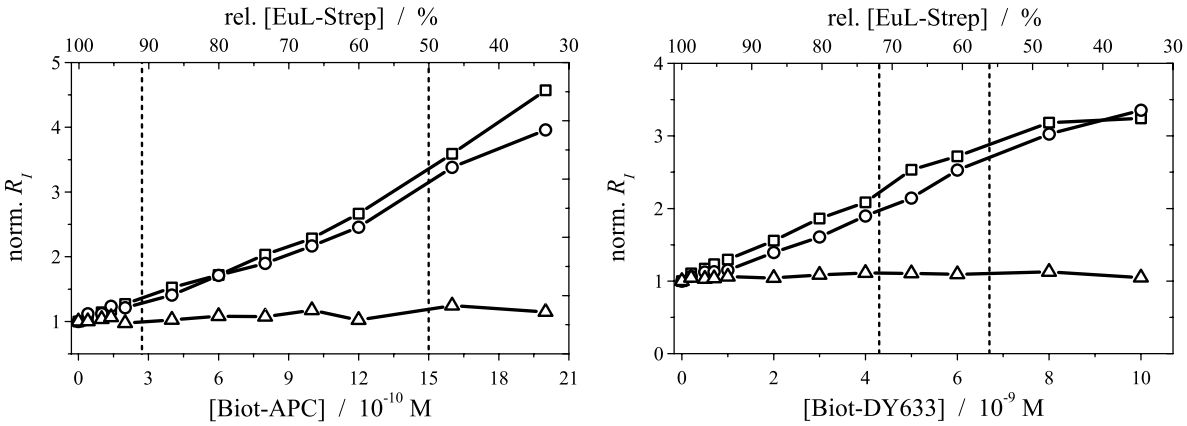

Figure 4.20: *Evolution of R_I as a function of [Biot-APC] ([Biot-DY633]) added to EuL-Strep in* ***SC*** *after ca. 1 h (1 h) incubation time (triangles),* ***SF*** *after ca. 1 h (1 h) (squares) and* ***SG*** *after ca. 2 h (1 h) (circles). Initial concentration [EuL-Strep] = $3 \cdot 10^{-9}$ M. The dotted lines indicate a ratio of 1 (at 50 % [EuL-Strep]) and 10 EuL-Strep per Biot-APC as well as 0.25 (at ca. 56 %) and 0.5 EuL-Strep per Biot-DY633.*

over acceptor concentration. This could not be observed for the free donors in the control experiments.

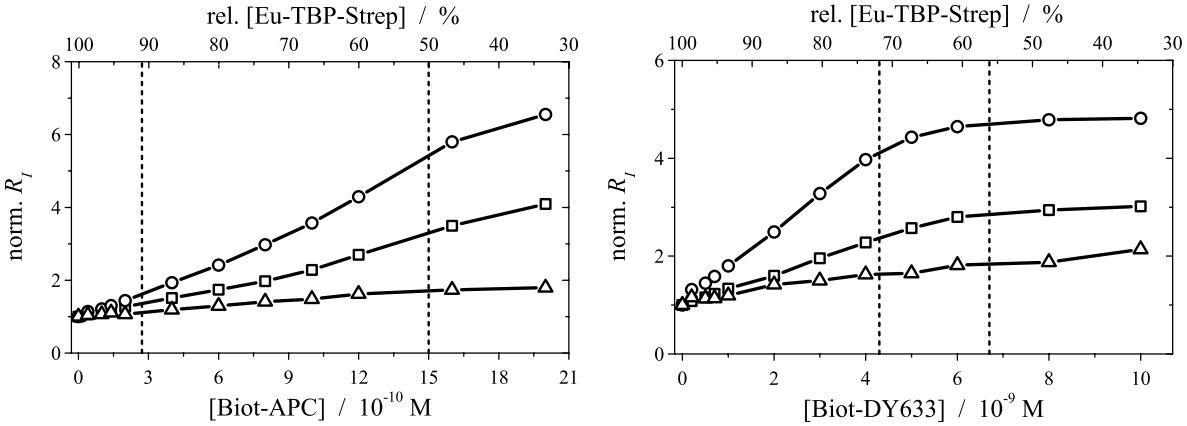

Figure 4.21: *Evolution of R_I as a function of [Biot-APC] ([Biot-DY633]) added to Eu-TBP-Strep in* ***SC*** *after ca. 1 h (1 h) incubation time (triangles),* ***SF*** *after ca. 2 h (1 h) (squares) and* ***SG*** *after ca. 2 h (1 h) (circles). Initial concentration [Eu-TBP-Strep] = $3 \cdot 10^{-9}$ M. The dotted lines indicate a ratio of 1 (at 50 % [Eu-TBP-Strep]) and 10 Eu-TBP-Strep per Biot-APC as well as 0.25 (at ca. 56 %) and 0.5 Eu-TBP-Strep per Biot-DY633.*

For Biot-DY633, R_I increases until the [Biot-DY633]/[Ln-Strep]-ratio reaches a value of approximately 2 to 4 and for larger [Biot-DY633], R_I remains stable to a plateau value. This indicates that all four biotin binding sites of streptavidin might be accessible for the relatively small Biot-DY633. Regarding Biot-APC, a plateau of stable R_I at higher Biot-APC concentrations is not reached for any of the donor-acceptor systems. However, the intensity I_A (Figures 6.36 to 6.38) levels off at a [Biot-APC]/[Ln-Strep] value of ca. 1. Due to the decrease of I_D, this cannot be monitored in the ratiometric analysis. The concentration range

of Biot-APC was chosen similar to that of Biot-QD655. Unlike the rigid nanocrystal acceptor, where approximately six streptavidin molecules bind to one Biot-QD655, Biot-APC seems to be very flexible. Hence, more than one binding site of streptavidin is accessible for Biot-APC. On the other hand, the 10 - 15 biotins per APC neither bind more than one streptavidin nor do they bind to more than one biotin binding site of the same streptavidin, because this would lead to a plateau at much lower Biot-APC concentrations.
Comparing the different donor-acceptor species, it becomes obvious that the Biot-QD655 systems have a much steeper rising intensity ratio, whereas the others are rather flat. Even for the often analytically applied and very sensitive Eu-TBP-APC system, comparable results could not be obtained. Another striking point is the necessary use of BSA inside the assays because all measurements within BSA free solutions (**SC**) lead to poor results. Having a high amount of 2 % BSA inside the assay leads to stable non-specific binding conditions within the biological medium as well as at the PS walls of the multiwell plate.

4.3.1.3 Detection limits

An important value for immunoassays is the limit of detection (LOD - Equation 2.48), which is three times the standard deviation of the blank sample devided by the slope of the signal over concentration curves. For comparison, the detection limits of all donor-acceptor systems inside **SF** and **SG** were calculated using the linear parts at low acceptor concentrations of the R_I curves. All LOD (calculated with 10 measurements for σ_0) are displayed in Table 4.5.

Table 4.5: LOD (in 10^{-12} M) of the different donor-acceptor systems.

	TbL-Strep		**EuL-Strep**		**Eu-TBP-Strep**	
Solution →	**SF**	**SG**	**SF**	**SG**	**SF**	**SG**
Biot-QD655	1.6	1.2	12	8.0	4.0	2.6
Biot-APC	15	14	63	54	59	19
Biot-DY633	14	13	250	230	210	54

Experimental uncertainty ca. ±50 %.

Regarding the LOD values, the advantage of using QD as FRET acceptors is obvious. The TbL-Strep-Biot-QD655 system has a more than 10-fold LOD improvement compared to the Eu-TBP-Strep-Biot-APC "gold standard". EuL-Strep provides the highest LOD, which is probably caused by the lower labeling ratio compared to the other donors. Generally, the detection limit is lowest for Biot-QD655, followed by Biot-APC and Biot-DY633. In contrast to the FRET systems using Eu donors, TbL-Strep-Biot-DY633 has the same LOD as TbL-Strep-Biot-APC. Looking at the Förster radii (Table 4.3), this is quite surprising because they are significantly larger for the Eu systems. A reason for the better sensitivity could be the higher overall quantum yield of TbL compared to EuL and Eu-TBP (quantum yields in pure water at 300 K: $\Phi_{tot}^{TbL} = 0.31, \Phi_{tot}^{EuL} = 0.08, \Phi_{tot}^{Eu-TBP} = 0.02$ [35, 86]). This allows for a higher total brightness of the sample, which has no effect on FRET efficiency but on the signal intensity (cf. Section

2.3.2). Thus, lower concentrations can be measured under the same experimental conditions. Regarding the FRET assay experiments, the best donor-acceptor system is the one of TbL-Strep with Biot-QD655. To optimize the LOD, the experiments for this donor-acceptor pair were repeated in **SE**, which does not contain NaN_3 and should therefore be the optimum solution. The titration experiment was performed with more measuring points in the lower concentration range because this part is used as linear part for the LOD analysis. Moreover, the storage conditions between the measurements were optimized for less sample evaporation and a laser system with much lower background emission and higher pulse to pulse stability could be used (laser system 2 instead of system 1 - cf. Section 3.3.2). The results are displayed in Figure 4.22.

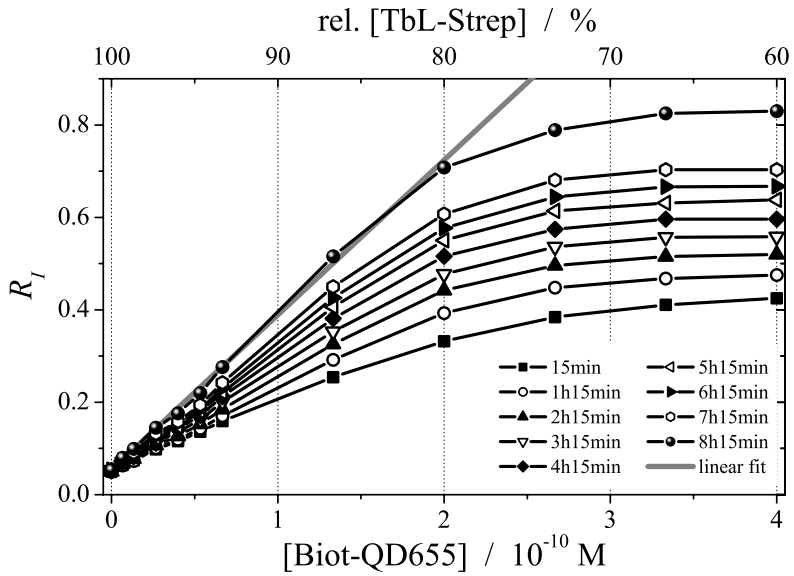

Figure 4.22: *Kinetic evolution of the intensity ratio R_I as a function of [Biot-QD655] and relative [TbL-Strep](**SE**, initial concentration [TbL-Strep] = $1 \cdot 10^{-9}$ M). A linear fit for LOD calculation is displayed in grey.*

Having improved the evaporation conditions for the samples and using the azide free measuring solution, the equilibration of the system takes even longer than before. The intensity ratio over [Biot-QD655] after ca. 8 hours incubation time shows a steep increase with excellent linearity up to a concentration of $2 \cdot 10^{-10}$ M Biot-QD655. For higher concentrations R_I is stable at a plateau value. The detection limit (with 12 measurements for σ_0) was improved by one order of magnitude to LOD = $1.2 \cdot 10^{-13}$ M Biot-QD655. Further improvement should be possible by optimizing the detection setup and careful examination of excitation wavelength and intensity as well as donor-acceptor concentrations.

4.3.2 HCG FRET immunoassays

Biotin-streptavidin binding is an excellent model for demonstrating FRET under physiological conditions. Nevertheless, there is no direct application for this system. In order to analyze the donor-acceptor properties in a real immunoassay, the IgG-HCG system (e.g. applied as pregnancy test) was used as a model and the first TbL to QD655 FRET experiments with this system are presented in this section.
Biotin, as well as streptavidin, can be coupled to antibodies or antigens [96, 195–197]. One

method for creating a FRET immunoassay would be an indirect labeling of antibody and antigen via biotin or streptavidin. Especially for streptavidin and QD the biological FRET system would be relatively large and a direct labeling of donor and acceptor would be preferable. QD655 is commercially available with a maleimide activated surface. Hence, direct QD655 labeling to the antibody hinge region can be performed, leading to two half antibodies with one QD655 each (cf. Section 2.5.3). For the donor side, sulfo-NHS activated TbL was coupled to lysine groups of HCG and IgG antibodies. In contrast to the maleimide activated labeling, where the label is positioned at the hinge region of the antibody, labeling to lysine could be achieved at almost any position of the antibody, depending on the number of accessible lysine groups. Labeling ratios of 2.1 TbL/IgG and 0.4 TbL/HCG were obtained by UV/Vis absorption measurements (see Figure 4.3). The following labeled biomolecules were used for immunoassay experiments:
TbL-HCG: HCG (human chorionic gonadotropin) labeled with an average number of 0.4 TbL.
TbL-B24BF10: Monoclonal anti-HCG mouse-IgG antibodies (B24BF10 [199]) labeled with an average number of 2.1 TbL.
QD655-B20CA2: Monoclonal anti-HCG mouse-IgG half antibodies (B20CA2 [199]) labeled with an average number of 1.0 QD655.
B24BF10 and B20CA2 are specific anti-HCG antibodies which bind to opposite sides of HCG as depicted in Figure 4.23. They belong to the class of proteins known as immunoglobulins (in this case immunoglobulin G - IgG) and have a molecular weight of approximately 150 kDa. The glycoprotein HCG is the analyte to be detected and has a molecular weight of ca. 40 kDa. Two kinds of experiments were performed. The first one is based on a sandwich immunoassay, where FRET should occur between TbL-B24BF10 and QD655-B20CA2 by binding to opposite regions of free HCG (see Figure 4.23). A very long donor-acceptor distance is possible especially in this case, because the antibodies (with an approximate diameter of 10 nm) were optimized to bind to opposite sides of HCG, which has ca. 6 nm diameter. Moreover, the binding region of TbL on B24BF10 is unknown, as there are several lysine groups available on the IgG antibody [198]. This leads to conjugates with a distribution of attachment sites, some of which may be located close to the antigen binding site, decreasing the affinity of the antibody [227]. Regarding a labeling ratio of 2.1 TbL/IgG, a decreased affinity is not expected. For Eu chelate labeling, immunoreactivity of IgG can still be observed at high labeling ratios of 20 or more [228].

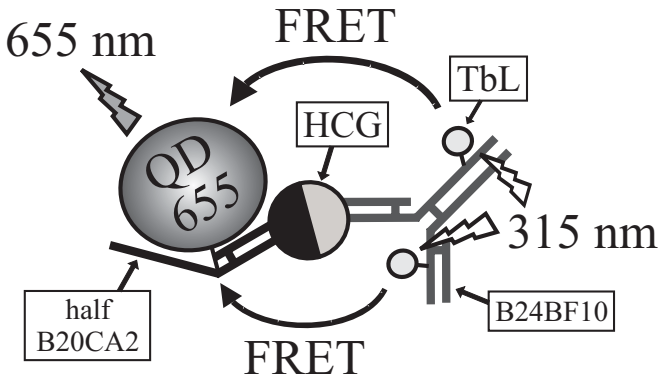

Figure 4.23: *Schematic representation of IgG-HCG-IgG FRET sandwich immunoassay with TbL labeled to one IgG antibody and QD655 labeled to the other.*

In order to overcome long distance problems, the second experiment is based on FRET from TbL-HCG to QD655-B20CA2. This system could be used in a competitive assay with free

HCG. Unfortunately, the labeling ratio was very low in this case with 0.4 TbL/HCG, which could also result in low FRET signals.
For the sandwich immunoassay, the HCG concentration in the multiwells was increased from 0 to 1000 ng/ml (0 to $2.5 \cdot 10^{-8}$ M) in a BSA containing solution with antibody concentrations of ca. $1 \cdot 10^{-7}$ M (15 μg/ml IgG) TbL-B24BF10, corresponding to ca. $2 \cdot 10^{-7}$ M TbL (a 10-fold lower concentration was also tested) and $2 \cdot 10^{-9}$ M (150 ng/ml half-IgG) QD655-B20CA2, corresponding to $2 \cdot 10^{-9}$ M QD655. Hence, an excess of donor antibodies is always present in the solutions and a signal increase due to FRET should be expected from 0 to 2 nM HCG (2 nM acceptor antibodies in the solution). In order to learn about this new type of immunoassay, the analyte (HCG) concentration range was chosen relatively large (compared to the small acceptor concentration) in these first experiments. To find out about the origin of the luminescence signals (FRET-signal or direct donor and acceptor signal, respectively) two control measurements with only one of both antibodies inside the solution were performed. A time delay of 0.3 ms and a gate time of 1.2 ms were used for the analysis of the obtained time-resolved luminescence signals. However, the results obtained with this assay were quite dissatisfying. Regarding Figure 4.24, an increase of the long-lived acceptor channel signal (I_A) can be measured at low concentrations which cannot be found for the control experiment without QD in the assay (the second control experiment is not shown because the signals without TbL inside the assay were negligibly low). Although the TbL concentration was equal for all the different analyte concentrations, a signal increase can also be found in the donor channel (I_D).

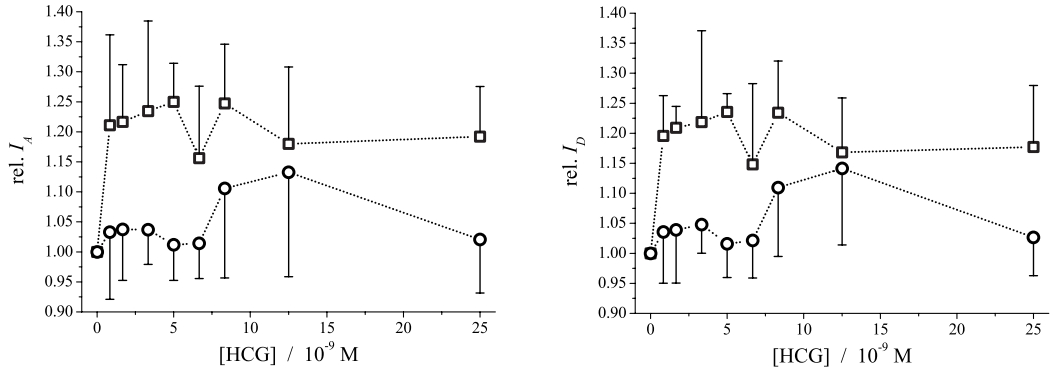

Figure 4.24: *Relative luminescence signals (delay: 0.3 ms, gate: 1.2 ms) in the acceptor channel (I_A) and the donor channel (I_D) as a function of [HCG]. Results for the sandwich immunoassay are displayed as squares, for the control experiment (no QD655-B20CA2 in the assay) as circles. For better illustration, error bars (3 times standard deviation of 5 measurements) are displayed in only positive or negative direction.*

In the ratiometric analysis (R_I) this leads to a very small difference between assay and control experiment and no evidence for FRET between TbL and QD655 can be concluded (see Figure 4.25).
The direct FRET immunoassay between TbL-HCG and QD655-B20CA2 leads to more promising results. Here, increasing concentrations of QD655-B20CA2 (0 - $6.7 \cdot 10^{-9}$ M) in a BSA containing solution with ca. $2 \cdot 10^{-8}$ M TbL-HCG (corresponding to ca. $1 \cdot 10^{-8}$ M TbL) were measured. As not all HCG are labeled with TbL (0.4 TbL/HCG), a 3-fold higher HCG concentration compared to the highest QD655-B20CA2 concentration was chosen. In a control

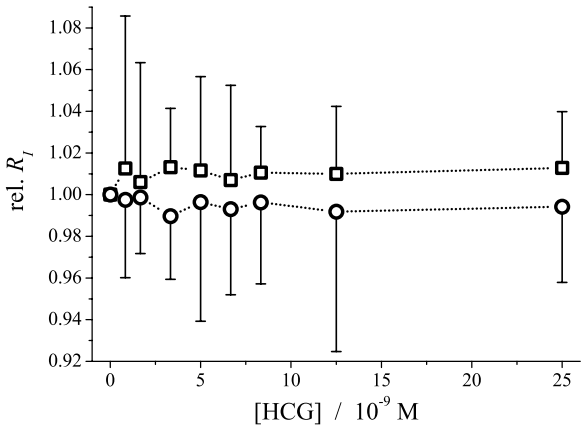

Figure 4.25: *Relative ratio (R_I) of I_A and I_D as a function of [HCG]. Results for the sandwich immunoassay are displayed as squares, for the control experiment (no QD655-B20CA2 in the assay) as circles. For better illustration, error bars (3 times standard deviation of 5 measurements) are displayed in only positive or negative direction.*

experiment, free HCG was present in the solution instead of TbL-HCG. Regarding Figure 4.26, I_A increases with QD655-B20CA2 concentration.

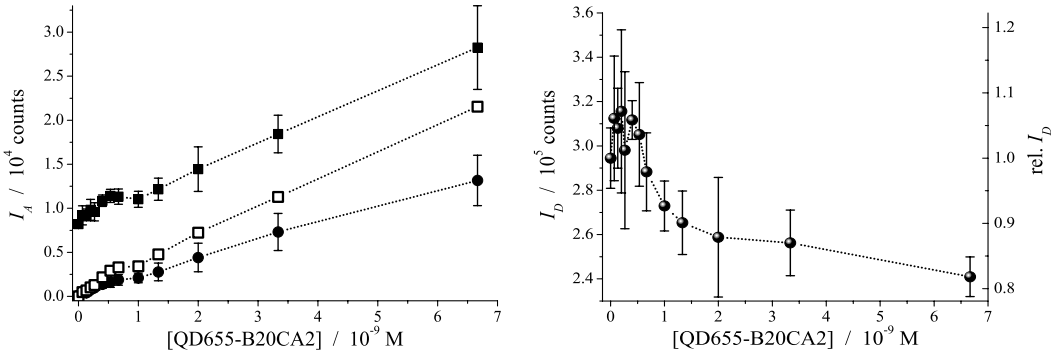

Figure 4.26: *Long-lived luminescence signals (delay: 0.3 ms, gate: 1.2 ms) in the acceptor channel (I_A) and the donor channel (I_D) as a function of [QD655-B20CA2]. Left: I_A for the FRET immunoassay (TbL-HCG-QD655-B20CA2) displayed as squares, open squares represent the TbL background corrected signal; control experiment (HCG-QD655-B20CA2) displayed as dots. Right: absolute and relative I_D for the direct immunoassay. Error bars represent 3 times standard deviation of 5 measurements.*

An increase can also be monitored for the control experiment due to very strong short-lived QD655 luminescence (direct QD655 excitation) still present at longer delay times at higher concentrations (cf. Section 4.3.1.1). Nevertheless, this increase is weaker and another evidence for FRET can be measured in the donor channel (I_D), where the long-lived TbL luminescence intensity decreases with increasing QD655-B20CA2 concentration, although the TbL-HCG concentration is equal for the whole experiment. Correcting I_A for the TbL background measured within the acceptor channel (I_A at [QD655-B20CA2] = 0 multiplied by the relative TbL emission (rel. I_D)), the steeper rising slope of I_A becomes obvious and the FRET intensity can be calculated by subtraction of the two I_A for the assay and the control experiment as displayed in Figure 4.27.

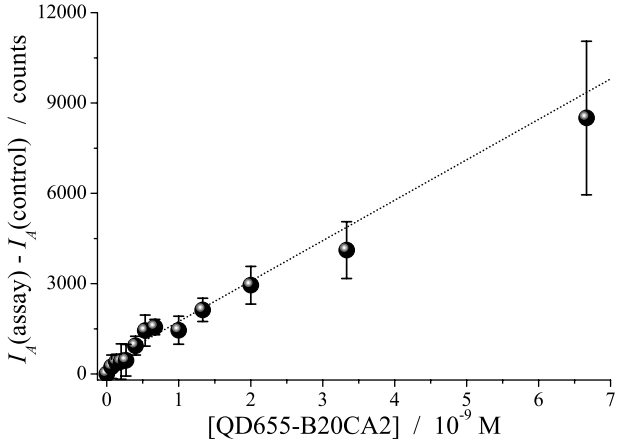

Figure 4.27: *FRET luminescence signal (delay: 0.3 ms, gate: 1.2 ms) in the acceptor channel (I_A) as a function of [QD655-B20CA2] and a linear fit (dotted line). Error bars represent 3 times standard deviation of 5 measurements.*

The increasing signal over QD655-B20CA2 concentration gives good evidence for FRET occurring between TbL and QD655 in this system. The linear fit displayed in the graph shows that the signal is not linear over the complete concentration range and starts to level off for higher concentrations, as it was found for the FRET experiments with biotin and streptavidin.
In conclusion these preliminary HCG assay experiments show the possibility of FRET between Ln complexes and QD in real life immunoassays, which are used for in vitro diagnostics. Nevertheless, further investigations have to be done to improve the experiments in order to get a highly sensitive immunoassay with low detection limit, as demonstrated for the biotin-streptavidin FRET system. Moreover, one of the well established FRET immunoassay with the Eu-TBP-APC donor-acceptor pair should be used in order to have the same direct comparison as for the Biot-Strep system.

Chapter 5

Summary and outlook

In this work the possibility of using quantum dot semiconductor nanocrystals (QD) as very efficient Förster resonance energy transfer (FRET) acceptors in combination with lanthanide (Ln) complexes as donors in biochemical systems is demonstrated with time-resolved laser spectroscopy experiments. The necessary theoretical and practical background of FRET, Ln complexes, QD and the applied biochemical models is outlined. In addition, scientific as well as commercial applications are presented.
Three Ln complexes (one with Tb^{3+} and two with Eu^{3+} as central ion) are used as FRET donors. TbL and EuL were synthesized at the Laboratoire de Chimie Moléculaire (CNRS - Strasbourg, France) whereas Europium tris(bipyridine) (Eu-TBP) is a commercial Ln complex distributed by CIS bio International (Bagnols-sur-Cèze, France). As a counterpart to these donors, three commercially available FRET acceptors are chosen. CdSe/ZnS core/shell QD emitting at 655 nm (QD655) are distributed by Invitrogen Corporation (Carlsbad, California, USA). The luminescent crosslinked biliprotein APC, which is used together with Eu-TBP in a commercial FRET immunoassay, can be purchased from various companies (e.g. Invitrogen Corporation). The organic fluorescence dye DY633 is distributed by Dyomics GmbH (Jena, Germany).
The very strong and well characterized binding process between streptavidin (Strep) and biotin (Biot) is used as a biomolecular model system. A FRET system is established by Strep conjugation with the donors and Biot conjugation with the acceptors. FRET occurs at distances ranging from ca. 1 to 10 nm, which corresponds very well to the donor-Strep to Biot-acceptor binding. In order to transfer this model system to a real-life in vitro diagnostic application, two kinds of immunoassays are investigated using human chorionic gonadotropin (HCG) as analyte. HCG itself, as well as two monoclonal anti-HCG mouse-IgG antibodies are labeled with TbL and QD655, respectively.
Bioconjugation of Strep with Ln complexes and HCG as well as IgG antibodies with TbL is described and analyzed by UV/Vis absorption spectroscopy and MALDI-TOF mass spectrometry. UV/Vis measurements of the conjugated complexes and comparison with a linear combination of their single constituents (e.g. TbL-Strep vs. linear combinaton of free TbL and unconjugated Strep) revealed average labeling ratios between 1 and 10 Ln complexes per Strep, depending on the Ln complex and on the labeling procedure. Labeled and unlabeled Strep were also analyzed by MALDI-TOF spectrometry confirming the ratios observed by UV/Vis measurements. For the immunoassay conjugates, average ratios of 2 TbL per IgG and 0.4 TbL per HCG are obtained.
Photophysical characterization of Ln-Strep conjugates and free Ln complexes is performed by

UV/Vis absorption as well as steady-state and time-resolved luminescence spectroscopy. Special attention is paid to the influence of different additives in aqueous solutions, namely borate buffer, potassium fluoride (KF), bovine serum albumin (BSA) and sodium azide (NaN_3). The impact on the donor properties is followed by fine-splitting analysis of the Ln Stark levels, which are sensitive to the surrounding medium. Eu-TBP and Eu-TBP-Strep show the strongest sensitivity to the different medium conditions followed by EuL and EuL-Strep and the relatively insensitive TbL and TbL-Strep. The luminecence decay times of the different donors are also influenced by the solution conditions. Decay times ranging from 600 to 2400 μs for TbL (or TbL-Strep), 600 to 1400 μs for EuL (or EuL-Strep) and 200 to 1200 μs for Eu-TBP (or Eu-TBP-Strep) are found with the Eu-TBP complexes showing bi-exponential decay behavior in some cases. The positive influence of the lanthanophilic KF, which replaces water molecules from the first Ln coordination sphere with fluoride anions, becomes obvious and the average number of water molecules for each Ln complex is calculated. Quantum yields of Ln centered luminescence, which are especially important for FRET calculations, are obtained by means of the measured luminescence kinetics. The donor quantum yields range from 0.2 to 0.8 for TbL (or TbL-Strep), 0.2 to 0.6 for EuL (or EuL-Strep) and 0.2 to 0.7 for Eu-TBP (or Eu-TBP-Strep).

The acceptors, which were purchased in both the free and biotinylated forms, are photophysically characterized by UV/Vis absorption and steady-state and time-resolved luminescence spectroscopy. All of them display very high extinction coefficients and a broad absorption spectrum. Biot-QD655 have the highest extinction values over the broadest wavelength range, which makes them ideally suited as FRET acceptors. The emission spectra are very similar, all with strong peaks between 650 and 660 nm and 30 to 40 nm full width at half maximum (FWHM). Acceptor emission can be well separated from the donor luminescence, which is only very weak in this region. Luminescence decay times are 1.5 ns for Biot-APC, 0.6 ns for Biot-DY633 and multiexponential with 23 ns, 47 ns and 160 ns for Biot-QD655, due to the QD size distribution and their anisotropy. Unlike the relatively small DY633 molecule (with 0.2 ns decay time), the other unbiotinylated acceptors show the same decay times as the Biot conjugates, which points out the weak influence of the small Biot molecule on the large APC protein and QD655 nanocrystal.

For the Strep-Biot FRET experiments, the Förster radii of the different donor-acceptor pairs are calculated. They range from ca. 50 Å for the TbL-DY633 pair to approximately 100 Å for TbL-QD655. Due to QD655 instability at low concentrations, FRET measurements are carried out in borate buffer with the additives mentioned above. Biot-acceptor is added to donor-Strep solutions and the measured time-resolved luminescence signals of donors and acceptors are analyzed. Donor and acceptor concentrations were in the 10^{-9} to 10^{-12} M range. In further experiments Biot-acceptors are added to free donor solutions for exclusion of dynamic energy transfer by freely diffusing donors and acceptors. The FRET systems using QD655 as acceptors, have long equilibration times of up to 8 hours, which can be attributed to non-specific binding of Ln-Strep to BSA and the rigidity of the large Biot-QD655 because the equilibration times are shorter for APC and DY633 as acceptors. For all donor-acceptor pairs, FRET is demonstrated by an increase of the long-lived acceptor emission signal measured by delayed detection in order to suppress background autofluorescence and emission from directly excited acceptors. For further evidence, a luminescence decay time analysis of the QD655 FRET systems is presented, showing a more than 1000-fold increased FRET sensitized Biot-QD655 decay time compared to pure Biot-QD655. FRET efficiencies between 30 and 70 % are calculated for the Ln-Strep-Biot-QD FRET systems with average donor-acceptor distances of 80 to 100 Å in

good agreement with the structural parameters of the FRET systems. The results show that QD655 can be very efficiently used as FRET acceptors. A more than 10-fold limit of detection (LOD) decrease compared to the extensively characterized and frequently used Eu-TBP-APC donor-acceptor pair is demonstrated for TbL-QD655 in the Biot-Strep FRET system. A sub-picomolar LOD for Biot-QD655 is achieved with TbL-Strep as donor in azide free borate buffer (pH 8.3) containing 2 % BSA and 0.5 M KF.

With the goal of showing the feasibilty of using the TbL-QD655 donor-acceptor pair for real-life immunoassays, first experiments with two kinds of HCG FRET assays are presented. For the sandwich immunoassay in which HCG is added to a stock solution of two different HCG specific antibodies labeled with TbL and QD655, respectively, only small differences between the TbL-IgG-HCG-IgG-QD655 model and the two control experiments (one without TbL and the other without QD655) are obtained. Hence, no evidence for FRET becomes obvious in this system. However, the average labeling ratios of 2 TbL per IgG and 1 QD655 per IgG are quite low and the large sandwich system with antibodies of ca. 10 nm and HCG of approximately 6 nm in diameter may lead to long donor-acceptor distances. This means that even the small increase of long-lived acceptor luminescence could point to the possibility of efficient FRET in this system, once the donor and acceptor concentrations and labeling conditions have been optimized. This perspective is further underlined by the direct TbL-HCG-IgG-QD655 assay results. Here, even with the very low labeling ratio of 0.4 TbL per HCG (in average), the increase of FRET sensitized QD luminescence is more obvious than for the sandwich assay and gives good evidence for FRET from TbL to QD655. Nevertheless, also for this assay the conditions have to be improved and the results show that a thorough investigation and several further experiments are necessary until a sensitive real-life FRET immunoassay with TbL and QD655 will be available. One of the well established FRET immunoassay with the Eu-TBP-APC donor-acceptor pair should be used in order to have the same direct comparison as for the Biot-Strep system.

Another very promising aspect of QD, which is not discussed in this work, is multiplexing analysis. Due to their broad absorption spectrum, several QD of the same material but different size can be excited by a single excitation source (with the same wavelength) and luminescence at different wavelengths depending on the QD size can de detected. Multiplexed FRET with four different QD as donors and a single acceptor has already been successfully performed [177]. In principle, the reverse format using one single Ln donor and several different QD as acceptors should also be possible, which offers very interesting perspectives, such as generating high sensitivity immunoassays with muliplexing analysis of several diagnostic markers in one sample. However, the health care market and the public demand for better and faster chemical and biological diagnostics as well as medical treatment are ever increasing. FRET spectroscopy using Ln complexes and QD can be an efficient tool in these fields, with the possibility of quantitative long-distance measurements due to Förster radii reaching 100 Å. These perspectives should motivate and stimulate further research in this interesting scientific area.

Chapter 6

Appendix

6.1 Fundamental constants

Symbol	Name	Numerical value
e	Electron charge	$1.60218 \cdot 10^{-19}$ C
m_e	Electron mass	$9.10938 \cdot 10^{-31}$ kg
m_p	Proton mass	$1.67262 \cdot 10^{-27}$ kg
ε_0	Permittivity of free space	$8.85419 \cdot 10^{-12}$ Fm^{-1}
c	Speed of light in vacuum	$2.99792 \cdot 10^{8}$ ms^{-1}
h	Planck's constant	$6.62607 \cdot 10^{-34}$ Js
$\hbar$	Planck's constant/2π	$1.05457 \cdot 10^{-34}$ Js
N_A	Avogadro's number	$6.02214 \cdot 10^{23}$ mol^{-1}
k	Boltzmann constant	$1.38065 \cdot 10^{-23}$ JK^{-1}

6.2 Abbreviations

A	acceptor
APC	crosslinked allophycocyanin
Asn	asparagine
Asp	aspartate
B20CA2	monoclonal anti-HCG mouse IgG (different from B24BF10)
B24BF10	monoclonal anti-HCG mouse IgG
BCPDA	4,7-bis(chlorosulfonylphenyl)-1,10-phenanthroline-2,9-dicarboxylic acid
Biot	biotin
BRET	bioluminescence resonance energy transfer
BSA	bovine serum albumin
ca.	circa
cf.	compare
CNRS	Centre National de Recherche Scientifique

D	donor
DELFIA	dissociation enhanced lanthanide fluoroimmunoassay
DMSO	dimethyl sulfoxide
DNA	deoxyribonucleic acid
DTA	dichlorotriazinyl
DTPA	diethylene triamine pentaacetic acid
DY633	dyomics dye DY633
ECPM	École Européenne de Chimie, Polymères et Matériaux de Strasbourg
ELISA	enzyme-linked immunosorbent assay
EuL	see LnL with Eu as Ln
Eu-TBP	europium tris(bipyridine)
FRET	Förster resonance energy transfer
FWHM	full width at half maximum
g	gerade
GmbH	Gesellschaft mit beschränkter Haftung
HCG	human chorionic gonadotropin
HOMO	highest occupied molecular orbital
HTRF	homogeneous time-resolved fluorescence
IgG	immunoglobulin G
ISC	intersystem crossing
IVD	in vitro diagnostics
KF	pottassium fluoride
L	luminophore
LANCE	lanthanide chelate excitation
LC	ligand-centered
LMCT	ligand to metal charge transfer
Ln	lanthanide
LnL	complex of Ln ion and ligand L
LOD	limit of detection or limits of detection
LRET	Luminescence resonance energy transfer
$L-S$ coupling	Russell-Saunders coupling
LUMO	lowest unoccupied molecular orbital
MALDI-TOF	matrix assisted laser desorption/ionization - time of flight
MC	metal-centered
NHS	N-hydroxysuccinimide
OPO	optical parametric oscillator
PBS	phosphate buffered saline
PMT	photomultiplier tube
PS	polystyrene
Q	quencher
QD	quantum dot or quantum dots
QD655	QD emitting at 655 nm
RET	resonance energy transfer
RNA	ribonucleic acid

SA	pure water
SB	pure water + 0.5 M KF
SC	50 mM borate buffer pH 8.3
SD	50 mM borate buffer pH 8.3 + 2 % BSA
SE	50 mM borate buffer pH 8.3 + 2 % BSA + 0.5 M KF
Ser	serine
SF	50 mM borate buffer pH 8.3 + 2 % BSA + 0.05 % NaN_3
SG	50 mM borate buffer pH 8.3 + 2 % BSA + 0.5 M KF + 0.05 % NaN_3
SPIE	The International Society for Optical Engineering (SPIE - Society of Photo-Optical Instrumentation Engineers)
Strep	streptavidin
TbL	see LnL with Tb as Ln
Thr	threonine
TMT	terpyridine-bis(methylenamine) tetraacetic acid
TOP	tri-*n*-octylphosphine
TOPO	tri-*n*-octylphosphine oxide
TPSA	total prostate specific antigen
TRACE	time-resolved amplified cryptate emission
TRFIA	time-resolved fluoroimmunoassays
Trp	tryptophan
Tyr	tyrosine
u	ungerade
UMR	Unité mixte de recherche
UV	ultraviolet
Vis	visible
YAG	yttrium aluminium garnet ($Y_3Al_5O_{12}$)
YAlO	yttrium aluminium perovskite ($YAlO_3$)

6.3 Emission spectra

In this section, the complete emission spectra (intensity-normalized to the maximum emission peak) of **TbL, TbL-Strep, EuL, EuL-Strep, Eu-TBP and Eu-TBP-Strep** in different measuring solutions are displayed. Figures 6.1, 6.2 and 6.3 are the same as Figures 4.5, 4.6 and 4.7. They are shown here again on bigger scale to allow for a closer look at the energy level fine-splitting within the different transitions.

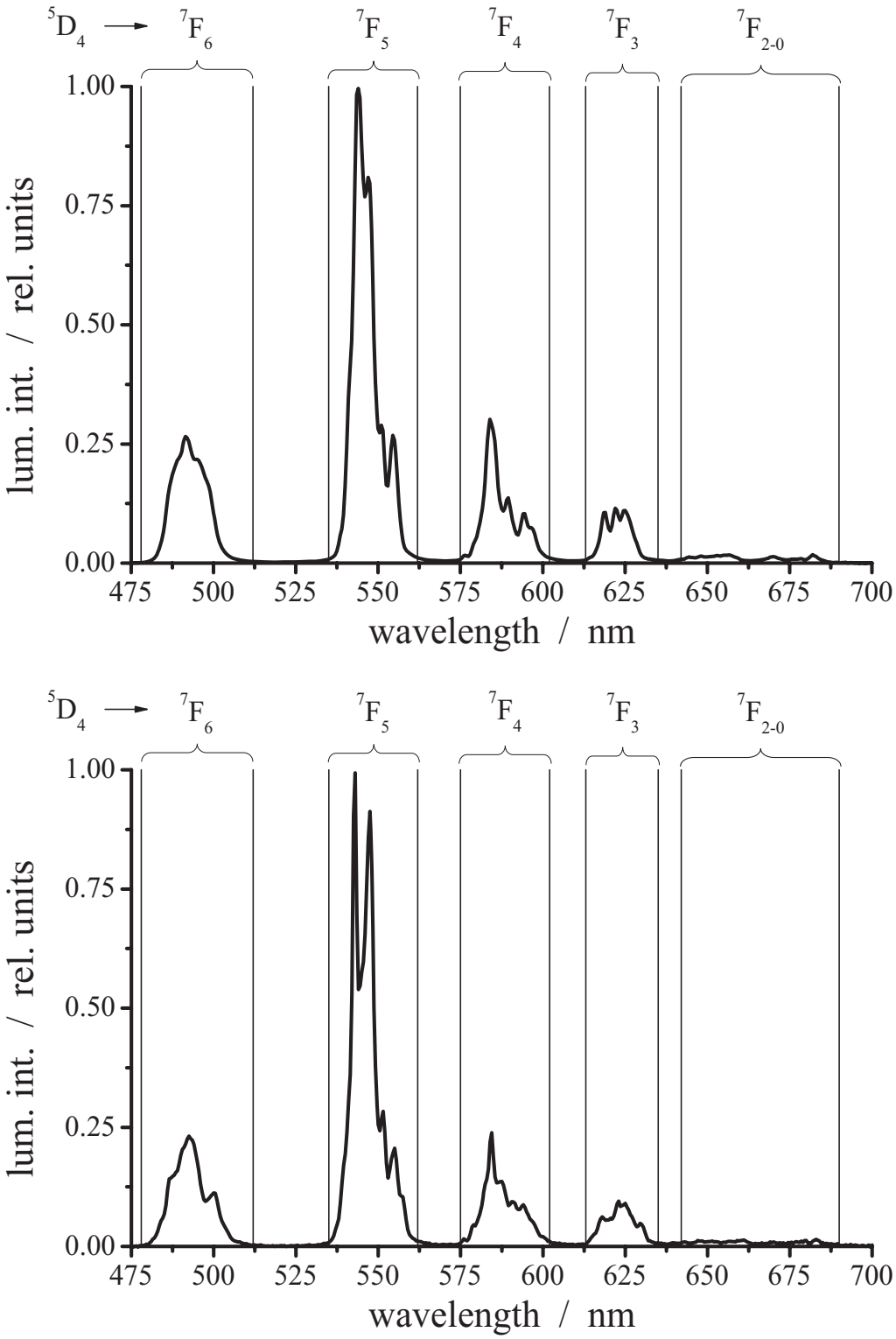

Figure 6.1: *Intensity-normalized emission spectra of TbL-Strep in* ***SA*** *(top) and TbL in* ***SG*** *(bottom). The optical transitions are displayed on top of the graphs.*

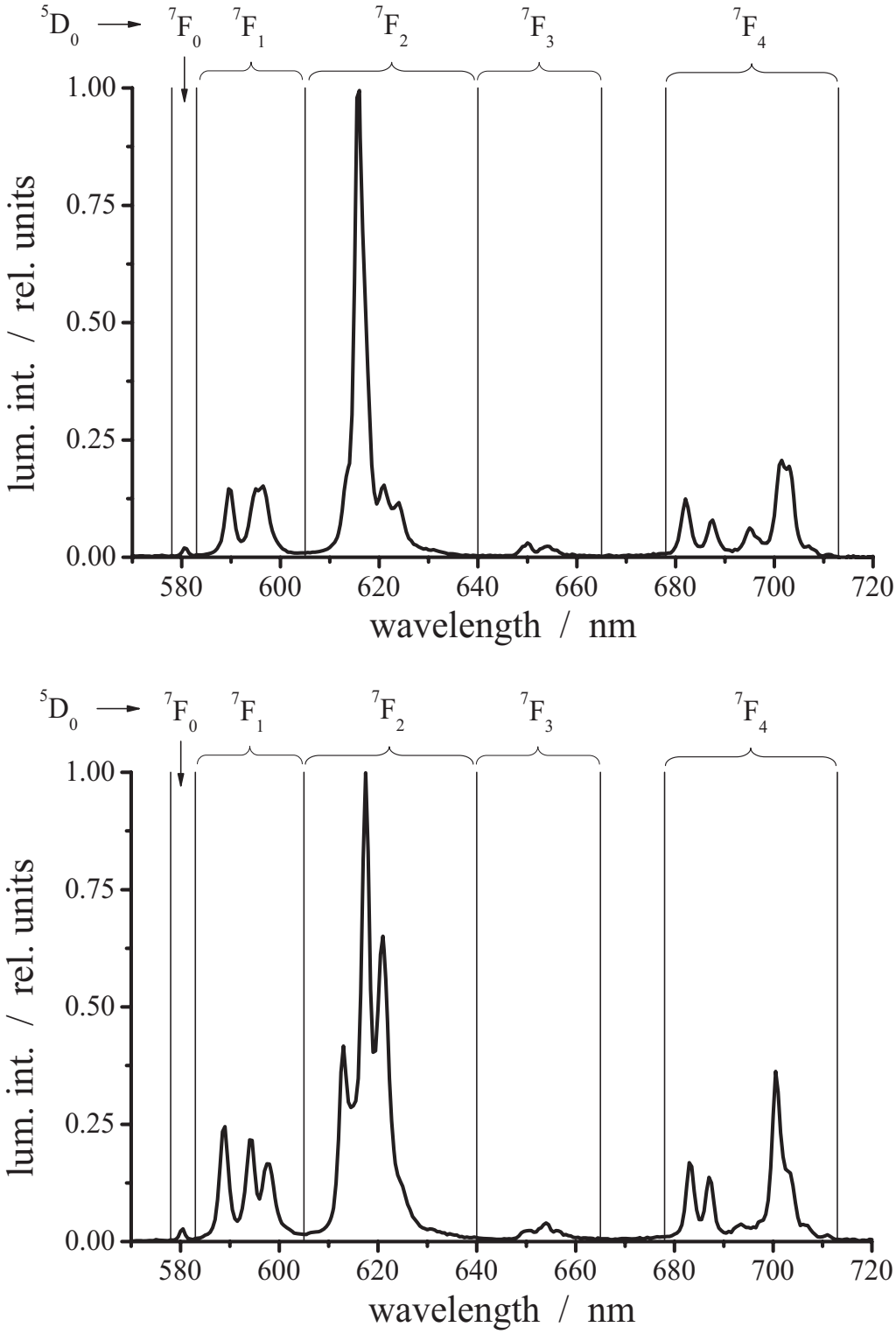

Figure 6.2: *Intensity-normalized emission spectra of EuL-Strep in* ***SA*** *(top) and EuL in* ***SG*** *(bottom). The optical transitions are displayed on top of the graphs.*

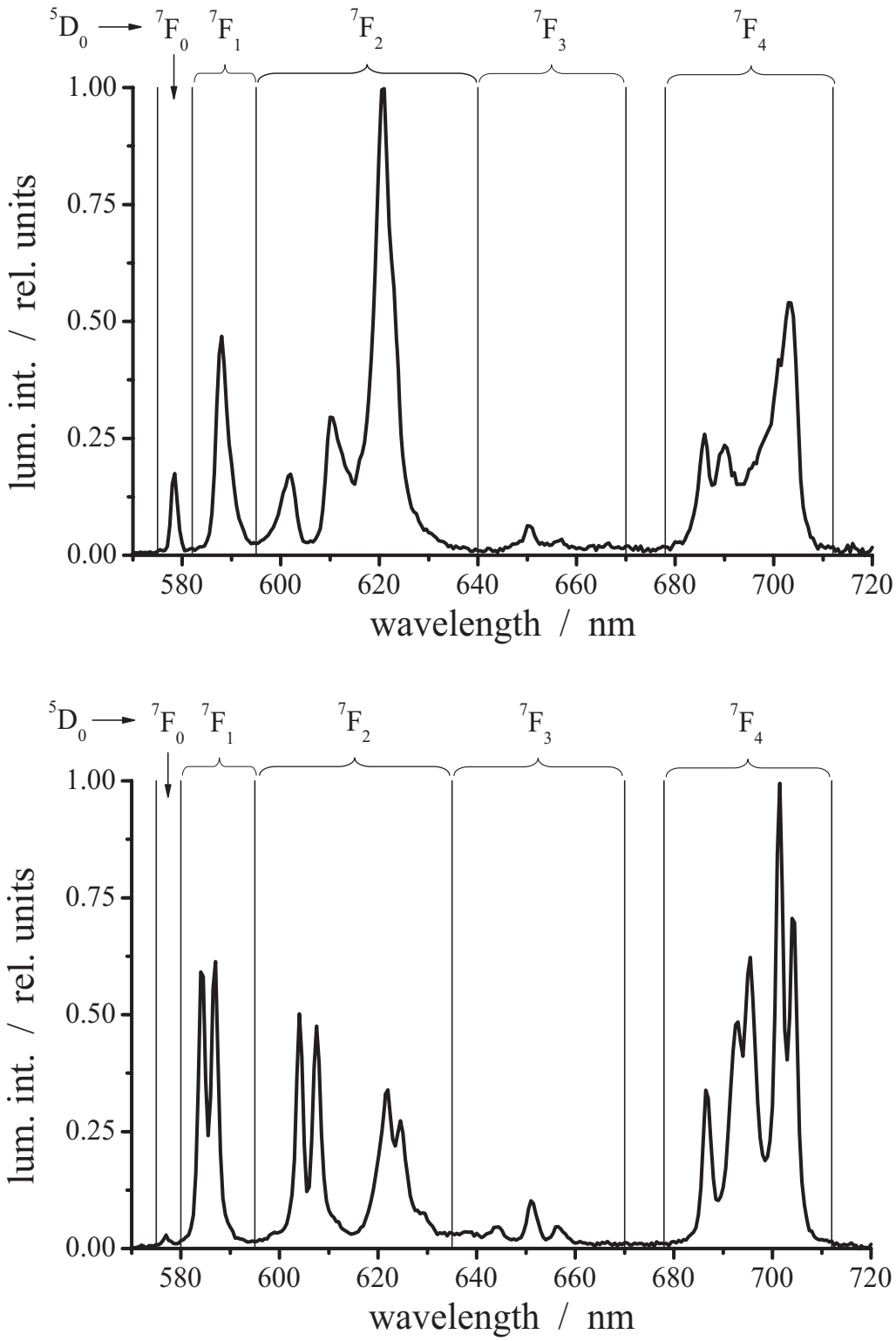

Figure 6.3: *Intensity-normalized emission spectra of Eu-TBP-Strep in* ***SA*** *(top) and Eu-TBP in* ***SG*** *(bottom). The optical transitions are displayed on top of the graphs.*

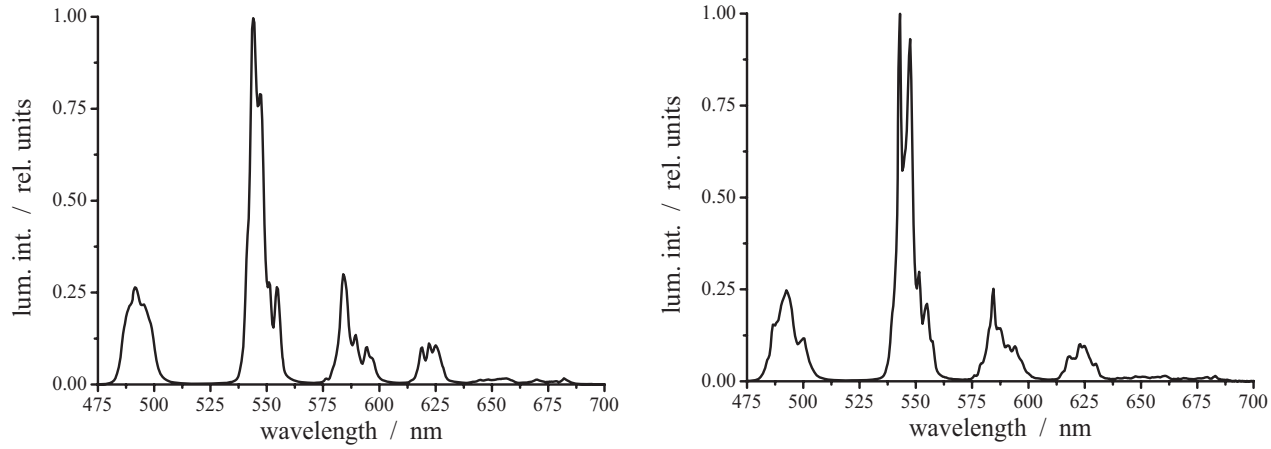

Figure 6.4: *Intensity-normalized emission spectra of TbL in* ***SA*** *(left) and in* ***SB*** *(right).*

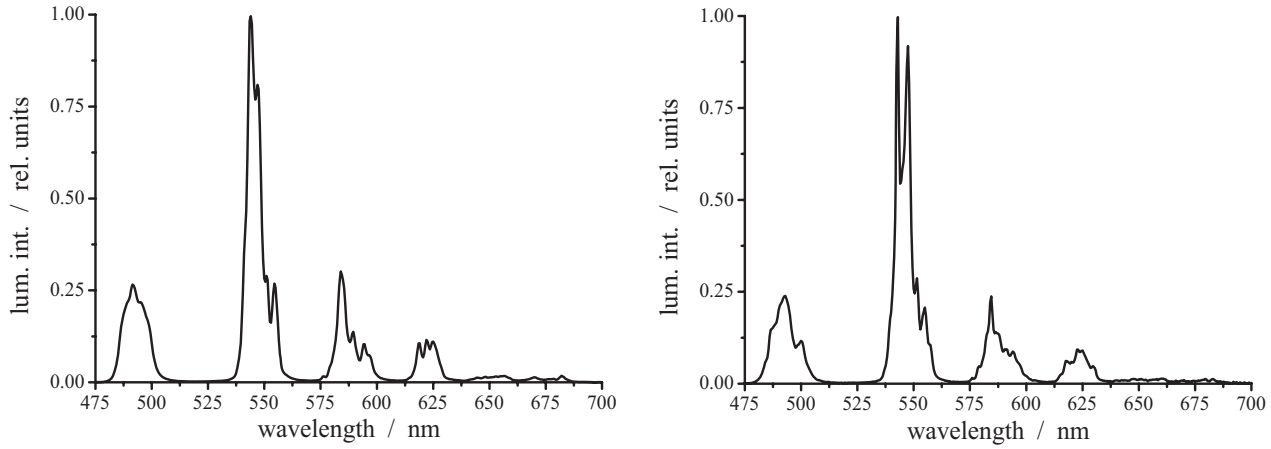

Figure 6.5: *Intensity-normalized emission spectra of TbL-Strep in* ***SA*** *(left) and in* ***SB*** *(right).*

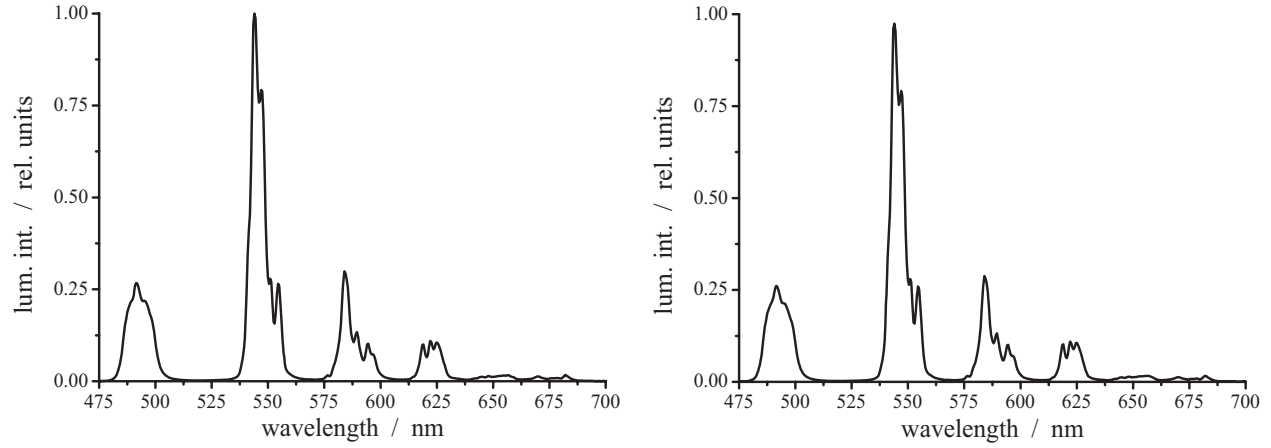

Figure 6.6: *Intensity-normalized emission spectra of TbL (left) and TbL-Strep (right) in* ***SC****.*

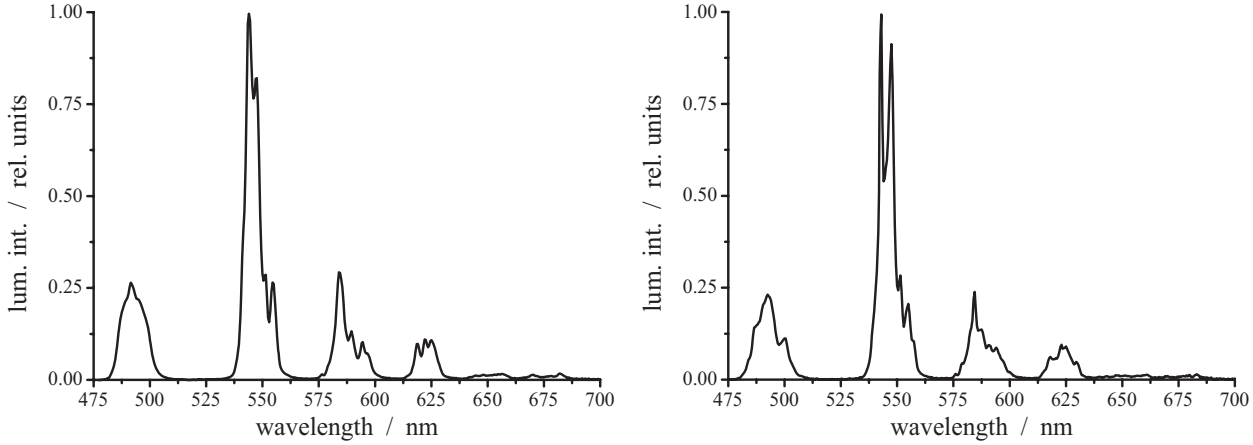

Figure 6.7: *Intensity-normalized emission spectra of TbL in* ***SF*** *(left) and in* ***SG*** *(right).*

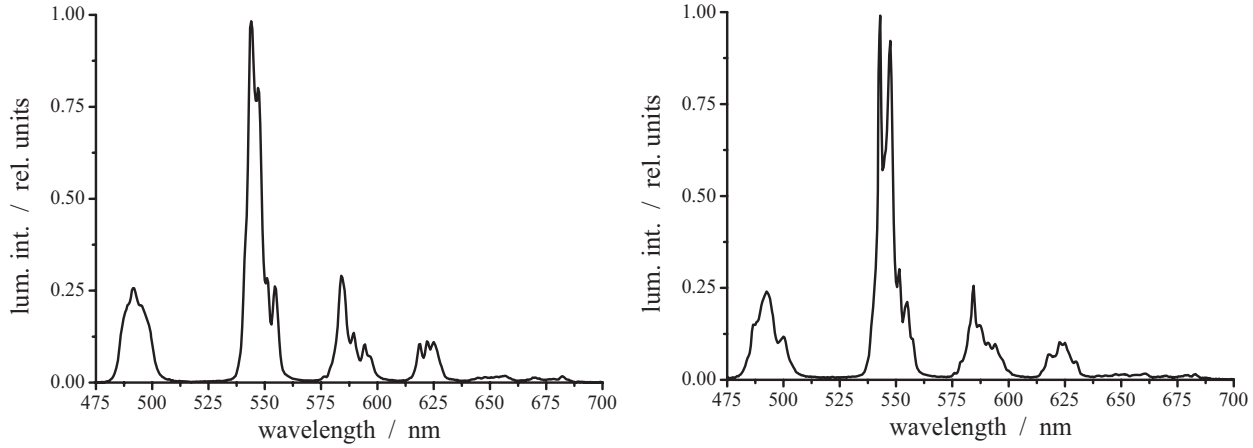

Figure 6.8: *Intensity-normalized emission spectra of TbL-Strep in* ***SF*** *(left) and in* ***SG*** *(right).*

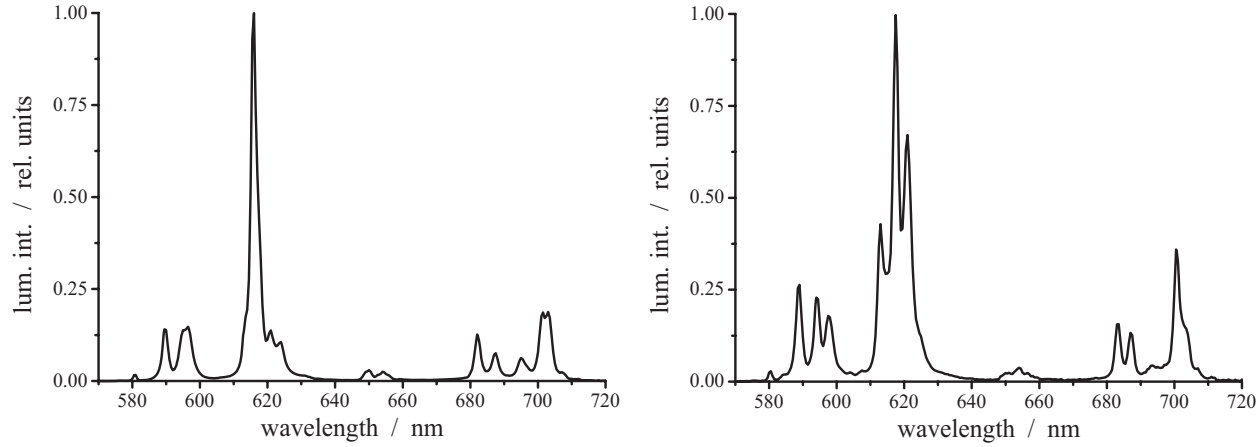

Figure 6.9: *Intensity-normalized emission spectra of EuL in* ***SA*** *(left) and in* ***SB*** *(right).*

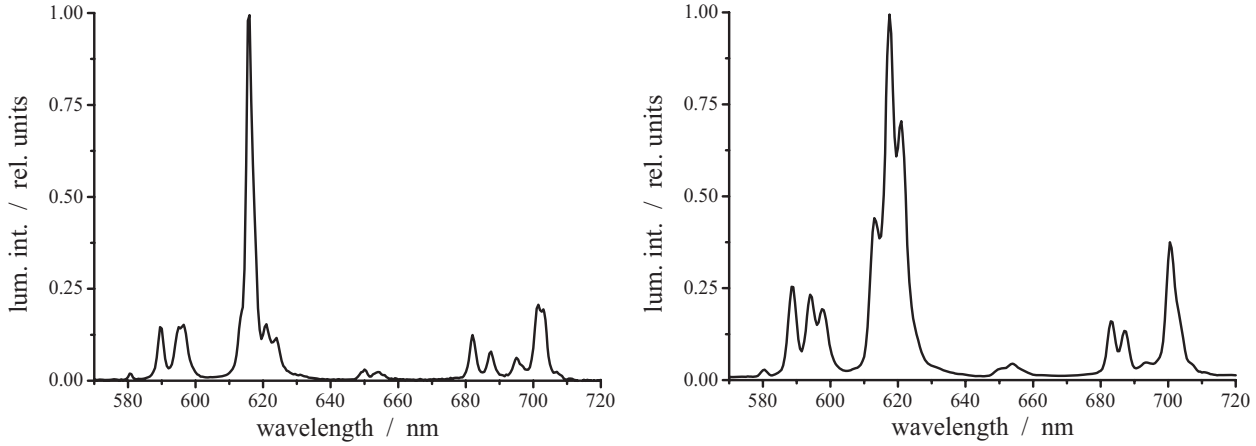

Figure 6.10: *Intensity-normalized emission spectra of EuL-Strep in* ***SA*** *(left) and in* ***SB*** *(right).*

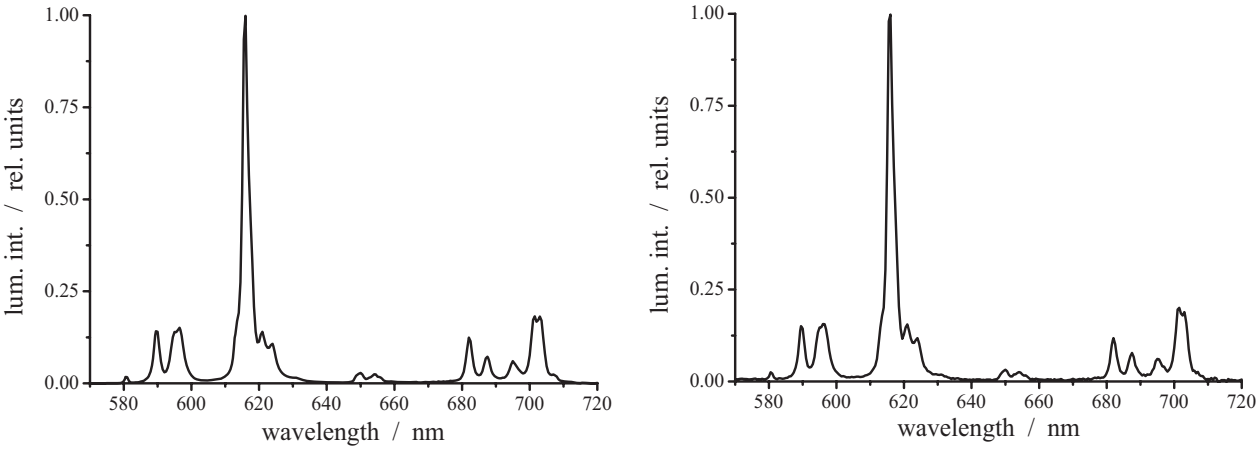

Figure 6.11: *Intensity-normalized emission spectra of EuL (left) and EuL-Strep (right) in* ***SC****.*

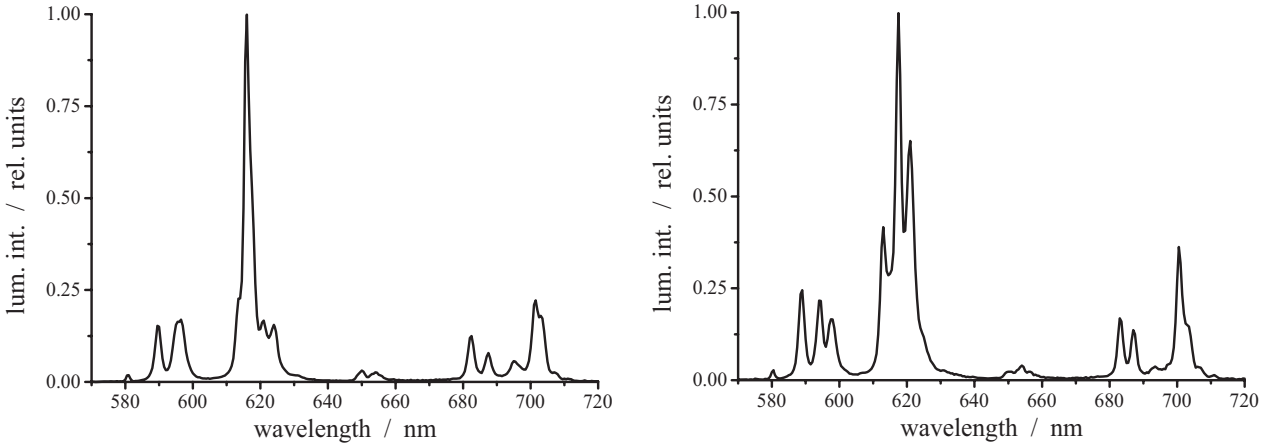

Figure 6.12: *Intensity-normalized emission spectra of EuL in* ***SF*** *(left) and in* ***SG*** *(right).*

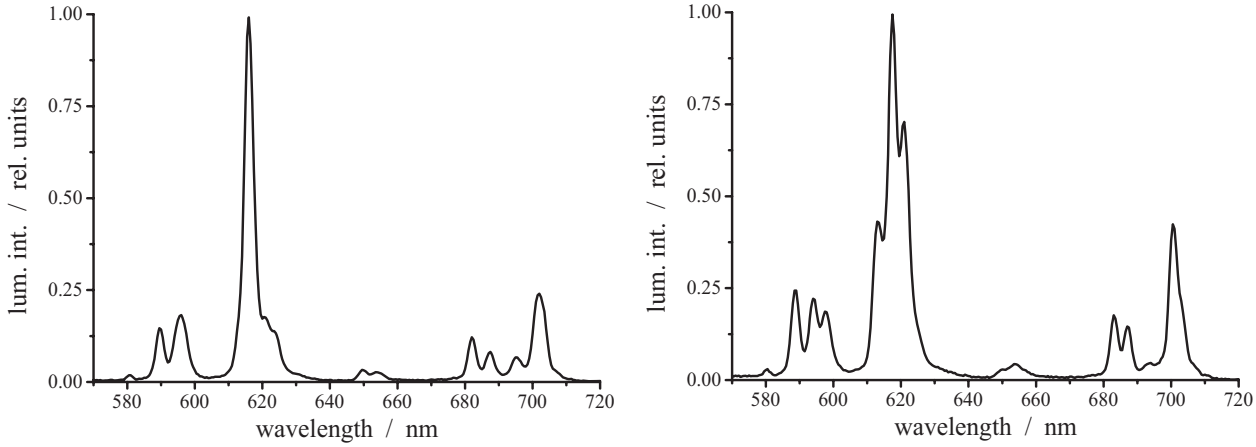

Figure 6.13: *Intensity-normalized emission spectra of EuL-Strep in* ***SF*** *(left) and in* ***SG*** *(right).*

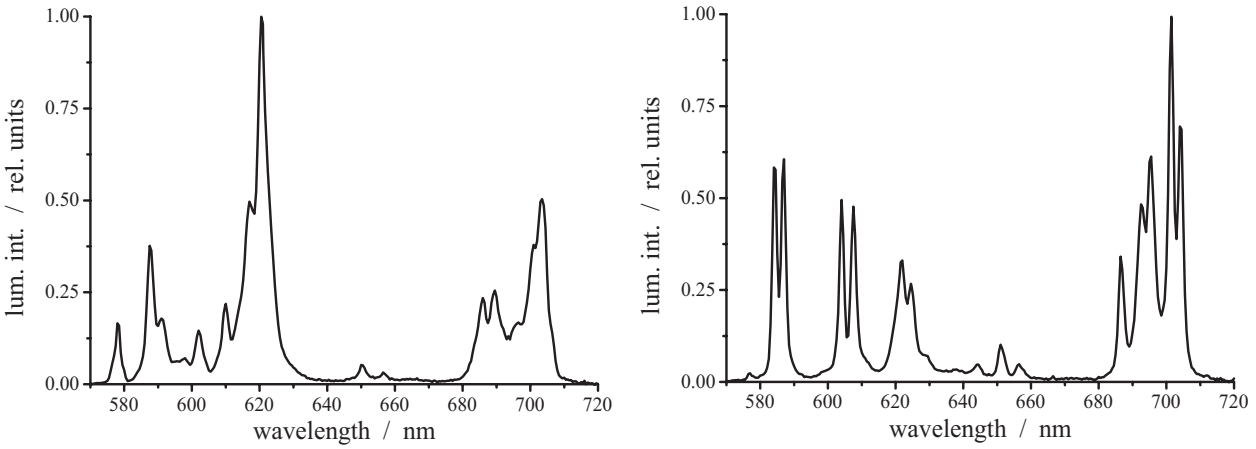

Figure 6.14: *Intensity-normalized emission spectra of Eu-TBP in* ***SA*** *(left) and in* ***SB*** *(right).*

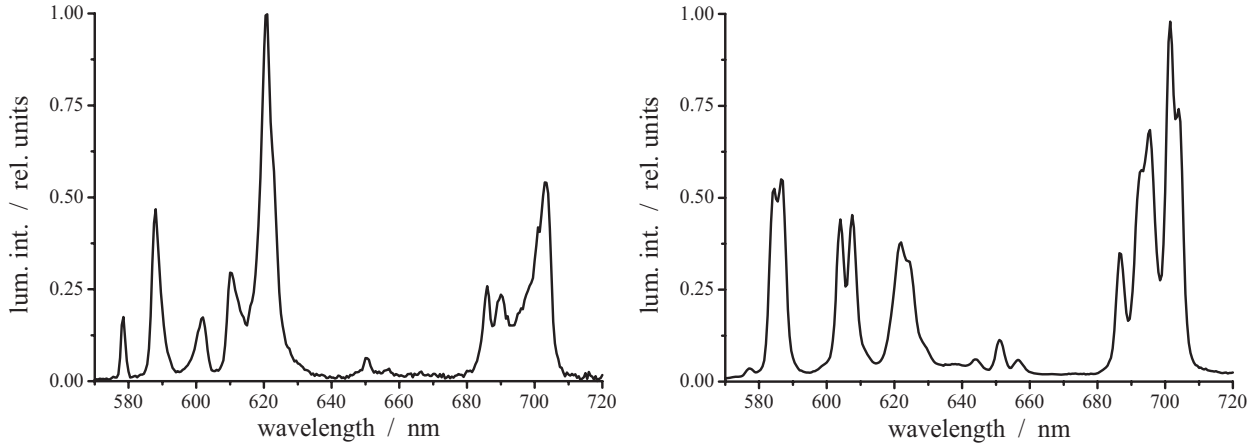

Figure 6.15: *Intensity-normalized emission spectra of Eu-TBP-Strep in* ***SA*** *(left) and in* ***SB*** *(right).*

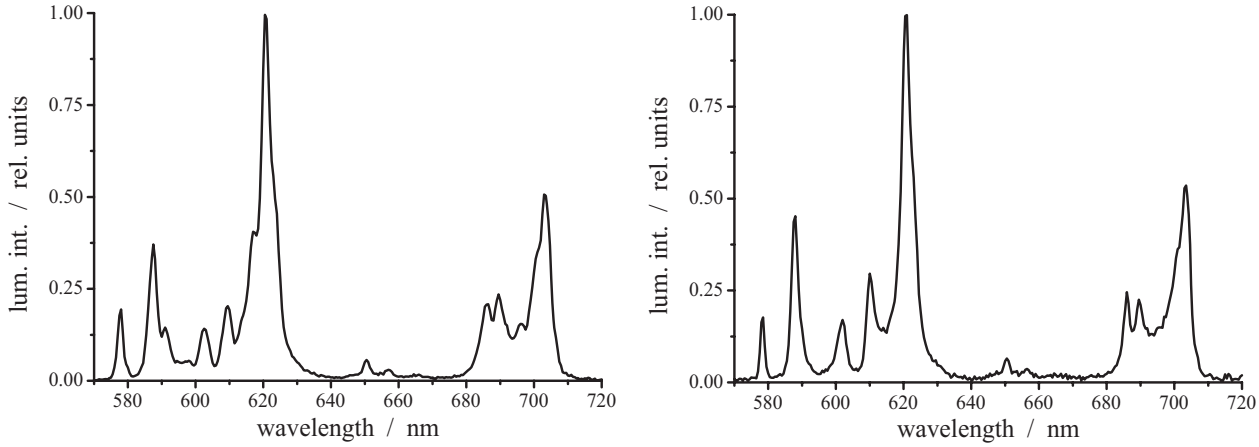

Figure 6.16: *Intensity-normalized emission spectra of Eu-TBP (left) and Eu-TBP-Strep (right) in* ***SC****.*

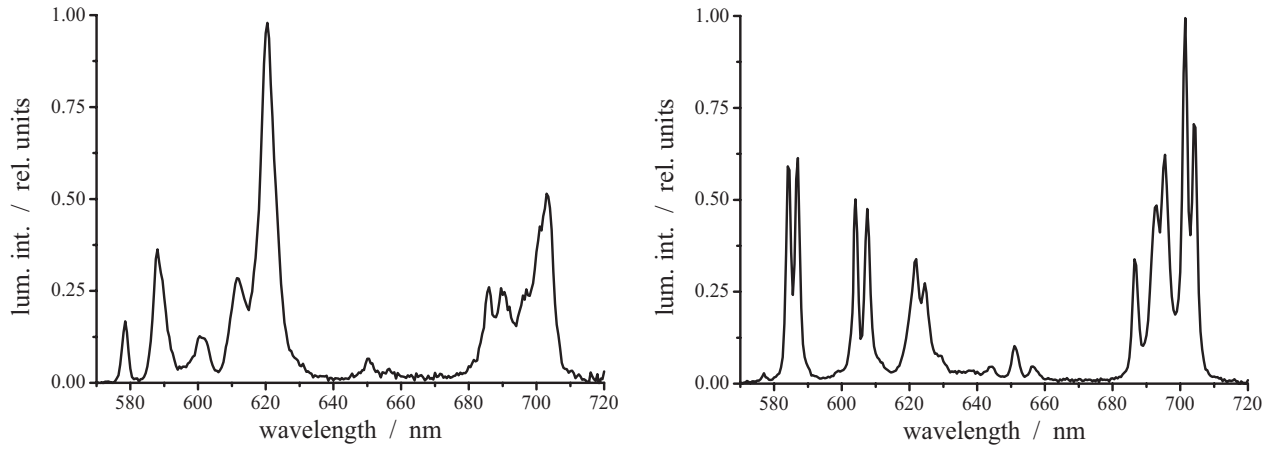

Figure 6.17: *Intensity-normalized emission spectra of Eu-TBP in* ***SF*** *(left) and in* ***SG*** *(right).*

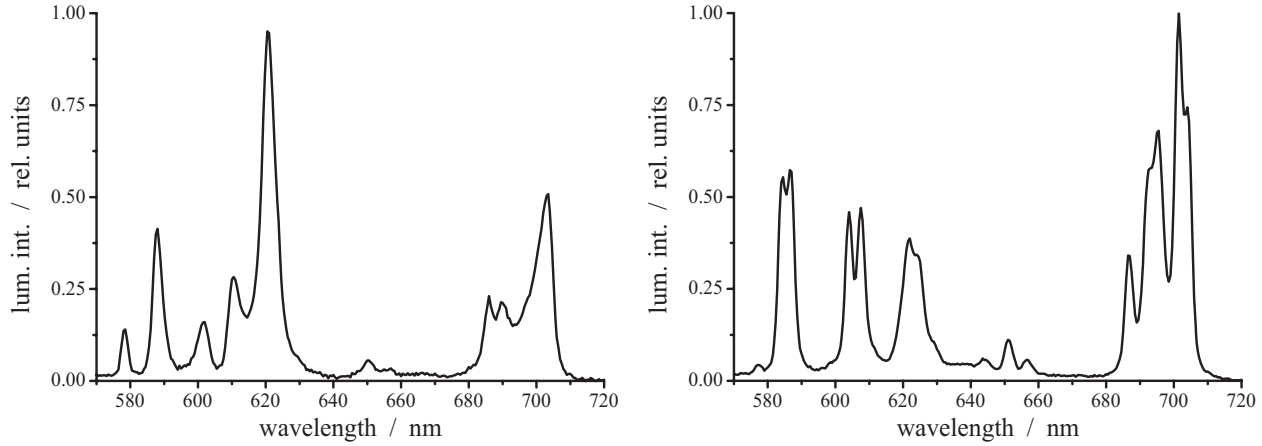

Figure 6.18: *Intensity-normalized emission spectra of Eu-TBP-Strep in* ***SF*** *(left) and in* ***SG*** *(right).*

6.4 Luminescence decay kinetics

Luminescence decay kinetics of TbL, TbL-Strep, EuL, EuL-Strep, Eu-TBP and Eu-TBP-Strep in measuring solutions **SA** to **SG**.

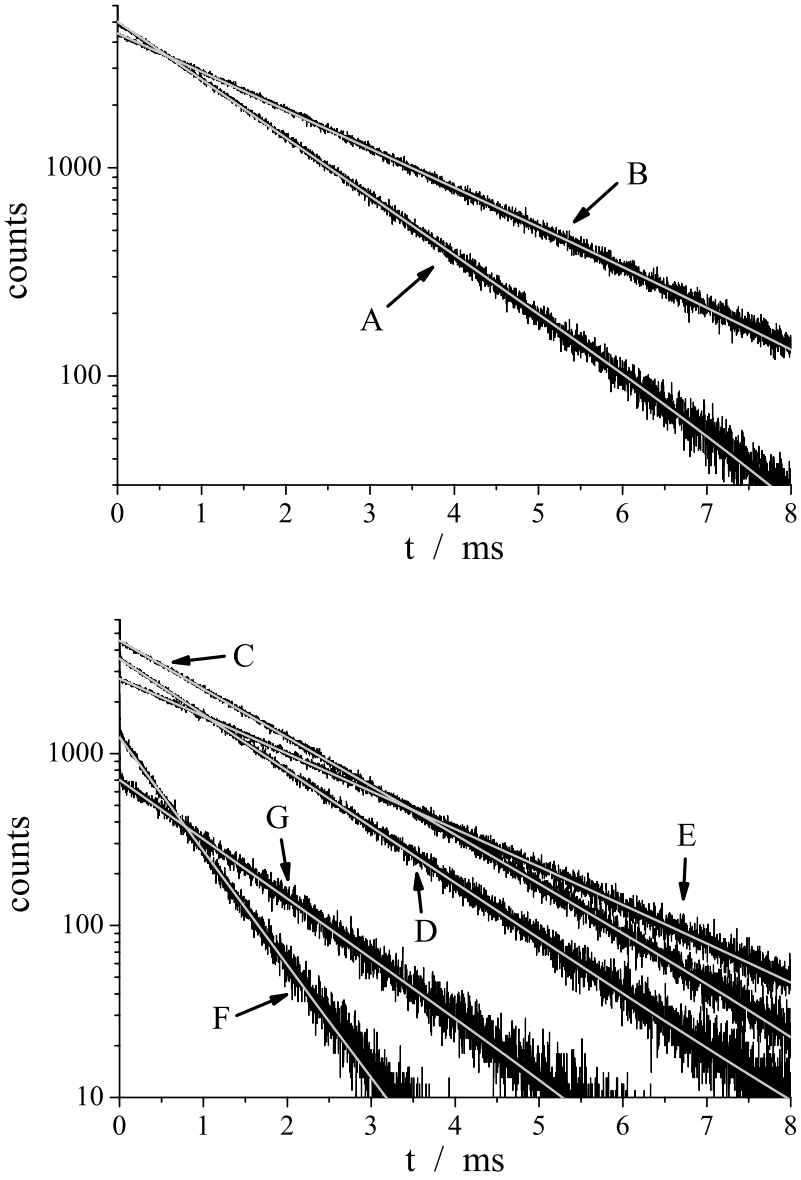

Figure 6.19: *Measured (black) and fitted (grey) luminescence decays of TbL in* ***SA*** *to* ***SG****. Approximate concentration of TbL: in* ***SA*** *to* ***SE****:* $1 \cdot 10^{-8}$ *M; in* ***SF*** *and* ***SG****:* $2 \cdot 10^{-9}$ *M.*

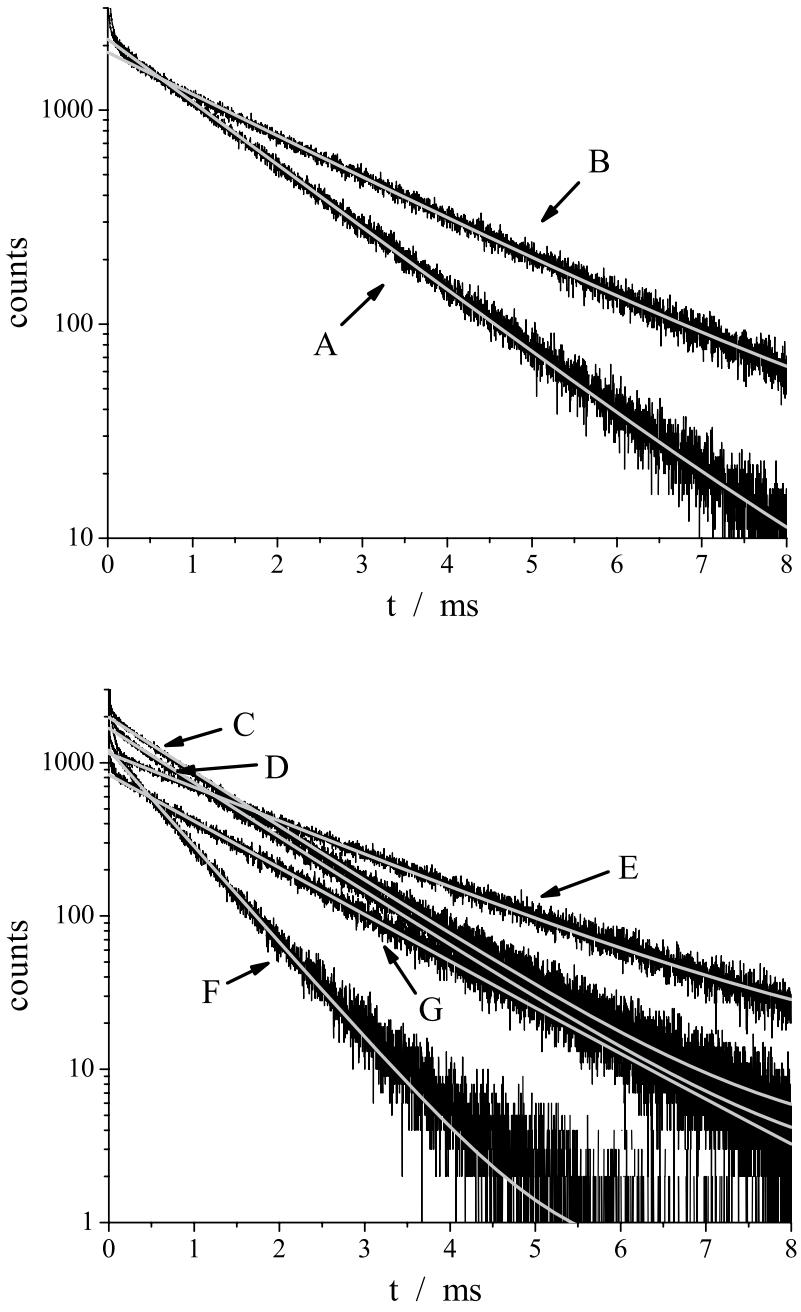

Figure 6.20: *Measured (black) and fitted (grey) luminescence decays of TbL-Strep in* ***SA*** *to* ***SG****. Approximate concentration of TbL-Strep:* $1 \cdot 10^{-9}$ *M.*

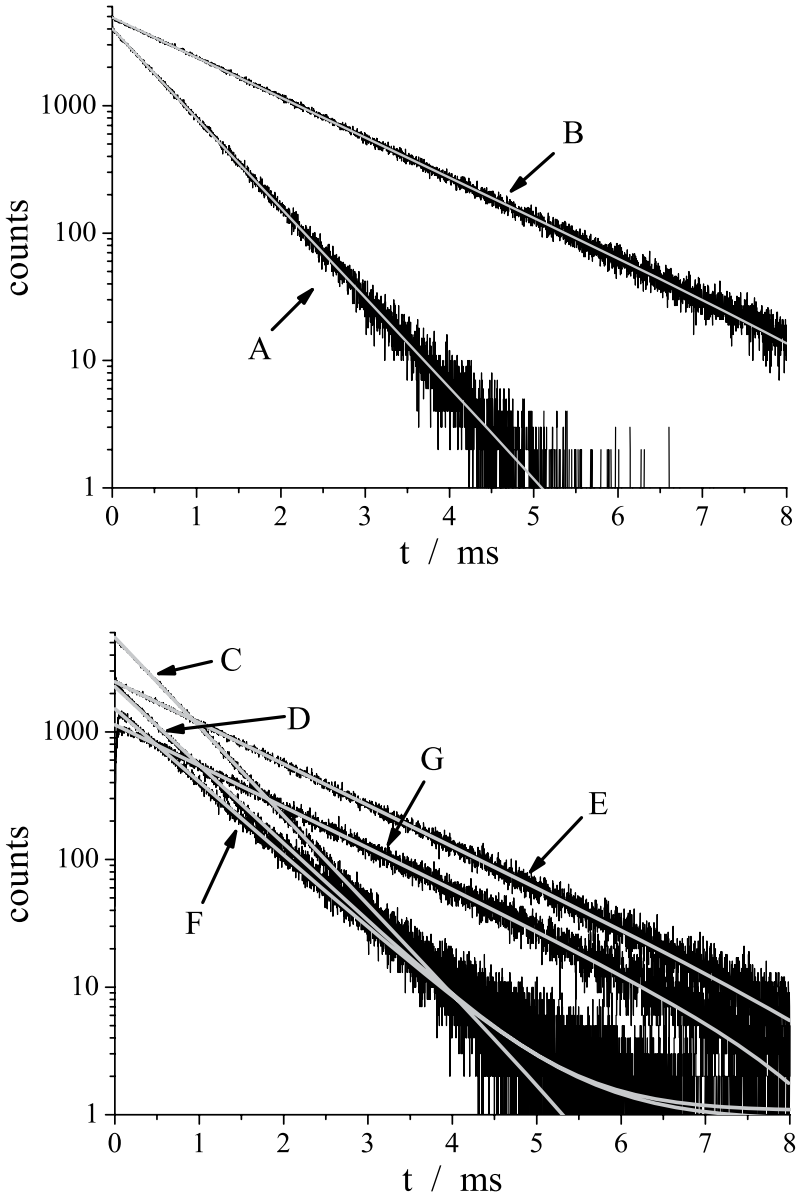

Figure 6.21: *Measured (black) and fitted (grey) luminescence decays of EuL in* ***SA*** *to* ***SG****. Approximate concentration of EuL: in* ***SA*** *to* ***SE****:* $5 \cdot 10^{-9}$ *M; in* ***SF*** *and* ***SG****:* $2 \cdot 10^{-9}$ *M.*

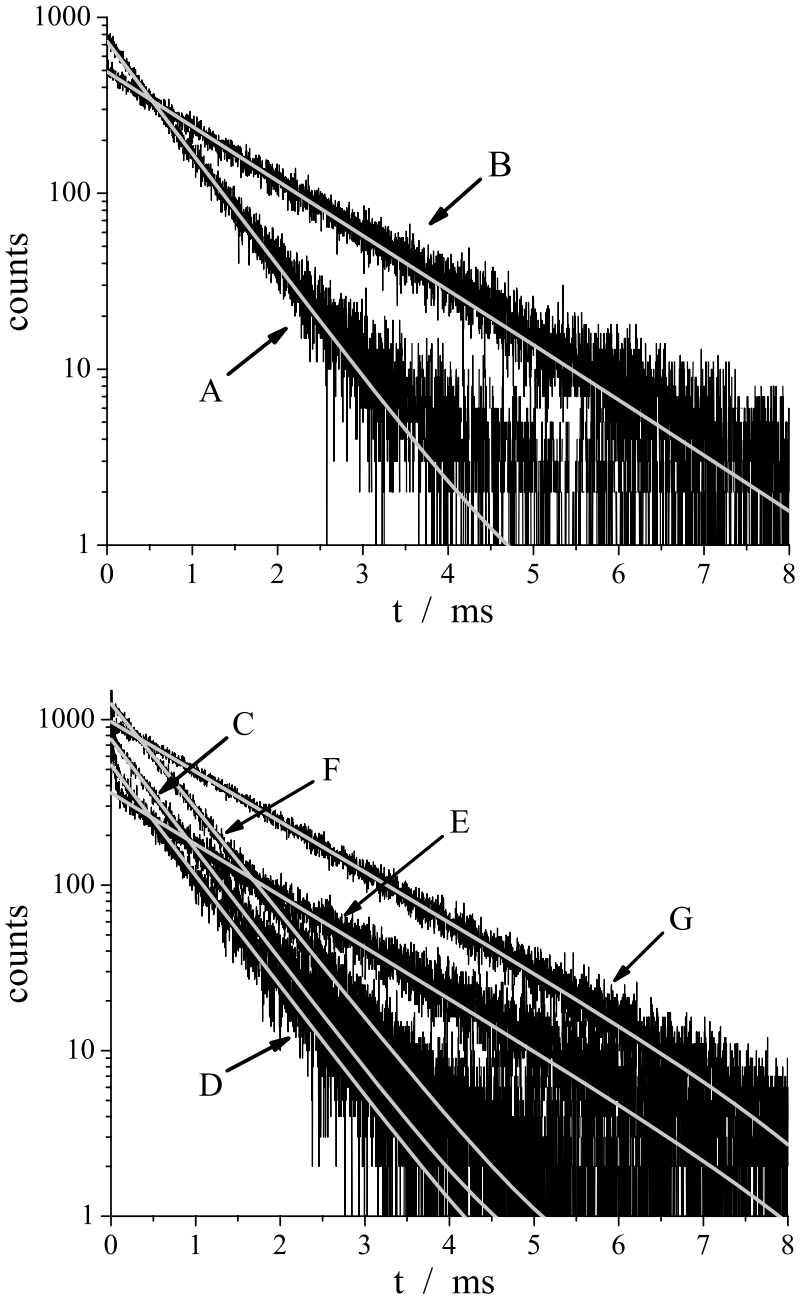

Figure 6.22: *Measured (black) and fitted (grey) luminescence decays of EuL-Strep in* ***SA*** *to* ***SG****. Approximate concentration of EuL-Strep:* $3 \cdot 10^{-9}$ *M.*

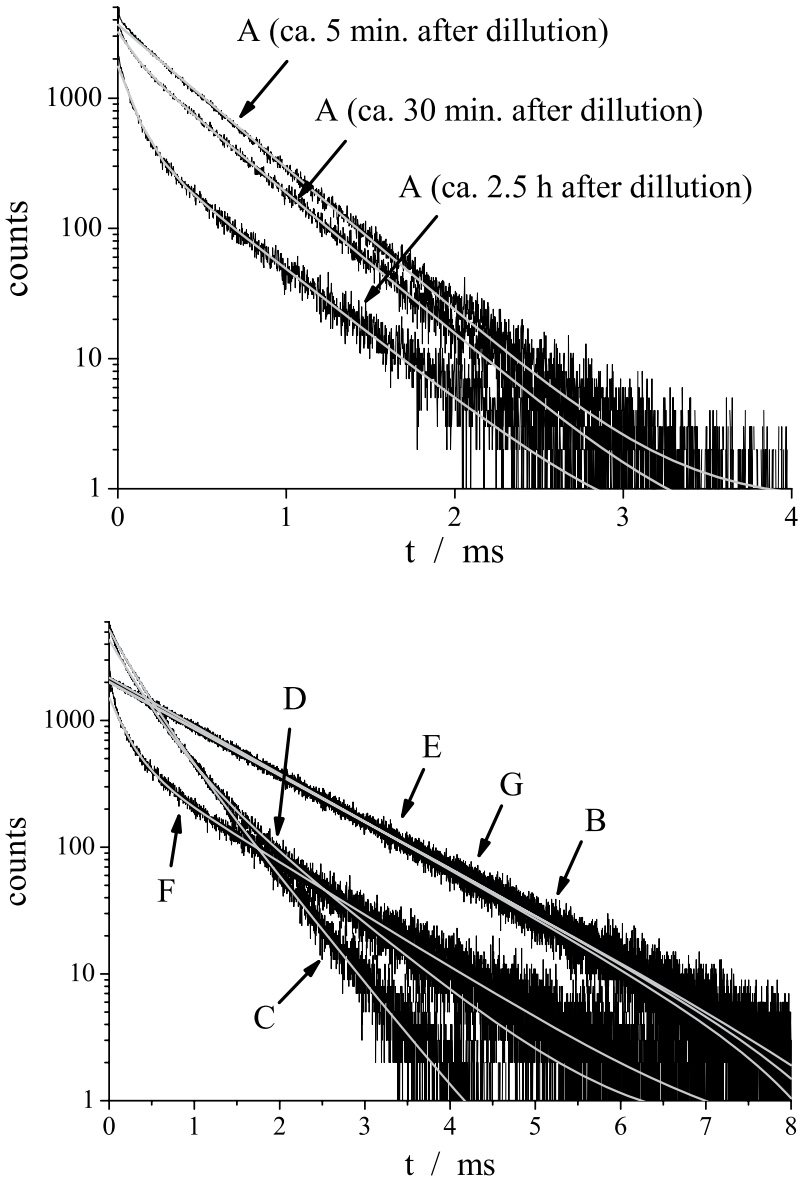

Figure 6.23: *Measured (black) and fitted (grey) luminescence decays of Eu-TBP in* ***SA*** *to* ***SG****. Approximate concentration of Eu-TBP:* $3 \cdot 10^{-8}$ *M.*

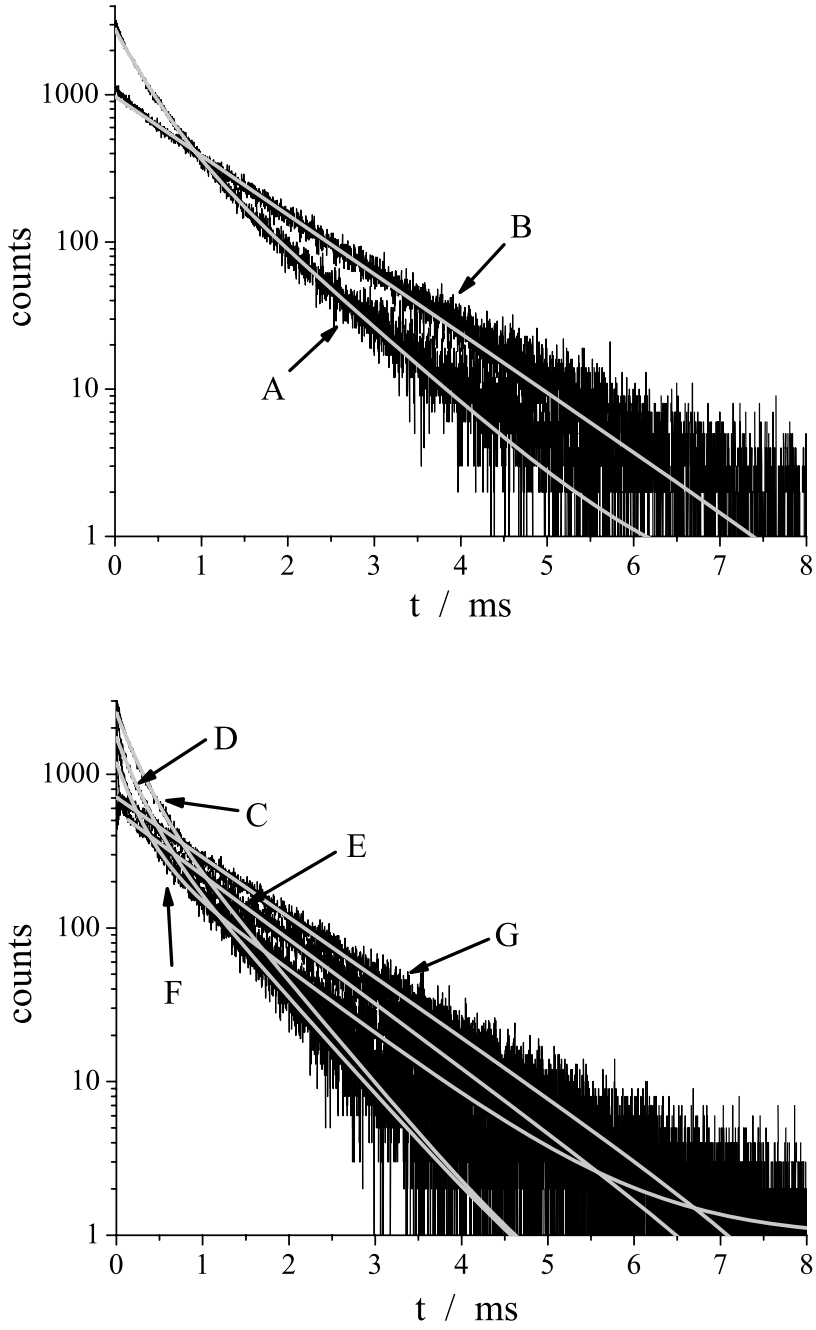

Figure 6.24: *Measured (black) and fitted (grey) luminescence decays of Eu-TBP-Strep in* ***SA*** *to* ***SG****. Approximate concentration of Eu-TBP-Strep:* $3 \cdot 10^{-9}$ *M*

6.5 FRET experiments

6.5.1 Biot-QD655 as acceptor

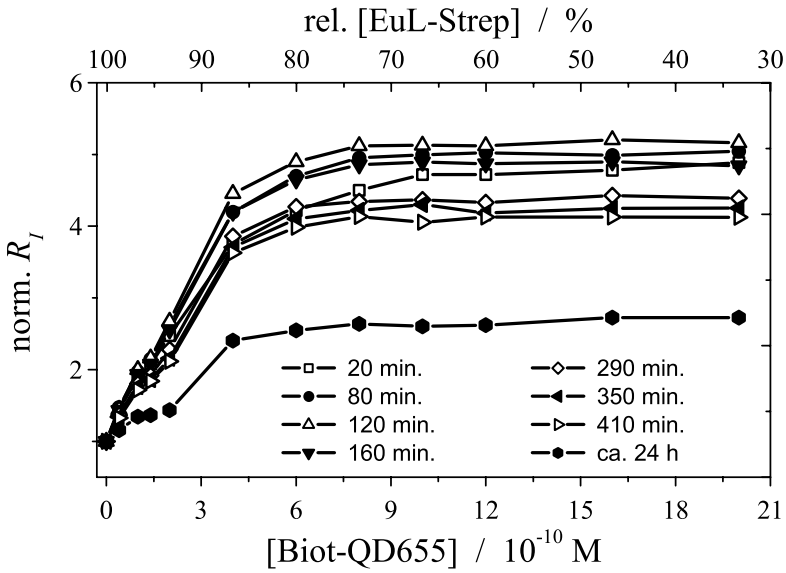

Figure 6.25: *Kinetic evolution of the normalized intensity ratio R_I as a function of [Biot-QD655] and relative [EuL-Strep] (in **SG**, initial concentration [EuL-Strep] $= 3 \cdot 10^{-9}$ M).*

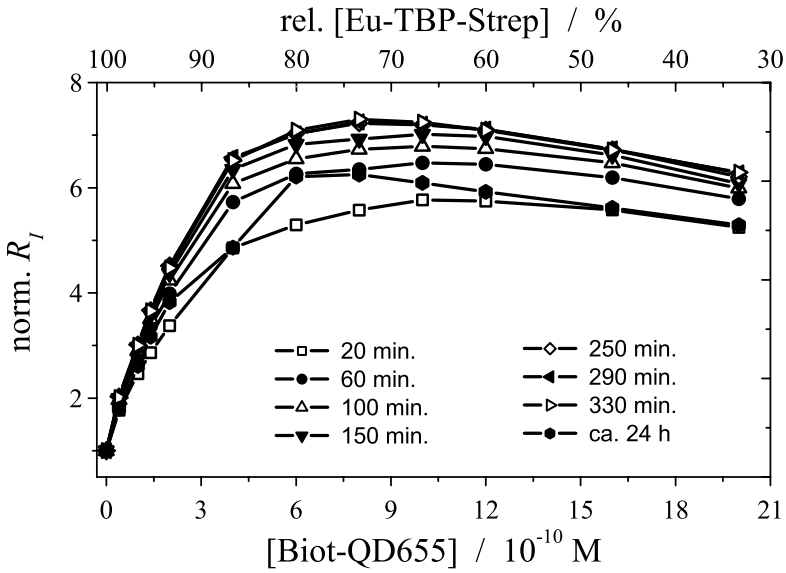

Figure 6.26: *Kinetic evolution of the normalized intensity ratio R_I as a function of [Biot-QD655] and relative [Eu-TBP-Strep] (in **SG**, initial concentration [Eu-TBP-Strep] $= 3 \cdot 10^{-9}$ M).*

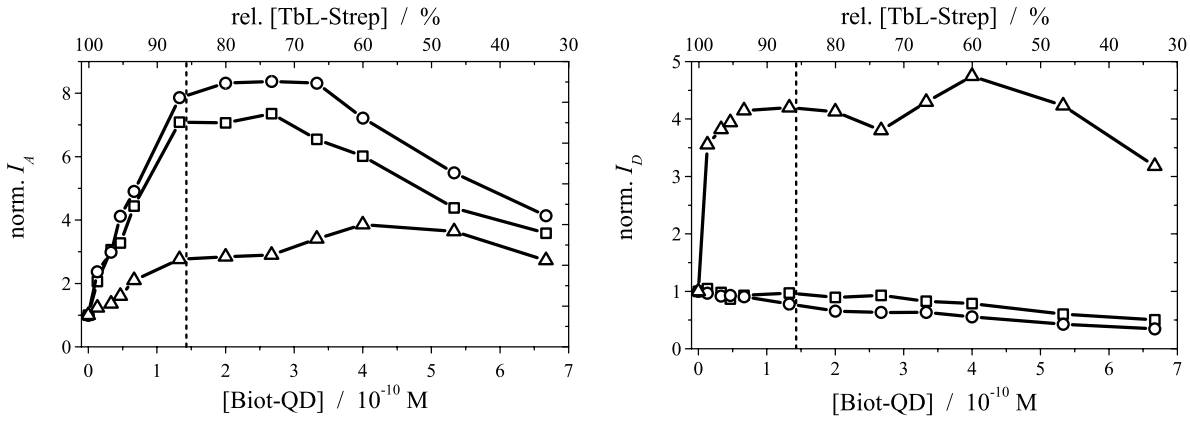

Figure 6.27: *Evolution of I_A and I_D as a function of [Biot-QD655] added to TbL-Strep in* ***SC*** *after ca. 7 hours incubation time (triangles),* ***SF*** *after ca. 5 hours (squares) and* ***SG*** *after ca. 4 hours (circles). Initial concentration [TbL-Strep] = $1 \cdot 10^{-9}$ M. The dotted line indicates a ratio of 6 TbL-Strep per Biot-QD655.*

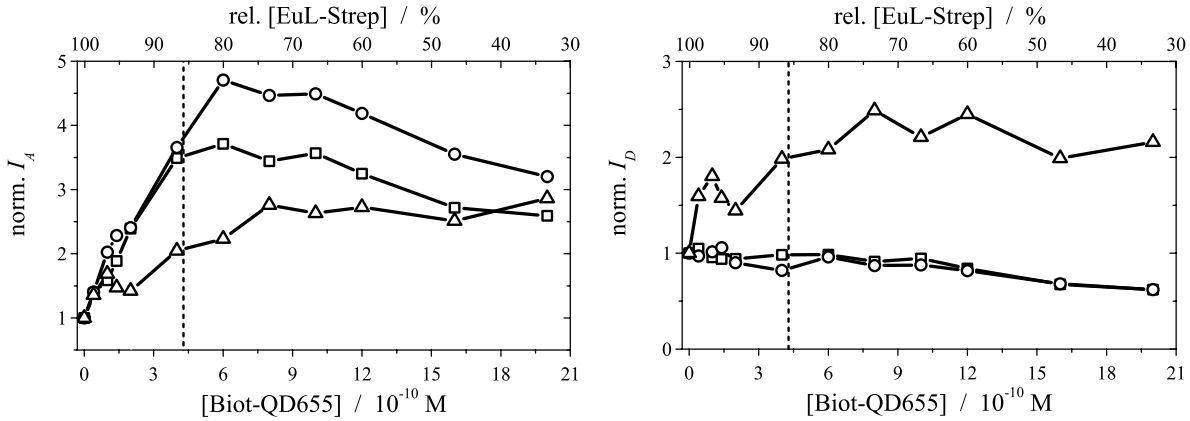

Figure 6.28: *Evolution of I_A and I_D as a function of [Biot-QD655] added to EuL-Strep in* ***SC*** *after ca. 1 hour incubation time (triangles),* ***SF*** *after ca. 3.5 hours (squares) and* ***SG*** *after ca. 2 hours (circles). Initial concentration [EuL-Strep] = $3 \cdot 10^{-9}$ M. The dotted line indicates a ratio of 6 EuL-Strep per Biot-QD655.*

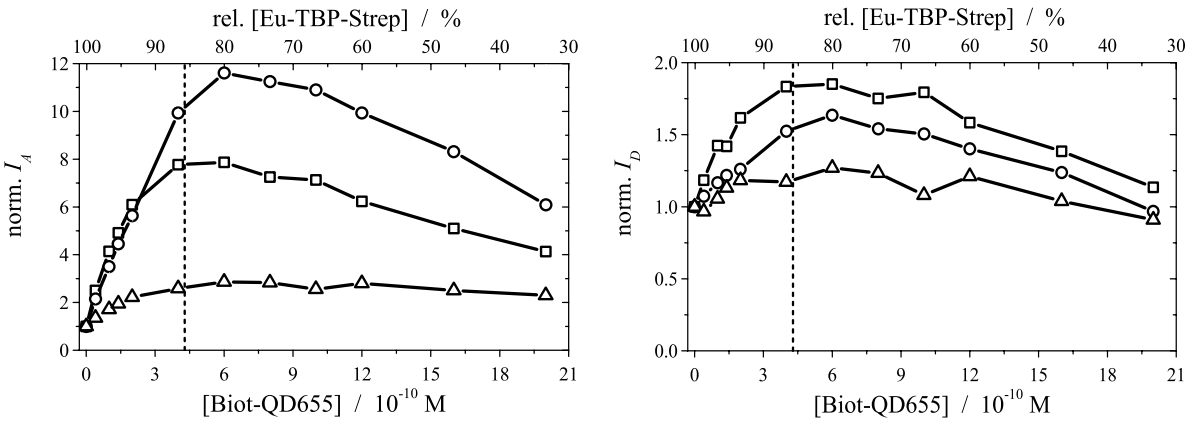

Figure 6.29: *Evolution of I_A and I_D as a function of [Biot-QD655] added to Eu-TBP-Strep in* ***SC*** *after ca. 2 hours incubation time (triangles),* ***SF*** *after ca. 5.5 hours (squares) and* ***SG*** *after ca. 5.5 hours (circles). Initial concentration [Eu-TBP-Strep] = $3 \cdot 10^{-9}$ M. The dotted line indicates a ratio of 6 Eu-TBP-Strep per Biot-QD655.*

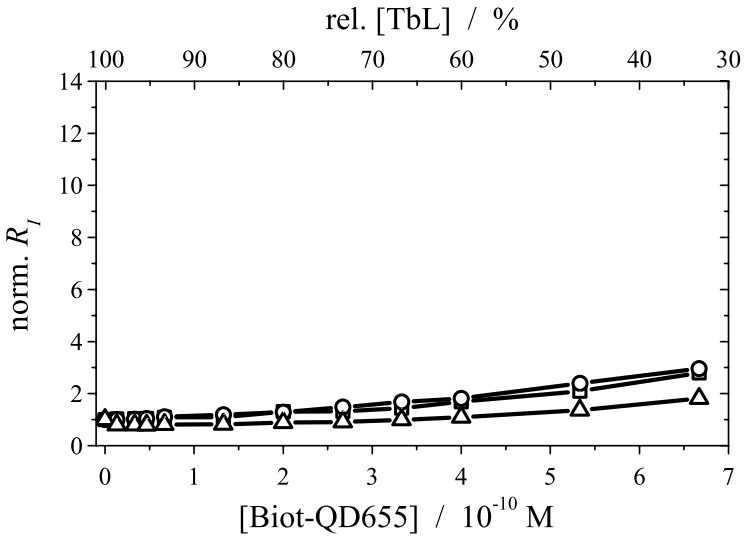

Figure 6.30: *TbL control experiments (cf. Figure 4.16), ruling out dynamic FRET.*

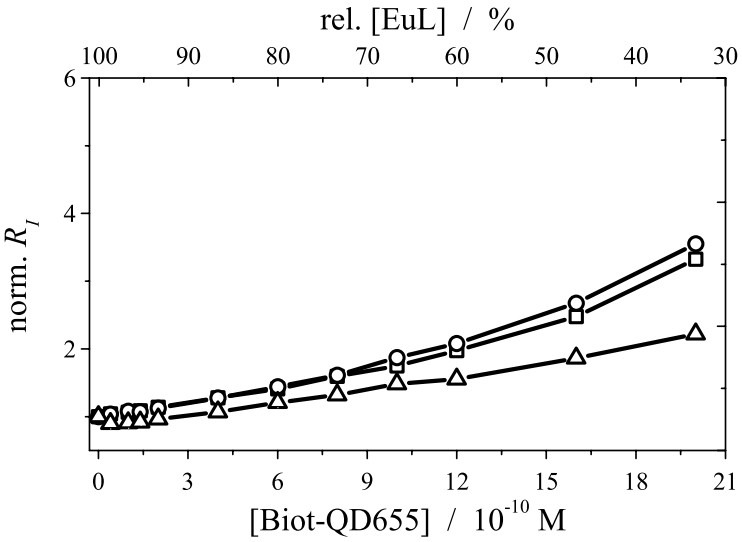

Figure 6.31: *EuL control experiments (cf. Figure 4.17), ruling out dynamic FRET.*

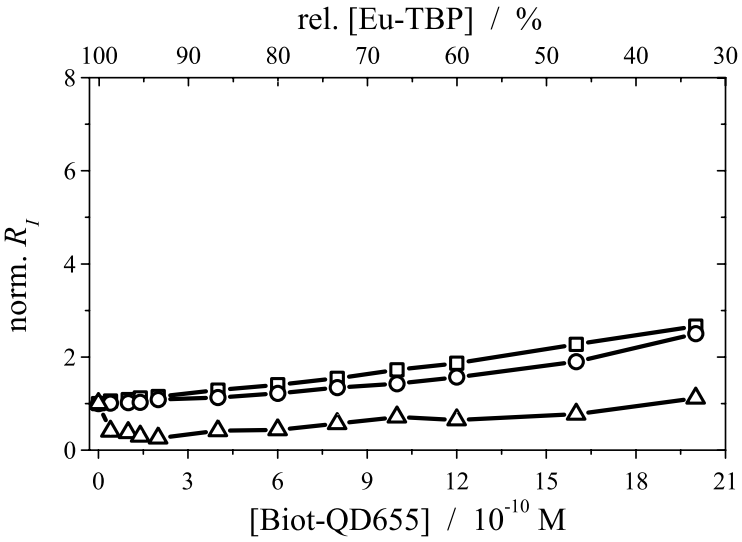

Figure 6.32: *Eu-TBP control experiments (cf. Figure 4.17), ruling out dynamic FRET.*

6.5.2 Biot-APC and Biot-DY633 as acceptors

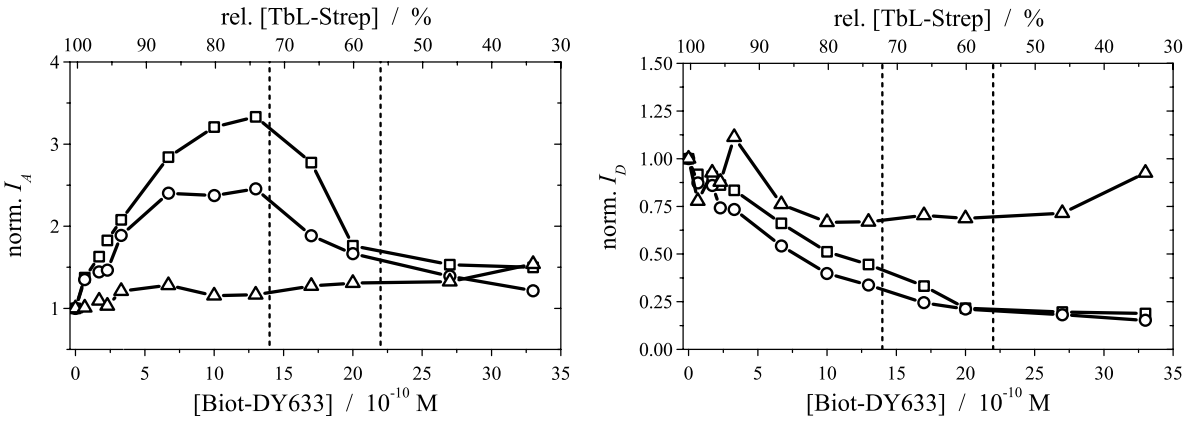

Figure 6.33: *Evolution of I_A and I_D as a function of [Biot-DY633] added to TbL-Strep after ca. 1 h incubation time in* ***SC*** *(triangles),* ***SF*** *(squares) and* ***SG*** *(circles). Initial concentration [TbL-Strep] = $1 \cdot 10^{-9}$ M. The dotted lines indicate a ratio of 0.25 (at ca. 56 %) and 0.5 TbL-Strep per Biot-DY633.*

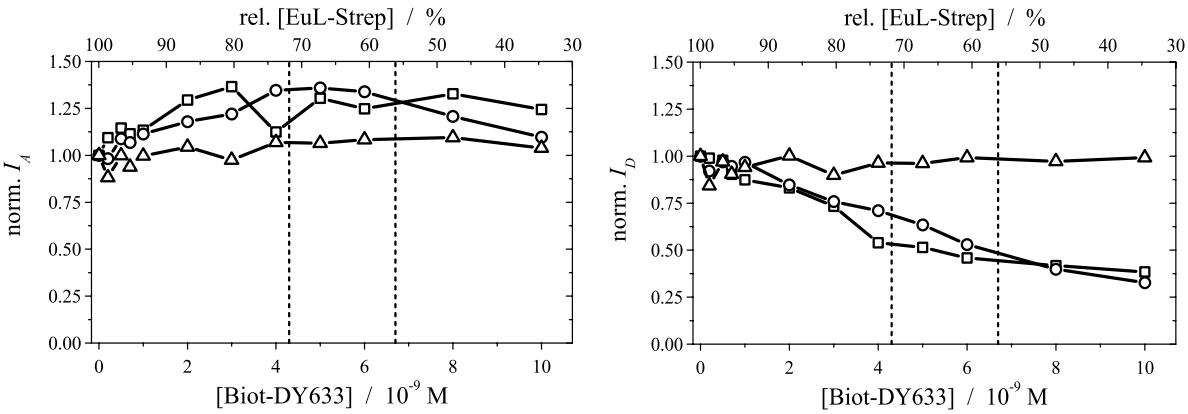

Figure 6.34: *Evolution of I_A and I_D as a function of [Biot-DY633] added to EuL-Strep after ca. 1 h incubation time in* ***SC*** *(triangles),* ***SF*** *(squares) and* ***SG*** *(circles). Initial concentration [EuL-Strep] = $3 \cdot 10^{-9}$ M. The dotted lines indicate a ratio of 0.25 (at ca. 56 %) and 0.5 EuL-Strep per Biot-DY633.*

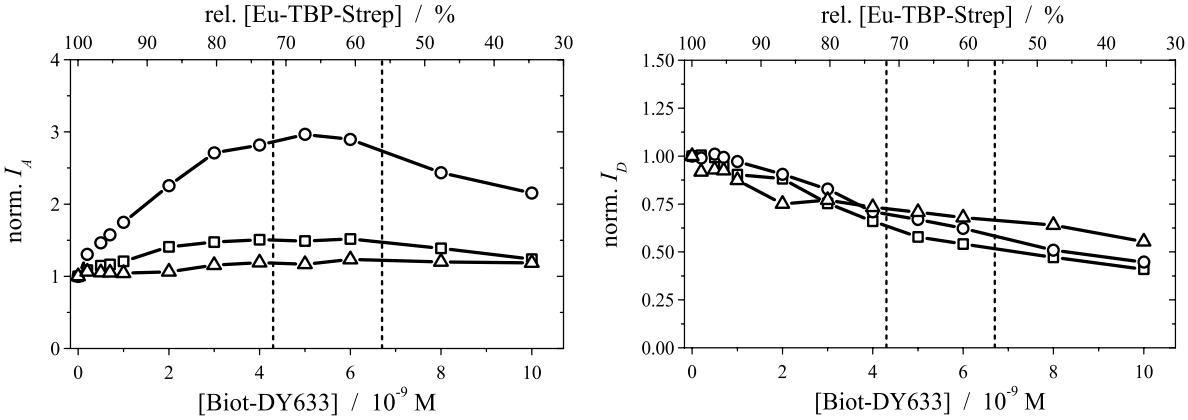

Figure 6.35: *Evolution of I_A and I_D as a function of [Biot-DY633] added to Eu-TBP-Strep after ca. 1 h incubation time in* ***SC*** *(triangles),* ***SF*** *(squares) and* ***SG*** *(circles). Initial concentration [Eu-TBP-Strep] = $3 \cdot 10^{-9}$ M. The dotted lines indicate a ratio of 0.25 (at ca. 56 %) and 0.5 Eu-TBP-Strep per Biot-DY633.*

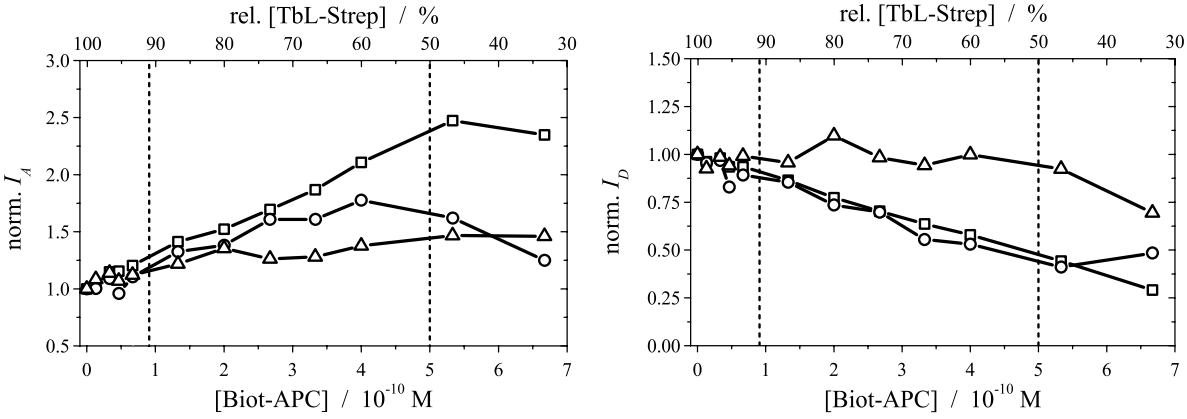

Figure 6.36: *Evolution of I_A and I_D as a function of [Biot-APC] added to TbL-Strep in* ***SC*** *after ca. 1 h incubation time (triangles),* ***SF*** *after ca. 2 h (squares) and* ***SG*** *after ca. 2 h (circles). Initial concentration [TbL-Strep] = $1 \cdot 10^{-9}$ M. The dotted lines indicate a ratio of 1 (at 50 % [TbL-Strep]) and 10 TbL-Strep per Biot-APC.*

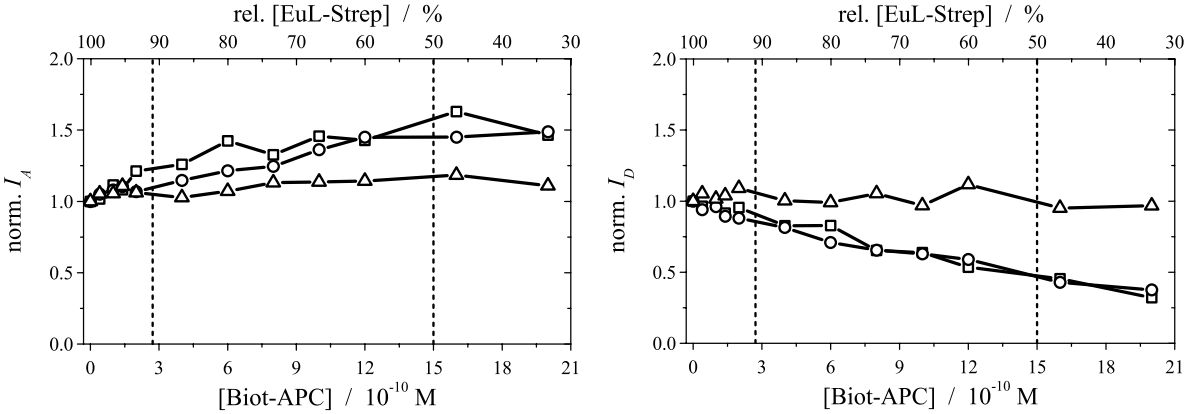

Figure 6.37: *Evolution of I_A and I_D as a function of [Biot-APC] added to EuL-Strep in* ***SC*** *after ca. 1 h incubation time (triangles),* ***SF*** *after ca. 1 h (squares) and* ***SG*** *after ca. 2 h (circles). Initial concentration [EuL-Strep] = $3 \cdot 10^{-9}$ M. The dotted lines indicate a ratio of 1 (at 50 % [EuL-Strep]) and 10 EuL-Strep per Biot-APC.*

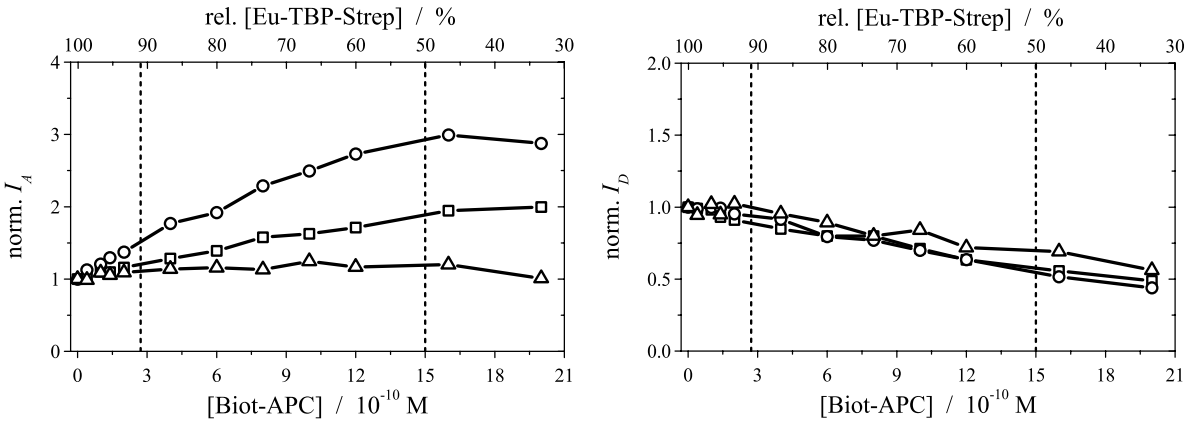

Figure 6.38: *Evolution of I_A and I_D as a function of [Biot-APC] added to Eu-TBP-Strep in* ***SC*** *after ca. 1 h incubation time (triangles),* ***SF*** *after ca. 2 h (squares) and* ***SG*** *after ca. 2 h (circles). Initial concentration [Eu-TBP-Strep] = $3 \cdot 10^{-9}$ M. The dotted lines indicate a ratio of 1 (at 50 % [Eu-TBP-Strep]) and 10 Eu-TBP-Strep per Biot-APC.*

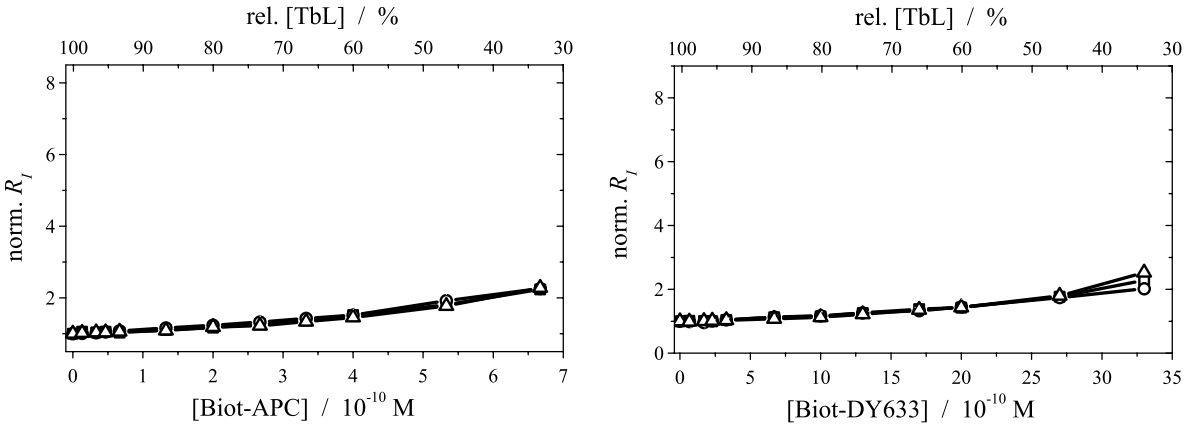

Figure 6.39: *TbL control experiments (cf. Figure 4.19), ruling out dynamic FRET.*

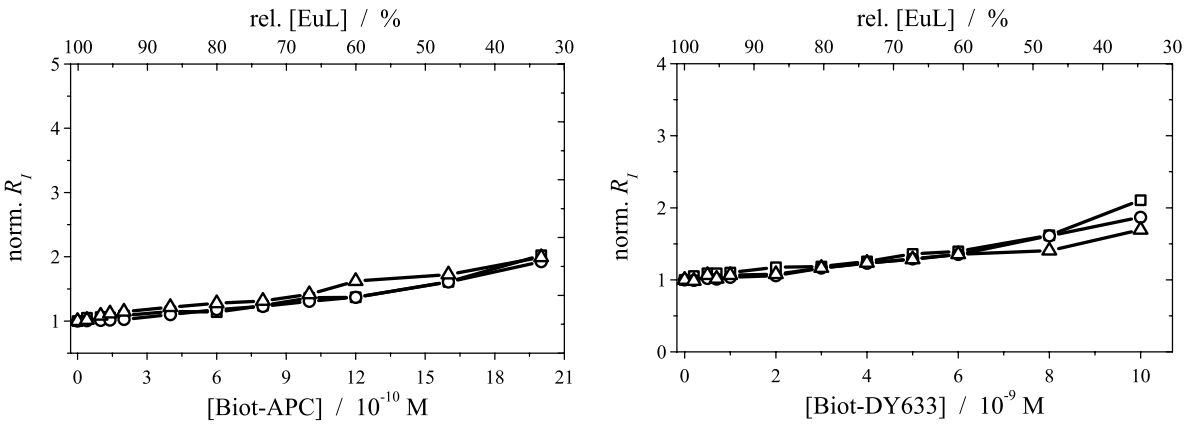

Figure 6.40: *EuL control experiments (cf. Figure 4.20), ruling out dynamic FRET.*

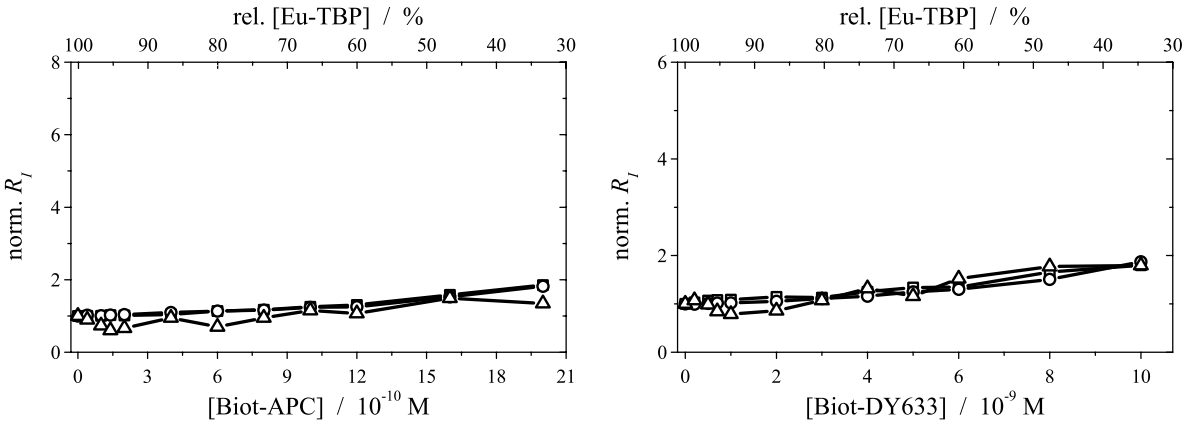

Figure 6.41: *EuL control experiments (cf. Figure 4.21), ruling out dynamic FRET.*

Bibliography

[1] Förster, Th.: Zwischenmolekulare Energiewanderung und Fluoreszenz. In: *Annalen der Physik* 2 (1948), Iss. 1-2, P. 55–75

[2] Clegg, R.M.: Fluorescence Resonance Energy Transfer. In: Wang, X.F. (Ed.); Herman, B. (Ed.): *Fluorescence Imaging Spectroscopy and Microscopy* Vol. 137. New York: John Wiley and Sons, Inc., 1996, P. 179 – 252

[3] Dale, R. E.; Eisinger, J.: Intramolecular Distances Determined by Energy-Transfer - Dependence on Orientational Freedom of Donor and Acceptor. In: *Biopolymers* 13 (1974), Iss. 8, P. 1573–1605

[4] Dale, R. E.; Eisinger, J.; Blumberg, W. E.: Orientational Freedom of Molecular Probes - Orientation Factor in Intra-Molecular Energy-Transfer. In: *Biophysical Journal* 26 (1979), Iss. 2, P. 161–193

[5] Förster, Th.: Experimentelle und theoretische Untersuchung des zwischenmolekularen Übergangs von Elektronenanregungsenergie. In: *Zeitschrift für Naturforschung Section a-a Journal of Physical Sciences* 4 (1949), Iss. 5, P. 321–327

[6] Förster, Th.: 10th Spiers Memorial Lecture - Transfer Mechanisms of Electronic Excitation. In: *Discussions of the Faraday Society* (1959), Iss. 27, P. 7–17

[7] Förster, Th.: Delocalized Excitation and Excitation Transfer. In: Sinanoglu, Oktay (Ed.): *Modern Quantum Chemistry. Istanbul Lectures. Part III: Action of Light and Organic Crystals.* New York ; London: Academic Press, 1965, P. 93–137

[8] Fung, B. K. K.; Stryer, L.: Surface Density Determination in Membranes by Fluorescence Energy Transfer. In: *Biochemistry* 17 (1978), Iss. 24, P. 5241–5248

[9] Haas, E.; Katchalskikatzir, E.; Steinberg, I. Z.: Effect of the Orientation of Donor and Acceptor on the Probability of Energy Transfer Involving Electronic Transitions of Mixed Polarization. In: *Biochemistry* 17 (1978), Iss. 23, P. 5064–5070

[10] Lakowicz, J. R.: *Principles of Fluorescence Spectroscopy.* 2nd. New York: Kluwer Academic/Plenum, 1999

[11] Morrison, L. E.: Time-Resolved Detection of Energy-Transfer - Theory and Application to Immunoassays. In: *Analytical Biochemistry* 174 (1988), Iss. 1, P. 101–120

[12] Sapsford, K. E.; Berti, L.; Medintz, I. L.: Materials for Fluorescence Resonance Energy Transfer Analysis: Beyond Traditional Donor-Acceptor Combinations. In: *Angewandte Chemie-International Edition* 45 (2006), Iss. 28, P. 4562–4588

[13] Selvin, P. R.: The Renaissance of Fluorescence Resonance Energy Transfer. In: *Nature Structural Biology* 7 (2000), Iss. 9, P. 730–734

[14] Steinberg, I. Z.: Long-Range Nonradiative Transfer of Electronic Excitation Energy in Proteins and Polypeptides. In: *Annual Review of Biochemistry* 40 (1971), P. 83–114

[15] Stryer, L.; Haugland, R. P.: Energy Transfer: A Spectroscopic Ruler. In: *Proceedings of the National Academy of Sciences of the United States of America* 58 (1967), Iss. 2, P. 716–726

[16] Stryer, L.: Fluorescence Energy-Transfer as a Spectroscopic Ruler. In: *Annual Review of Biochemistry* 47 (1978), P. 819–846

[17] Van der Meer, B. W.; Coker, G.; Simon Chen, S. Y.: *Resonance Energy Transfer: Theory and Data*. New York ; Cambridge: Vch, 1994

[18] Wu, P. G.; Brand, L.: Resonance Energy-Transfer - Methods and Applications. In: *Analytical Biochemistry* 218 (1994), Iss. 1, P. 1–13

[19] Didenko, V. V.: DNA Probes Using Fluorescence Resonance Energy Transfer (FRET): Designs and Applications. In: *Biotechniques* 31 (2001), Iss. 5, P. 1106–1116

[20] Fairclough, R.H.; Cantor, C.R.: The Use of Singlet-Singlet Energy Transfer to Study Macromolecular Assemblies. In: Hirs, C.H.W. (Ed.); Timasheff, S.N. (Ed.): *Methods in Enzymology* Vol. 48. New York: Academic Press, 1978, P. 347–379

[21] Jares-Erijman, E. A.; Jovin, T. M.: FRET imaging. In: *Nature Biotechnology* 21 (2003), Iss. 11, P. 1387–1395

[22] Lakowicz, J. R.; Geddes, C. D.: *Topics in Fluorescence Spectroscopy*. New York: Plenum Press, 1991

[23] Schuler, B.: Single-molecule fluorescence spectroscopy of protein folding. In: *ChemPhysChem* 6 (2005), Iss. 7, P. 1206–1220

[24] Selvin, P. R.: Principles and Biophysical Applications of Lanthanide-Based Probes. In: *Annual Review of Biophysics and Biomolecular Structure* 31 (2002), P. 275–302

[25] Szollosi, J.; Damjanovich, S.; Matyus, L.: Application of Fluorescence Resonance Energy Transfer in the Clinical Laboratory: Routine and Research. In: *Cytometry* 34 (1998), Iss. 4, P. 159–179

[26] Schuler, B.; Lipman, E. A.; Steinbach, P. J.; Kumke, M.; Eaton, W. A.: Polyproline and the "Spectroscopic Ruler" Revisited with Single-Molecule Fluorescence. In: *Proceedings of the National Academy of Sciences of the United States of America* 102 (2005), Iss. 8, P. 2754–2759

[27] Kumke, M. U.; Eidner, S.; Kruger, T.: Fluorescence Quenching and Luminescence Sensitization in Complexes of Tb3+ and Eu3+ with Humic Substances. In: *Environmental Science and Technology* 39 (2005), Iss. 24, P. 9528–9533

[28] Bünzli, J.-C. G.: Luminescent Probes. In: Bünzli, J.-C. G. (Ed.); Choppin, G. R. (Ed.): *Lanthanide Probes in Life, Chemical, and Earth Sciences: Theory and Practice*. Amsterdam ; New York: Elsevier, 1989

[29] Bünzli, J. C. G.: Luminescent Lanthanide Probes as Diagnostic and Therapeutic Tools. In: Sigel, A. (Ed.); Sigel, H. (Ed.): *Metal Ions in Biolgical Systems, Vol 42: Metal Complexes in Tumor Diagnosis and as Anticancer Agents* Vol. 42. New York: Marcel Dekker Inc., 2004, P. 39–75

[30] Richardson, F. S.: Terbium(III) and Europium(III) Ions as Luminescent Probes and Stains for Biomolecular Systems. In: *Chemical Reviews* 82 (1982), Iss. 5, P. 541–552

[31] Ekimov, A. I.; Onushchenko, A. A.; Tsekhomskii, V.A.: Exciton Light Absorption by CuCl Microcrystals in a Glass Matrix. In: *The Soviet Journal of Glass Physics and Chemistry* 6 (1980), P. 511–512

[32] Éfros, Al. L.; Éfros, A. L.: Interband Absorption of Light in a Semiconductor Sphere. In: *Soviet Physics-Semiconductors* 16 (1982), Iss. 7, P. 772–775

[33] Rossetti, R.; Ellison, J. L.; Gibson, J. M.; Brus, L. E.: Size Effects in the Excited Electronic States of Small Colloidal CdS Crystallites. In: *Journal of Chemical Physics* 80 (1984), Iss. 9, P. 4464–4469

[34] Clapp, A. R.; Medintz, I. L.; Fisher, B. R.; Anderson, G. P.; Mattoussi, H.: Can Luminescent Quantum Dots Be Efficient Energy Acceptors with Organic Dye Donors? In: *Journal of the American Chemical Society* 127 (2005), Iss. 4, P. 1242–1250

[35] Weibel, N.; Charbonnière, L. J.; Guardigli, M.; Roda, A.; Ziessel, R.: Engineering of Highly Luminescent Lanthanide Tags Suitable for Protein Labeling and Time-Resolved Luminescence Imaging. In: *Journal of the American Chemical Society* 126 (2004), Iss. 15, P. 4888–4896

[36] Hildebrandt, N.; Charbonnière, L. J.; Beck, M.; Ziessel, R. F.; Löhmannsröben, H.-G.: Quantum Dots As Efficient Energy Acceptors in a Time-Resolved Fluoroimmunoassay. In: *Angewandte Chemie - International Edition* 44 (2005), Iss. 46, P. 7612–7615

[37] Charbonnière, L. J.; Hildebrandt, N.; Ziessel, R. F.; Löhmannsröben, H.-G.: Lanthanides to Quantum Dots Resonance Energy Transfer in Time-Resolved FluoroImmunoAssays and Luminescence Microscopy. In: *Journal of the American Chemical Society* 128 (2006), Iss. 39, P. 12800–12809

[38] Alpha, B.; Lehn, J. M.; Mathis, G.: Energy-Transfer Luminescence of Europium(III) and Terbium(III) Cryptates of Macrobicyclic Polypyridine Ligands. In: *Angewandte Chemie - International Edition* 26 (1987), Iss. 3, P. 266–267

[39] Perrin, J. B.: Fluorescence et lois générales relatives aux vitesses de réaction. In: *Comptes Rendus Hebdomadaires des Séances de l'Académie des Sciences* 178 (1924), P. 1401–1406

[40] Perrin, J. B.: Fluorescence et induction moléculaire par résonance. In: *Comptes Rendus Hebdomadaires des Séances de l'Académie des Sciences* 184 (1927), P. 1097–1100

[41] Perrin, F.: Théorie quantique des transferts d'activation entre molécules de même espèce. Cas des solutions fluorescentes. In: *Annales de Chimie et de Physique* 17 (1932), P. 283–313

[42] Förster, Th.: Energiewanderung und Fluoreszenz. In: *Naturwissenschaften* 33 (1946), Iss. 6, P. 166–175

[43] Förster, Th.: *Fluoreszenz organischer Verbindungen.* Gottingen: Vandenhoeck und Ruprecht, 1951

[44] Valeur, B.: *Molecular Fluorescence: Principles and Applications.* Weinheim ; New York: Wiley-VCH, 2002

[45] Haas, E.; Wilchek, M.; Katchalskikatzir, E.; Steinberg, I. Z.: Distribution of End-to-End Distances of Oligopeptides in Solution as Estimated by Energy-Transfer. In: *Proceedings of the National Academy of Sciences of the United States of America* 72 (1975), Iss. 5, P. 1807–1811

[46] Haas, E.; Katchalski-Katzir, E.; Steinberg, I. Z.: Brownian-Motion of Ends of Oligopeptide Chains in Solution as Estimated by Energy-Transfer between Chain Ends. In: *Biopolymers* 17 (1978), Iss. 1, P. 11–31

[47] Grinvald, A.; Haas, E.; Steinberg, I.Z.: Evaluation of Distribution of Distances between Energy Donors and Acceptors by Fluorescence Decay. In: *Proceedings of the National Academy of Sciences of the United States of America* 69 (1972), Iss. 8, P. 2273–2277

[48] Loosli, A.; Rusbandi, U. E.; Gradinaru, J.; Bernauer, K.; Schlaepfer, C. W.; Meyer, M.; Mazurek, S.; Novic, M.; Ward, T. R.: (Strept)avidin as Host for Biotinylated Coordination Complexes: Stability, Chiral Discrimination, and Cooperativity. In: *Inorganic Chemistry* 45 (2006), Iss. 2, P. 660–668

[49] Lakowicz, J. R.; Weber, G.: Quenching of Protein Fluorescence by Oxygen - Detection of Structural Fluctuations in Proteins on Nanosecond Time Scale. In: *Biochemistry* 12 (1973), Iss. 21, P. 4171–4179

[50] Weber, G.; Lakowicz, J. R.: Subnanosecond Solvent Relaxation Studies by Oxygen Quenching of Fluorescence. In: *Chemical Physics Letters* 22 (1973), Iss. 2, P. 419–423

[51] Seidel, C. A. M.; Schulz, A.; Sauer, M. H. M.: Nucleobase-specific quenching of fluorescent dyes .1. Nucleobase one-electron redox potentials and their correlation with static and dynamic quenching efficiencies. In: *Journal of Physical Chemistry* 100 (1996), Iss. 13, P. 5541–5553

[52] Choppin, G. R.: Chemical Properties of the Rare Earth Elements. In: Bünzli, J.-C. G. (Ed.); Choppin, G. R. (Ed.): *Lanthanide Probes in Life, Chemical, and Earth Sciences: Theory and Practice.* Amsterdam ; New York: Elsevier, 1989

[53] Carnall, W. T.: The Absorption and Fluorescence Spectra of Rare Earth Ions in Solution. In: Gschneidner, K. A. (Ed.); Eyring, L. (Ed.): *Handbook on the Physics and Chemistry of Rare Earths*. North-Holland

[54] Carnall, W. T.; Beitz, J.V.; Crosswhite, H.; Rajnak, K.; Mann, J.B.: Spectroscopic Properties of the f-Elements in Compounds and Solutions. In: Sinha, S. P. (Ed.): *Systematics and the Properties of the Lanthanides*. D. Reidel; Hingham

[55] Görller-Walrand, C.; Binnemans, K.: Rationalization of Crystal-Field Parametrization. In: Gschneidner, K. A. (Ed.); Eyring, L. (Ed.): *Handbook on the Physics and Chemistry of Rare Earths* Vol. 23. Amsterdam ; London: North-Holland, 1996

[56] Görller-Walrand, C.; Binnemans, K.: Spectral Intensities of f-f Transitions. In: Gschneidner, K. A. (Ed.); Eyring, L. (Ed.): *Handbook on the Physics and Chemistry of Rare Earths* Vol. 25. Amsterdam ; London: North-Holland, 1998

[57] Sinha, A.P.B.: Fluorescence and Laser Action in Rare Earth Chelates. In: Rao, C. N. R. (Ed.); Ferraro, J. R. (Ed.): *Spectroscopy in Inorganic Chemistry* Vol. 2. New York ; London: Academic Press, 1971

[58] Sinha, S. P.: Fluorescence Spectra and Lifetimes of the Lanthanide Aquo Ions and their Complexes. In: Sinha, S. P. (Ed.): *Systematics and the Properties of the Lanthanides*. D. Reidel; Hingham

[59] Racah, G.: Theory of Complex Spectra. I. In: *Physical Review* 61 (1942), Iss. 3-4, P. 186–197

[60] Racah, G.: Theory of Complex Spectra. II. In: *Physical Review* 62 (1942), Iss. 9-10, P. 438–462

[61] Racah, G.: Theory of Complex Spectra. III. In: *Physical Review* 63 (1943), Iss. 9-10, P. 367–382

[62] Racah, G.: Theory of Complex Spectra. IV. In: *Physical Review* 76 (1949), Iss. 9, P. 1352–1365

[63] Slater, J. C.: *International Series in Pure and Applied Physics*. Vol. II: *Quantum Theory of Atomic Structure*. New York: McGraw-Hill, 1960

[64] Judd, B. R.: *Operator Techniques in Atomic Spectroscopy*. New York ; London: McGraw-Hill Book Co, 1963 (McGraw-Hill Advanced Physics Monograph Series)

[65] Nielson, C. W.; Koster, G. F.: *Spectroscopic Coefficients for the pn, dn, and fn Configurations*. Cambridge, Mass.: M.I.T. Press, 1963

[66] Blasse, G.; Grabmaier, B. C.: *Luminescent Materials*. Berlin ; London: Springer, 1994

[67] Broer, L. J. F.; Gorter, C. J.; Hoogschagen, J.: On the Intensities and the Multipole Character in the Spectra of the Rare Earth Ions. In: *Physica* 11 (1945), Iss. 4, P. 231–250

[68] Judd, B. R.: Optical Absorption Intensities of Rare-Earth Ions. In: *Physical Review* 127 (1962), Iss. 3, P. 750–761

[69] Ofelt, G. S.: Intensities of Crystal Spectra of Rare-Earth Ions. In: *Journal of Chemical Physics* 37 (1962), Iss. 3, P. 511–520

[70] Chrysochoos, J.; Evers, A.: Effect of Primary and Secondary Solvation Spheres of Eu^{3+} Upon Electric-Quadrupole Transitions ($\Delta J = 2$). In: *Chemical Physics Letters* 18 (1973), Iss. 1, P. 115–119

[71] Selwood, P.W.: Deformation of Electron Shells II. Absorption Spectrum, Molecular Volume and Refraction of Certain Rare Earth Salts. In: *Journal of the American Chemical Society* 52 (1930), Iss. 11, P. 4308–4316

[72] Moeller, T.; Brantley, J. C.: Observations on the Rare Earths. LVIII. Reaction Between Neodymium and Ethylenediaminetetraacetate Ions in Aqueous Solution. In: *Journal of the American Chemical Society* 72 (1950), Iss. 12, P. 5447–5451

[73] Moeller, T.; Jackson, D. E.: The Rare Earths - Separative Extraction of Certain Rare Earth Elements as 5,7-Dichloro-8-Quinolinol Chelates. In: *Analytical Chemistry* 22 (1950), Iss. 11, P. 1393–1397

[74] Peacock, R.D.: Rare Earths. In: Dunitz, J. D. (Ed.): *Structure and Bonding* Vol. 22. New York, NY: Springer-Verlag, 1975, P. 83–122

[75] Henrie, D. E.; Fellows, R. L.; Choppin, G. R.: Hypersensitivity in Electronic-Transitions of Lanthanide and Actinide Complexes. In: *Coordination Chemistry Reviews* 18 (1976), Iss. 2, P. 199–224

[76] Misra, S. N.: Energy Interaction Parameters and Intensity Analysis of Praseodymium and Neodymium Complexes. In: *Journal of Scientific and Industrial Research* 44 (1985), Iss. 7, P. 366–375

[77] Misra, S. N.; Sommerer, S. O.: Absorption-Spectra of Lanthanide Complexes in Solution. In: *Applied Spectroscopy Reviews* 26 (1991), Iss. 3, P. 151–202

[78] Atkins, P. W.; Friedman, R. S.: *Molecular quantum mechanics.* Oxford: Oxford University Press, 2005

[79] Gruen, D. M.; De Kock, C. W.: Absorption Spectra of Gaseous $NdBr_3$ and NdI_3. In: *Journal of Chemical Physics* 45 (1966), Iss. 2, P. 455–460

[80] Weissman, S. I.: Intramolecular Energy Transfer: The Fluorescence of Complexes of Europium. In: *Journal of Chemical Physics* 10 (1942), P. 214–217

[81] Crosby, G. A.; Alire, R. M.; Whan, R. E.: Intramolecular Energy Transfer in Rare Earth Chelates - Role of Triplet State. In: *Journal of Chemical Physics* 34 (1961), Iss. 3, P. 743–748

[82] Balzani, V.; Scandola, F.: *Supramolecular Photochemistry.* Chichester: Ellis Horwood, 1991 (Ellis Horwood series in physical chemistry)

[83] Hemmilä, I.; Mukkala, V. M.: Time-Resolution in Fluorometry Technologies, Labels, and Applications in Bioanalytical Assays. In: *Critical Reviews in Clinical Laboratory Sciences* 38 (2001), Iss. 6, P. 441–519

[84] Jorgensen, C. K.: Electron Transfer Spectra of Lanthanide Complexes. In: *Molecular Physics* 5 (1962), Iss. 3, P. 271–277

[85] Latva, M.; Takalo, H.; Mukkala, V. M.; Matachescu, C.; RodriguezUbis, J. C.; Kankare, J.: Correlation between the lowest triplet state energy level of the ligand and lanthanide(III) luminescence quantum yield. In: *Journal of Luminescence* 75 (1997), Iss. 2, P. 149–169

[86] Alpha, B.; Ballardini, R.; Balzani, V.; Lehn, J. M.; Perathoner, S.; Sabbatini, N.: Antenna Effect in Luminescent Lanthanide Cryptates - a Photophysical Study. In: *Photochemistry and Photobiology* 52 (1990), Iss. 2, P. 299–306

[87] Horrocks, W. D.; Sudnick, D. R.: Lanthanide Ion Probes of Structure in Biology - Laser-Induced Luminescence Decay Constants Provide a Direct Measure of the Number of Metal-Coordinated Water-Molecules. In: *Journal of the American Chemical Society* 101 (1979), Iss. 2, P. 334–340

[88] Xiao, M.; Selvin, P. R.: Quantum Yields of Luminescent Lanthanide Chelates and Far-Red Dyes Measured by Resonance Energy Transfer. In: *Journal of the American Chemical Society* 123 (2001), Iss. 29, P. 7067–7073

[89] Diamandis, E. P.: Immunoassays with Time-Resolved Fluorescence Spectroscopy - Principles and Applications. In: *Clinical Biochemistry* 21 (1988), Iss. 3, P. 139–150

[90] Diamandis, E. P.: Analytical Methodology for Immunoassays and DNA Hybridization Assays - Current Status and Selected Systems - Critical-Review. In: *Clinica Chimica Acta* 194 (1990), Iss. 1, P. 19–50

[91] Dickson, E. F. G.; Pollak, A.; Diamandis, E. P.: Ultrasensitive Bioanalytical Assays Using Time-Resolved Fluorescence Detection. In: *Pharmacology and Therapeutics* 66 (1995), Iss. 2, P. 207–235

[92] Hemmilä, Ilkka A.: *Applications of Fluorescence in Immunoassays*. New York: J. Wiley and Sons, 1991

[93] Horrocks, W. D.; Sudnick, D. R.: Lanthanide Ion Luminescence Probes of the Structure of Biological Macromolecules. In: *Accounts of Chemical Research* 14 (1981), Iss. 12, P. 384–392

[94] Sabbatini, N.; Guardigli, M.; Lehn, J. M.: Luminescent Lanthanide Complexes as Photochemical Supramolecular Devices. In: *Coordination Chemistry Reviews* 123 (1993), Iss. 1-2, P. 201–228

[95] Soini, E.; Hemmilä, I.: Fluoroimmunoassay - Present Status and Key Problems. In: *Clinical Chemistry* 25 (1979), Iss. 3, P. 353–361

[96] Wild, D.: *The Immunoassay Handbook*. 2nd. London: Nature Pub. Group, 2001

[97] Yuan, J. L.; Wang, G. L.: Lanthanide Complex-Based Fluorescence Label for Time-Resolved Fluorescence Bioassay. In: *Journal of Fluorescence* 15 (2005), Iss. 4, P. 559–568

[98] Inventors: Soini, E.; Hemmilä, I.: *European Patent EP0064484*. 1982

[99] Inventor: Evangelista, R.A.: *European Patent EP0171978*. 1986

[100] Evangelista, R. A.; Pollak, A.; Allore, B.; Templeton, E. F.; Morton, R. C.; Diamandis, E. P.: A New Europium Chelate for Protein Labeling and Time-Resolved Fluorometric Applications. In: *Clinical Biochemistry* 21 (1988), Iss. 3, P. 173–178

[101] Sammes, P. G.; Yahioglu, G.: Modern Bioassays Using Metal Chelates as Luminescent Probes. In: *Natural Product Reports* 13 (1996), Iss. 1, P. 1–28

[102] Lehn, J. M.: Supramolecular Chemistry - Scope and Perspectives. Molecules, Supermolecules, and Molecular Devices. In: *Angewandte Chemie - International Edition* 27 (1988), Iss. 1, P. 89–112

[103] Hemmilä, I.; Laitala, V.: Progress in Lanthanides as Luminescent Probes. In: *Journal of Fluorescence* 15 (2005), Iss. 4, P. 529–542

[104] Mathis, G.: HTRF™ Technology. In: *Journal of Biomolecular Screening* 4 (1999), Iss. 6, P. 309–313

[105] Takalo, H.; Mukkala, V. M.; Mikola, H.; Liitti, P.; Hemmila, I.: Synthesis of Europium(III) Chelates Suitable for Labeling of Bioactive Molecules. In: *Bioconjugate Chemistry* 5 (1994), Iss. 3, P. 278–282

[106] Hemmilä, I.: LANCE™: Homogeneous Assay Platform for HTS. In: *Journal of Biomolecular Screening* 4 (1999), Iss. 6, P. 303–307

[107] Saha, A. K.; Kross, K.; Kloszewski, E. D.; Upson, D. A.; Toner, J. L.; Snow, R. A.; Black, C. D. V.; Desai, V. C.: Time-Resolved Fluorescence of a New Europium Chelate Complex - Demonstration of Highly Sensitive Detection of Protein and DNA Samples. In: *Journal of the American Chemical Society* 115 (1993), Iss. 23, P. 11032–11033

[108] Hildebrandt, N.; Charbonnière, L. J.; Ziessel, R. F.; Löhmannsröben, H.-G.: Quantum Dots as Resonance Energy Transfer Acceptors for Monitoring Biological Interactions. In: Grzymala, R. (Ed.); Haeberle, O. (Ed.): *Proceedings of SPIE Vol. 6191 - Biophotonics and New Therapy Frontiers* Vol. 6191, 2006, P. 61910W (9 pages)

[109] Kubo, R.: Electronic Properties of Metallic Fine Particles. I. In: *Journal of the Physical Society of Japan* 17 (1962), Iss. 6, P. 975–986

[110] Fröhlich, H.: Die spezifische Wärme der Elektronen kleiner Metallteilchen bei tiefen Temperaturen. In: *Physica* 4 (1937), Iss. 5, P. 406–412

[111] Wise, F. W. (Ed.): *Selected Papers on Semiconductor Quantum Dots*. Bellingham, Wash.: SPIE Press, 2005 (SPIE Milestone Series; Volume MS 180)

[112] Banyai, L.; Koch, S. W.: *Semiconductor Quantum Dots*. Singapore; London: World Scientific, 1993 (World Scientific Series on Atomic, Molecular, and Optical Physics; Vol.2)

[113] Gaponenko, S. V.: *Optical Properties of Semiconductor Nanocrystals*. Cambridge: Cambridge University Press, 2005 (Cambridge studies in modern optics ; 23)

[114] Schmid, G. (Ed.): *Nanoparticles: From Theory to Application*. Weinheim: Wiley-VCH, 2004

[115] Bawendi, M. G.; Wilson, W. L.; Rothberg, L.; Carroll, P. J.; Jedju, T. M.; Steigerwald, M. L.; Brus, L. E.: Electronic-Structure and Photoexcited-Carrier Dynamics in Nanometer-Size CdSe Clusters. In: *Physical Review Letters* 65 (1990), Iss. 13, P. 1623–1626

[116] Steigerwald, M. L.; Brus, L. E.: Semiconductor Crystallites - A Class of Large Molecules. In: *Accounts of Chemical Research* 23 (1990), Iss. 6, P. 183–188

[117] Murray, C. B.; Norris, D. J.; Bawendi, M. G.: Synthesis and Characterization of Nearly Monodisperse CdE (E = S, Se, Te) Semiconductor Nanocrystallites. In: *Journal of the American Chemical Society* 115 (1993), Iss. 19, P. 8706–8715

[118] Weller, H.: Quantized Semiconductor Particles - A Novel State of Matter for Materials Science. In: *Advanced Materials* 5 (1993), Iss. 2, P. 88–95

[119] Alivisatos, A. P.: Semiconductor Clusters, Nanocrystals, and Quantum Dots. In: *Science* 271 (1996), Iss. 5251, P. 933–937

[120] Murphy, C. J.; Coffer, J. L.: Quantum Dots: A Primer. In: *Applied Spectroscopy* 56 (2002), Iss. 1, P. 16a–27a

[121] Davydov, A. S.: *Quantum Mechanics*. Oxford; New York: Pergamon Press, 1965 (International Series of Monographs in Natural Philosophy; Vol. 1)

[122] Flügge, S.: *Die Grundlehren der mathematischen Wissenschaften in Einzeldarstellungen; Bd. 177-178*. Vol. 1: *Practical Quantum Mechanics*. Berlin; London: Springer-Verlag, 1971

[123] Brus, L. E.: Electron-Electron and Electron-Hole Interactions in Small Semiconductor Crystallites: The Size Dependence of the Lowest Excited Electronic State. In: *Journal of Chemical Physics* 80 (1984), Iss. 9, P. 4403–4409

[124] Schmidt, H. M.; Weller, H.: Quantum Size Effects in Semiconductor Crystallites: Calculation of the Energy Spectrum for the Confined Exciton. In: *Chemical Physics Letters* 129 (1986), Iss. 6, P. 615–618

[125] Brus, L.: Electronic Wave Functions in Semiconductor Clusters: Experiment and Theory. In: *Journal of Physical Chemistry* 90 (1986), Iss. 12, P. 2555–2560

[126] Kayanuma, Y.: Wannier Exciton in Microcrystals. In: *Solid State Communications* 59 (1986), Iss. 6, P. 405–408

[127] Gerion, D.; Pinaud, F.; Williams, S. C.; Parak, W. J.; Zanchet, D.; Weiss, S.; Alivisatos, A. P.: Synthesis and Properties of Biocompatible Water-Soluble Silica-Coated CdSe/ZnS Semiconductor Quantum Dots. In: *Journal of Physical Chemistry B* 105 (2001), Iss. 37, P. 8861–8871

[128] Hines, M. A.; Guyot-Sionnest, P.: Synthesis and Characterization of Strongly Luminescing ZnS-Capped CdSe Nanocrystals. In: *Journal of Physical Chemistry* 100 (1996), Iss. 2, P. 468–471

[129] Norris, D. J.; Sacra, A.; Murray, C. B.; Bawendi, M. G.: Measurement of the Size Dependent Hole Spectrum in CdSe Quantum Dots. In: *Physical Review Letters* 72 (1994), Iss. 16, P. 2612–2615

[130] Dabbousi, B. O.; RodriguezViejo, J.; Mikulec, F. V.; Heine, J. R.; Mattoussi, H.; Ober, R.; Jensen, K. F.; Bawendi, M. G.: (CdSe)ZnS Core-Shell Quantum Dots: Synthesis and Characterization of a Size Series of Highly Luminescent Nanocrystallites. In: *Journal of Physical Chemistry B* 101 (1997), Iss. 46, P. 9463–9475

[131] Kortan, A. R.; Hull, R.; Opila, R. L.; Bawendi, M. G.; Steigerwald, M. L.; Carroll, P. J.; Brus, L. E.: Nucleation and Growth of CdSe on ZnS Quantum Crystallite Seeds, and Vice Versa, in Inverse Micelle Media. In: *Journal of the American Chemical Society* 112 (1990), Iss. 4, P. 1327–1332

[132] Wang, S. P.; Mamedova, N.; Kotov, N. A.; Chen, W.; Studer, J.: Antigen/Antibody Immunocomplex from CdTe Nanoparticle Bioconjugates. In: *Nano Letters* 2 (2002), Iss. 8, P. 817–822

[133] Tran, P. T.; Goldman, E. R.; Anderson, G. P.; Mauro, J. M.; Mattoussi, H.: Use of Luminescent CdSe-ZnS Nanocrystal Bioconjugates in Quantum Dot-Based Nanosensors. In: *Physica Status Solidi B - Basic Research* 229 (2002), Iss. 1, P. 427–432

[134] Parak, W. J.; Gerion, D.; Zanchet, D.; Woerz, A. S.; Pellegrino, T.; Micheel, C.; Williams, S. C.; Seitz, M.; Bruehl, R. E.; Bryant, Z.; Bustamante, C.; Bertozzi, C. R.; Alivisatos, A. P.: Conjugation of DNA to Silanized Colloidal Semiconductor Nanocrystalline Quantum Dots. In: *Chemistry of Materials* 14 (2002), Iss. 5, P. 2113–2119

[135] Guo, W. Z.; Li, J. J.; Wang, Y. A.; Peng, X. G.: Conjugation Chemistry and Bioapplications of Semiconductor Box Nanocrystals Prepared via Dendrimer Bridging. In: *Chemistry of Materials* 15 (2003), Iss. 16, P. 3125–3133

[136] Chan, W. C. W.; Nie, S. M.: Quantum Dot Bioconjugates for Ultrasensitive Nonisotopic Detection. In: *Science* 281 (1998), Iss. 5385, P. 2016–2018

[137] Potapova, I.; Mruk, R.; Hubner, C.; Zentel, R.; Basche, T.; Mews, A.: CdSe/ZnS Nanocrystals with Dye-Functionalized Polymer Ligands Containing Many Anchor Groups. In: *Angewandte Chemie - International Edition* 44 (2005), Iss. 16, P. 2437–2440

[138] Mamedova, N. N.; Kotov, N. A.; Rogach, A. L.; Studer, J.: Albumin-CdTe Nanoparticle Bioconjugates: Preparation, Structure, and Interunit Energy Transfer with Antenna Effect. In: *Nano Letters* 1 (2001), Iss. 6, P. 281–286

[139] Chen, F. Q.; Gerion, D.: Fluorescent CdSe/ZnS Nanocrystal-Peptide Conjugates for Long-Term, Nontoxic Imaging and Nuclear Targeting in Living Cells. In: *Nano Letters* 4 (2004), Iss. 10, P. 1827–1832

[140] Pinaud, F.; King, D.; Moore, H. P.; Weiss, S.: Bioactivation and Cell Targeting of Semiconductor CdSe/ZnS Nanocrystals with Phytochelatin-Related Peptides. In: *Journal of the American Chemical Society* 126 (2004), Iss. 19, P. 6115–6123

[141] Warner, J. H.; Hoshino, A.; Yamamoto, K.; Tilley, R. D.: Water-soluble Photoluminescent Silicon Quantum Dots. In: *Angewandte Chemie - International Edition* 44 (2005), Iss. 29, P. 4550–4554

[142] Uyeda, H. T.; Medintz, I. L.; Jaiswal, J. K.; Simon, S. M.; Mattoussi, H.: Synthesis of Compact Multidentate Ligands to Prepare Stable Hydrophilic Quantum Dot Fluorophores. In: *Journal of the American Chemical Society* 127 (2005), Iss. 11, P. 3870–3878

[143] Mattoussi, H.; Mauro, J. M.; Goldman, E. R.; Anderson, G. P.; Sundar, V. C.; Mikulec, F. V.; Bawendi, M. G.: Self-Assembly of CdSe-ZnS Quantum Dot Bioconjugates Using an Engineered Recombinant Protein. In: *Journal of the American Chemical Society* 122 (2000), Iss. 49, P. 12142–12150

[144] Gaponik, N.; Talapin, D. V.; Rogach, A. L.; Hoppe, K.; Shevchenko, E. V.; Kornowski, A.; Eychmuller, A.; Weller, H.: Thiol-Capping of CdTe Nanocrystals: An Alternative to Organometallic Synthetic Routes. In: *Journal of Physical Chemistry B* 106 (2002), Iss. 29, P. 7177–7185

[145] Querner, C.; Reiss, P.; Bleuse, J.; Pron, A.: Chelating Ligands for Nanocrystals' Surface Functionalization. In: *Journal of the American Chemical Society* 126 (2004), Iss. 37, P. 11574–11582

[146] Bruchez, M. P.: Turning All the Lights on: Quantum Dots in Cellular Assays. In: *Current Opinion in Chemical Biology* 9 (2005), Iss. 5, P. 533–537

[147] Arya, H.; Kaul, Z.; Wadhwa, R.; Taira, K.; Hirano, T.; Kaul, S. C.: Quantum Dots in Bio-Imaging: Revolution by the Small. In: *Biochemical and Biophysical Research Communications* 329 (2005), Iss. 4, P. 1173–1177

[148] Dubertret, B.; Skourides, P.; Norris, D. J.; Noireaux, V.; Brivanlou, A. H.; Libchaber, A.: In Vivo Imaging of Quantum Dots Encapsulated in Phospholipid Micelles. In: *Science* 298 (2002), Iss. 5599, P. 1759–1762

[149] Larson, D. R.; Zipfel, W. R.; Williams, R. M.; Clark, S. W.; Bruchez, M. P.; Wise, F. W.; Webb, W. W.: Water-Soluble Quantum Dots for Multiphoton Fluorescence Imaging in Vivo. In: *Science* 300 (2003), Iss. 5624, P. 1434–1436

[150] Xu, H. X.; Sha, M. Y.; Wong, E. Y.; Uphoff, J.; Xu, Y. H.; Treadway, J. A.; Truong, A.; O'Brien, E.; Asquith, S.; Stubbins, M.; Spurr, N. K.; Lai, E. H.; Mahoney, W.: Multiplexed SNP Genotyping Using the Qbead^{TM} System: A Quantum Dot-Encoded Microsphere-Based Assay. In: *Nucleic Acids Research* 31 (2003), Iss. 8, P. e43, 10 pages

[151] Taylor, J. R.; Fang, M. M.; Nie, S. M.: Probing Specific Sequences on Single DNA Molecules with Bioconjugated Fluorescent Nanoparticles. In: *Analytical Chemistry* 72 (2000), Iss. 9, P. 1979–1986

[152] Chan, W. C.; Maxwell, D. J.; Gao, X.; Bailey, R. E.; Han, M.; Nie, S.: Luminescent Quantum Dots for Multiplexed Biological Detection and Imaging. In: *Current Opinion in Biotechnology* 13 (2002), Iss. 1, P. 40–46

[153] Han, M. Y.; Gao, X. H.; Su, J. Z.; Nie, S.: Quantum-Dot-Tagged Microbeads for Multiplexed Optical Coding of Biomolecules. In: *Nature Biotechnology* 19 (2001), Iss. 7, P. 631–635

[154] Goldman, E. R.; Clapp, A. R.; Anderson, G. P.; Uyeda, H. T.; Mauro, J. M.; Medintz, I. L.; Mattoussi, H.: Multiplexed Toxin Analysis Using Four Colors of Quantum Dot Fluororeagents. In: *Analytical Chemistry* 76 (2004), Iss. 3, P. 684–688

[155] Alivisatos, A. P.; Gu, W. W.; Larabell, C.: Quantum Dots as Cellular Probes. In: *Annual Review of Biomedical Engineering* 7 (2005), P. 55–76

[156] Alivisatos, P.: The Use of Nanocrystals in Biological Detection. In: *Nature Biotechnology* 22 (2004), Iss. 1, P. 47–52

[157] Bruchez, M.; Moronne, M.; Gin, P.; Weiss, S.; Alivisatos, A. P.: Semiconductor Nanocrystals as Fluorescent Biological Labels. In: *Science* 281 (1998), Iss. 5385, P. 2013–2016

[158] Medintz, I. L.; Uyeda, H. T.; Goldman, E. R.; Mattoussi, H.: Quantum Dot Bioconjugates for Imaging, Labelling and Sensing. In: *Nature Materials* 4 (2005), Iss. 6, P. 435–446

[159] Michalet, X.; Pinaud, F. F.; Bentolila, L. A.; Tsay, J. M.; Doose, S.; Li, J. J.; Sundaresan, G.; Wu, A. M.; Gambhir, S. S.; Weiss, S.: Quantum Dots for Live Cells, in Vivo Imaging, and Diagnostics. In: *Science* 307 (2005), Iss. 5709, P. 538–544

[160] Parak, W. J.; Gerion, D.; Pellegrino, T.; Zanchet, D.; Micheel, C.; Williams, S. C.; Boudreau, R.; Le Gros, M. A.; Larabell, C. A.; Alivisatos, A. P.: Biological Applications of Colloidal Nanocrystals. In: *Nanotechnology* 14 (2003), Iss. 7, P. R15–R27

[161] Parak, W. J.; Pellegrino, T.; Plank, C.: Labelling of Cells with Quantum Dots. In: *Nanotechnology* 16 (2005), Iss. 2, P. R9–R25

[162] Hardman, R.: A Toxicologic Review of Quantum Dots: Toxicity Depends on Physicochemical and Environmental Factors. In: *Environmental Health Perspectives* 114 (2006), Iss. 2, P. 165–172

[163] Ma, H. L.; Lu, H. Z.; Wang, L. P.; Xu, S. K.; Li, W.: Application of Fluorescence Resonance Energy Transfer of Quantum Dots in Biological Assay. In: *Chinese Journal of Analytical Chemistry* 33 (2005), Iss. 9, P. 1335–1338

[164] Zhang, C. Y.; Yeh, H. C.; Kuroki, M. T.; Wang, T. H.: Single-quantum-dot-based DNA nanosensor. In: *Nature Materials* 4 (2005), Iss. 11, P. 826–831

[165] Ma, Q.; Su, X. G.; Wang, X. Y.; Wan, Y.; Wang, C. L.; Yang, B.; Jin, Q. H.: Fluorescence Resonance Energy Transfer in Doubly-Quantum Dot Labeled IgG System. In: *Talanta* 67 (2005), Iss. 5, P. 1029–1034

[166] Jares-Erijman, E.; Giordano, L.; Spagnuolo, C.; Lidke, K.; Jovin, T. M.: Imaging Quantum Dots Switched On and Off by Photochromic Fluorescence Resonance Energy Transfer (pcFRET). In: *Molecular Crystals and Liquid Crystals* 430 (2005), P. 257–265

[167] Hohng, S.; Ha, T.: Single-Molecule Quantum-Dot Fluorescence Resonance Energy Transfer. In: *ChemPhysChem* 6 (2005), Iss. 5, P. 956–960

[168] Oh, E.; Hong, M. Y.; Lee, D.; Nam, S. H.; Yoon, H. C.; Kim, H. S.: Inhibition Assay of Biomolecules Based on Fluorescence Resonance Energy Transfer (FRET) Between Quantum Dots and Gold Nanoparticles. In: *Journal of the American Chemical Society* 127 (2005), Iss. 10, P. 3270–3271

[169] Clapp, A. R.; Medintz, I. L.; Mauro, J. M.; Fisher, B. R.; Bawendi, M. G.; Mattoussi, H.: Fluorescence Resonance Energy Transfer Between Quantum Dot Donors and Dye-Labeled Protein Acceptors. In: *Journal of the American Chemical Society* 126 (2004), Iss. 1, P. 301–310

[170] Medintz, I. L.; Clapp, A. R.; Mattoussi, H.; Goldman, E. R.; Fisher, B.; Mauro, J. M.: Self-Assembled Nanoscale Biosensors Based on Quantum Dot FRET Donors. In: *Nature Materials* 2 (2003), Iss. 9, P. 630–638

[171] Willard, D. M.; Carillo, L. L.; Jung, J.; Van Orden, A.: CdSe-ZnS Quantum Dots as Resonance Energy Transfer Donors in a Model Protein-Protein Binding Assay. In: *Nano Letters* 1 (2001), Iss. 9, P. 469–474

[172] Kagan, C. R.; Murray, C. B.; Bawendi, M. G.: Long-Range Resonance Transfer of Electronic Excitations in Close-Packed CdSe Quantum-Dot Solids. In: *Physical Review B* 54 (1996), Iss. 12, P. 8633–8643

[173] Kagan, C. R.; Murray, C. B.; Nirmal, M.; Bawendi, M. G.: Electronic Energy Transfer in CdSe Quantum Dot Solids. In: *Physical Review Letters* 76 (1996), Iss. 9, P. 1517–1520

[174] Beck, M.; Hildebrandt, N.; Löhmannsröben, H.-G.: Quantum Dots as Acceptors in FRET Assays Containing Serum. In: Grzymala, R. (Ed.); Haeberle, O. (Ed.): *Proceedings of SPIE Vol. 6191 - Biophotonics and New Therapy Frontiers* Vol. 6191, 2006, P. 61910X (8 pages)

[175] Clapp, A. R.; Medintz, I. L.; Mattoussi, H.: Förster Resonance Energy Transfer Investigations Using Quantum-Dot Fluorophores. In: *ChemPhysChem* 7 (2006), Iss. 1, P. 47–57

[176] Pons, T.; Medintz, I. L.; Sykora, M.; Mattoussi, H.: Spectrally Resolved Energy Transfer Using Quantum Dot Donors: Ensemble and Single-Molecule Photoluminescence Studies. In: *Physical Review B* 73 (2006), Iss. 24, P. 245302 (7 pages)

[177] Clapp, A. R.; Medintz, I. L.; Uyeda, H. T.; Fisher, B. R.; Goldman, E. R.; Bawendi, M. G.; Mattoussi, H.: Quantum Dot-Based Multiplexed Fluorescence Resonance Energy Transfer. In: *Journal of the American Chemical Society* 127 (2005), Iss. 51, P. 18212–18221

[178] Achermann, M.; Petruska, M. A.; Kos, S.; Smith, D. L.; Koleske, D. D.; Klimov, V. I.: Energy-Transfer Pumping of Semiconductor Nanocrystals Using an Epitaxial Quantum Well. In: *Nature* 429 (2004), Iss. 6992, P. 642–646

[179] Anni, M.; Manna, L.; Cingolani, R.; Valerini, D.; Creti, A.; Lomascolo, M.: Förster Energy Transfer from Blue-Emitting Polymers to Colloidal CdSe/ZnS Core Shell Quantum Dots. In: *Applied Physics Letters* 85 (2004), Iss. 18, P. 4169–4171

[180] So, M. K.; Xu, C. J.; Loening, A. M.; Gambhir, S. S.; Rao, J. H.: Self-Illuminating Quantum Dot Conjugates for In Vivo Imaging. In: *Nature Biotechnology* 24 (2006), Iss. 3, P. 339–343

[181] Mathis, G.: Rare-Earth Cryptates and Homogeneous Fluoroimmunoassays with Human Sera. In: *Clinical Chemistry* 39 (1993), Iss. 9, P. 1953–1959

[182] ACS Committee on Environmental Improvement; Subcommittee on Environmental Analytical Chemistry: Guidelines for Data Acquisition and Data Quality Evaluation in Environmental Chemistry. In: *Analytical Chemistry* 52 (1980), Iss. 14, P. 2242–2249

[183] Wilchek, M.; Bayer, E. A.: The Avidin Biotin Complex in Immunology. In: *Immunology Today* 5 (1984), Iss. 2, P. 39–43

[184] Wilchek, M.; Bayer, E. A.: The Avidin Biotin Complex in Bioanalytical Applications. In: *Analytical Biochemistry* 171 (1988), Iss. 1, P. 1–32

[185] Diamandis, E. P.; Christopoulos, T. K.: The Biotin (Strept)Avidin System - Principles and Applications in Biotechnology. In: *Clinical Chemistry* 37 (1991), Iss. 5, P. 625–636

[186] Green, N. M.: Avidin and Streptavidin. In: *Methods in Enzymology* 184 (1990), P. 51–67

[187] Wilchek, Meir (Ed.); Bayer, Edward A. (Ed.): *Avidin-Biotin Technology.* San Diego, Calif. ; London: Academic Press (Methods in Enzymology 184)

[188] Freitag, S.; Le Trong, I.; Chilkoti, A.; Klumb, L. A.; Stayton, P. S.; Stenkamp, R. E.: Structural Studies of Binding Site Tryptophan Mutants in the High-Affinity Streptavidin-Biotin Complex. In: *Journal of Molecular Biology* 279 (1998), Iss. 1, P. 211–221

[189] Green, N. M.: Avidin. In: Anfinsen, C.B. (Ed.); Edsall, J.T. (Ed.); Richards, F.M. (Ed.): *Advances in Protein Chemistry* Vol. 29. 1975, P. 85–133

[190] Freitag, S.: http://faculty.washington.edu/stenkamp/stefanieweb/abstract.html.

[191] Weber, P. C.; Ohlendorf, D. H.; Wendoloski, J. J.; Salemme, F. R.: Structural Origins of High-Affinity Biotin Binding to Streptavidin. In: *Science* 243 (1989), Iss. 4887, P. 85–88

[192] Hendrickson, W. A.; Pahler, A.; Smith, J. L.; Satow, Y.; Merritt, E. A.; Phizackerley, R. P.: Crystal-Structure of Core Streptavidin Determined from Multiwavelength Anomalous Diffraction of Synchrotron Radiation. In: *Proceedings of the National Academy of Sciences of the United States of America* 86 (1989), Iss. 7, P. 2190–2194

[193] Freitag, S.; LeTrong, I.; Klumb, L.; Stayton, P. S.; Stenkamp, R. E.: Structural Studies of the Streptavidin Binding Loop. In: *Protein Science* 6 (1997), Iss. 6, P. 1157–1166

[194] Chu, V.; Freitag, S.; Le Trong, I.; Stenkamp, R. E.; Stayton, P. S.: Thermodynamic and structural consequences of flexible loop deletion by circular permutation in the streptavidin-biotin system. In: *Protein Science* 7 (1998), Iss. 4, P. 848–859

[195] Aslam, M.; Dent, A. (Eds.): *Bioconjugation: Protein Coupling Techniques for the Biomedical Sciences*. London; New-York: Macmillan Reference ltd: Grove's Dictionnaries Inc., 1998

[196] Hermanson, G. T.: *Bioconjugate Techniques*. San Diego; London: Academic Press, 1995

[197] Wong, S. S.: *Chemistry of Protein Conjugation and Cross-Linking*. Boca Raton: CRC Press, 1991

[198] Brinkley, M.: A Brief Survey of Methods for Preparing Protein Conjugates with Dyes, Haptens, and Cross-Linking Reagents. In: *Bioconjugate Chemistry* 3 (1992), Iss. 1, P. 2–13

[199] Böttger, V.; Micheel, B.; Scharte, G.; Kaiser, G.; Wolf, G.; Schmechta, H.: Monoclonal-Antibodies to Human Chorionic-Gonadotropin (Hcg) and Their Use in 2-Site Binding Enzyme Immunoassays. In: *Hybridoma* 12 (1993), Iss. 1, P. 81–91

[200] Invitrogen Corporation: http://www.qdots.com.

[201] Ong, L. J.; Glazer, A. N.: Crosslinking of Allophycocyanin. In: *Physiologie Vegetale* 23 (1985), Iss. 5, P. 777–787

[202] Walsh Yeh, S. W.; Ong, L. J.; Clark, J. H.; Glazer, A. N.: Fluorescence Properties of Allophycocyanin and a Cross-Linked Allophycocyanin Trimer. In: *Cytometry* 8 (1987), Iss. 1, P. 91–95

[203] Dyomics GmbH: http://www.dyomics.com.

[204] Lottspeich, F.; Zorbas, H. (Eds.): *Bioanalytik*. Heidelberg; Berlin: Spektrum, Akad. Verl., 1998

[205] Pace, C. N.; Vajdos, F.; Fee, L.; Grimsley, G.; Gray, T.: How to Measure and Predict the Molar Absorption Coefficient of a Protein. In: *Protein Science* 4 (1995), Iss. 11, P. 2411–2423

[206] Cohen, L. R. H.; Strupat, K.; Hillenkamp, F.: Analysis of Quaternary Protein Ensembles by Matrix Assisted Laser Desorption/Ionization Mass Spectrometry. In: *Journal of the American Society for Mass Spectrometry* 8 (1997), Iss. 10, P. 1046–1052

[207] Hildebrandt, N.; Flehr, R.; Bois, E.; Löhmannsröben, H.-G.: Optimized Homogeneous Immunoassay Based on XeCl-Laser Excited Förster Resonance Energy Transfer. In: *CLEO/EUROPE 2005 - Conferences on Lasers and Electro-Optics/Europe - Photonic Manipulation and Bio-Sensing (CL4-6)*, 2005

[208] Niederkrüger, M.; Salb, C.; Marowsky, G.; Beck, M.; Hildebrandt, N.; Löhmannsröben, H.-G.: Improvement of a Fluorescence Immunoassay with a Compact Diode-Pumped Solid State Laser at 315 nm. In: *Proceedings of SPIE Vol. 6380 - Smart Medical and Biomedical Sensor Technology IV* Vol. 6380, 2006, P. 63800M (9 pages)

[209] Tsukube, H.; Shinoda, S.: Lanthanide complexes in molecular recognition and chirality sensing of biological substrates. In: *Chemical Reviews* 102 (2002), Iss. 6, P. 2389–2403

[210] Charbonniere, L. J.; Ziessel, R.; Montalti, M.; Prodi, L.; Zaccheroni, N.; Boehme, C.; Wipff, G.: Luminescent lanthanide complexes of a bis-bipyridine-phosphine-oxide ligand as tools for anion detection. In: *Journal of the American Chemical Society* 124 (2002), Iss. 26, P. 7779–7788

[211] Lis, S.; Kimura, T.; Yoshida, Z.: Luminescence Lifetime of Lanthanide(III) Ions In Aqueous Solution Containing Azide Ion. In: *Journal of Alloys and Compounds* 323 (2001), P. 125–127

[212] Blasse, G.; Dirksen, G. J.; Sabbatini, N.; Perathoner, S.; Lehn, J. M.; Alpha, B.: Luminescence Processes In [Tb Bpy.Bpy.Bpy]3+ Cryptate - A Low-Temperature Solid-State Study. In: *Journal of Physical Chemistry* 92 (1988), Iss. 9, P. 2419–2422

[213] Sabbatini, N.; Guardigli, M.; Lehn, J. M.; Mathis, G.: Luminescence of Lanthanide Cryptates - Effects of Phosphate and Iodide Anions. In: *Journal of Alloys and Compounds* 180 (1992), P. 363–367

[214] Adams, E.W.; Bruchez, M.P.Jr.: *Surface-Modified Semiconductive and Metallic Nanoparticles Having Enhanced Dispersibility In Aqueous Media.* 2003

[215] Glazer, A. N.: Phycobilisome - A Macromolecular Complex Optimized for Light Energy Transfer. In: *Biochimica Et Biophysica Acta* 768 (1984), Iss. 1, P. 29–51

[216] Liu, J. Y.; Jiang, T.; Zhang, J. P.; Liang, D. C.: Crystal Structure of Allophycocyanin from Red Algae Porphyra yezoensis at 2.2-Angstrom Resolution. In: *Journal of Biological Chemistry* 274 (1999), Iss. 24, P. 16945–16952

[217] Buschmann, V.; Weston, K. D.; Sauer, M.: Spectroscopic Study and Evaluation of Red-Absorbing Fluorescent Dyes. In: *Bioconjugate Chemistry* 14 (2003), Iss. 1, P. 195–204

[218] Berlier, J. E.; Rothe, A.; Buller, G.; Bradford, J.; Gray, D. R.; Filanoski, B. J.; Telford, W. G.; Yue, S.; Liu, J. X.; Cheung, C. Y.; Chang, W.; Hirsch, J. D.; Beechem, J. M.; Haugland, R. P.; Haugland, R. P.: Quantitative Comparison of Long-Wavelength Alexa Fluor Dyes to Cy Dyes: Fluorescence of the Dyes and Their Bioconjugates. In: *Journal of Histochemistry and Cytochemistry* 51 (2003), Iss. 12, P. 1699–1712

[219] Kronick, M. N.: The Use of Phycobiliproteins as Fluorescent Labels in Immunoassay. In: *Journal of Immunological Methods* 92 (1986), Iss. 1, P. 1–13

[220] Schlegel, G.; Bohnenberger, J.; Potapova, I.; Mews, A.: Fluorescence decay time of single semiconductor nanocrystals. In: *Physical Review Letters* 88 (2002), Iss. 13, P. 137401 (4 pages)

[221] Fisher, B. R.; Eisler, H. J.; Stott, N. E.; Bawendi, M. G.: Emission Intensity Dependence and Single-Exponential Behavior In Single Colloidal Quantum Dot Fluorescence Lifetimes. In: *Journal of Physical Chemistry B* 108 (2004), Iss. 1, P. 143–148

[222] Geissbuehler, I.; Hovius, R.; Martinez, K. L.; Adrian, M.; Thampi, K. R.; Vogel, H.: Lipid-Coated Nanocrystals as Multifunctionalized Luminescent Scaffolds for Supramolecular Biological Assemblies. In: *Angewandte Chemie-International Edition* 44 (2005), Iss. 9, P. 1388–1392

[223] Gabourdes, M.; Bourgine, V.; Mathis, G.; Bazin, H.; Alpha-Bazin, W.: A Homogeneous Time-Resolved Fluorescence Detection of Telomerase Activity. In: *Analytical Biochemistry* 333 (2004), Iss. 1, P. 105–113

[224] Enomoto, K.; Nagasaki, T.; Yamauchi, A.; Onoda, J.; Sakai, K.; Yoshida, T.; Maekawa, K.; Kinoshita, Y.; Nishino, I.; Kikuoka, S.; Fukunaga, T.; Kawamoto, K.; Numata, Y.; Takemoto, H.; Nagata, K.: Development of High-Throughput Spermidine Synthase Activity Assay Using Homogeneous Time-Resolved Fluorescence. In: *Analytical Biochemistry* 351 (2006), Iss. 2, P. 229–240

[225] Erkens, J. H. F.; Dieleman, S. J.; Dressendorfer, R. A.; Strasburger, C. J.: A Time-Resolved Fluoroimmunoassay for Cortisol in Unextracted Bovine Plasma or Serum with Optimized Procedures to Eliminate Steroid Binding Protein Interference and to Minimize Non-Specific Streptavidin-Europium Binding. In: *Journal of Steroid Biochemistry and Molecular Biology* 67 (1998), Iss. 2, P. 153–161

[226] Beck, M.: *Personal communication at the Institut für Chemie, Interdisziplinäres Zentrum für Photonik, Physikalische Chemie, Universität Potsdam.* 2006

[227] Rodwell, J. D.; Alvarez, V. L.; Chyi, L.; Lopes, A. D.; Goers, J. W. F.; King, H. D.; Powsner, H. J.; Mckearn, T. J.: Site-Specific Covalent Modification of Monoclonal-Antibodies: In Vitro and In Vivo Evaluations. In: *Proceedings of the National Academy of Sciences of the United States of America* 83 (1986), Iss. 8, P. 2632–2636

[228] Lövgren, T.; Petterson, K.: Time-Resolved Fluoroimmunoassay, Advantages and Limitations. In: Van Dyke, Knox (Ed.); Van Dyke, Richard (Ed.): *Luminescence Immunoassay and Molecular Applications.* Boca Raton, Fla.: CRC Press, 1990, P. 233–254

Acknowledgment

My sincere personal thanks are given to the following people:

Prof. Dr. Hans-Gerd Löhmannsröben for letting me work on various interesting research subjects (especially the fascinating field of FRET laser spectroscopy with quantum dots and lanthanides) and for his constant support, motivation and scientific advice.

Dr. Loïc Charbonnière for the very interesting and pleasant scientific cooperation. It has been (and hopefully will be) great fun working with him.

Emmanuel Bois, Dominique Nuti and Arnaud Lavigne from Cezanne SA (Nîmes, France) for fruitful and friendly cooperation.

Christine Frankovitch, Dr. Michael Beck, Dr. Michael U. Kumke and Monique Chan Huot for fruitful discussions, advice and corrections.

All members of the Löhmannsröben Group for the fantastic working atmosphere, many discussions, scientific and personal support and a lot of unforgettable parties.

All my family and friends for love, trust, support and creative stimulation. Without them this work would have never been possible.